THE EFFECTS OF AIR DRYING ON THE STRENGTH OF SAND-LIGNOSULFONATE-WATER MIXES

by

WILSON ANTHONY SMITH JR

B.S., Kansas State University, 2009

A REPORT

submitted in partial fulfillment of the requirements for the degree

MASTER OF SCIENCE

Department of Civil Engineering
College of Engineering

KANSAS STATE UNIVERSITY
Manhattan, Kansas

2012

Approved by:

Major Professor
Dr. Dunja Peric

Abstract

The purpose of this research was to investigate the effects of drying on the strength gain of masonry sand stabilized with a co-product from wood pulping called calcium lignosulfonate. Lignin is an amorphous polymer found in plant cell walls. It provides protection against disease and allows the transport of water and nutrients. Adhesive properties of lignin generated interest in adding its modifications to soils as means to prevent erosion from wind and vehicle traffic on unpaved roads. Lignin has the potential to become a more sustainable alternative to traditional stabilizers because its source is renewable and abundant, and its toxicity is negligible.

Extensive testing has recently been completed to quantify the stress-strain relationships and Mohr-Coulomb strength parameters of sand- calcium lignosulfonate-water (S-CaL-W) mixes at early age (Bartley, 2011). The experimental program consisted of performing Standard Proctor Tests to determine maximum densities and optimum moisture contents for mixes having different gravimetric lignin contents and direct shear tests on selected sample configurations. Based on these results, it was decided to conduct shear strength testing of the samples containing 4%, 6% and 9% of calcium lignosulfonate after they had been exposed to air drying. To this end, responses of the selected sample configurations to drying at 71° F and 27% relative humidity were measured to determine the target water contents for shear strength testing. Drying curves were obtained by plotting the measured water content or water to CaL ratio versus the elapsed time. Drying times for shear strength were chosen based on how long it took the moisture contents to decrease by specified levels. The available results of direct shear tests show that drying significantly increases both the cohesion and the friction angle of the S-CaL-W mixes with respect to the early age cohesion and friction angle. In addition to the direct shear test program a laboratory compaction test was conducted on CaL and water only, thus providing the maximum dry density of CaL and the corresponding optimum water to CaL ratio.

It is also noted that relative humidity was discovered to be the limiting factor in the strength gain of S-CaL-W mixes. The reasons behind its sensitivity to water are due to the presence of HPLC sugars within the calcium lignosulfonate structure. These sugars hold the water through the chemical interaction of the sugars with hydrogen ions and water molecules.

Table of Contents

List of Figures

List of Tables

Acknowledgements

This research project was a unique experience in which I grew not just as student but as an individual. Individuals throughout the university and beyond contributed to the success of this project and I am forever grateful for them. I want to thank the faculty and staff within the Department of Civil Engineering at Kansas State University. I appreciate Dr Stokes and Dr. Davis for being on my supervisory committee as well as Dr. Najjar for giving me scholastic insight into the field of geotechnical engineering. I want to include a special thanks to Danita Deters and Peggy Selvidge for always being able to answers questions about payroll, university transactions, and departmental funding etc.

I want to express gratitude to my advisor Dr. Peric for her expertise and guidance throughout the duration of this project. Her vast knowledge is inspirational and I will try to emulate her quest to always learn more and never stop asking questions in order to learn and grow within the profession. I am also thankful for the countless hours that she dedicated to this project from its conception to its completion.

Borregaard LignoTech USA was the source of calcium lignosulfonate for the project and I would like to thank both Roland Taff and Tim McNally for being thoughtful and generous in their donations. The University Transportation Center funded me during researching and I am humbled and appreciative by the fact that I was voted student of the year. I want to thank Dr. Mbaki Onyango for her postdoctoral work in calcium lignosulfonate as a soil stabilizer which was the initial starting point for the entire research project.

Finally, I must thank my loving family for their constant support throughout this process. School could be an extremely difficult process and I could not have done this without my parents, Wilson and Valerie Smith. I am grateful to my sister, Jocelyn, for giving practical advice in challenging situations which has been indispensible to me. I want to acknowledge my friends particularly my colleagues, Paul Bartley and Hakan Yasarer, for being helpful during laboratory challenges and for being a pleasure to work with.

Chapter 1 - Literature Review

1.1 Introduction

Lignin is an amorphous polymer found within the cell walls of plants. Lignin products are available as sodium or calcium salts and have been utilized in industry for their deflocculating properties. For example, lignin is added to concrete as a superplasticizer to reduce the water demand of concrete mixes. Lignin products have also been used in the food industry as an emulsifier for animal feed. The specific role of calcium lignosulfonate in food production has been as a carrier for carotenoids and fat-soluble vitamins [Cecilia et al, 2008]. Only recently have the investigations of lignin as a soil stabilizer been undertaken for a few different types of soils. The ability of lignin to bond soil particles together has potential to significantly reduce damage to unpaved roads which is caused by traffic and wind erosion.

1.2 Lignin in Plant Structure

Lignin is bound in the cellular structure of plants with the polysaccharides cellulose and hemicelluloses in a heterogeneous complex known as lignocellulosic biomass which is typically 55 to 75% percent carbohydrate [Mosier et al., 2004]. The presence of lignin in the cell wall protects the plant from disease and pests and creates a hydrophobic surface for the transportation of water and nutrients throughout the plant structure [Novaes et al, 2010]. However, it impedes the separation of the polysaccharides which is necessary for the production of biofuels. Lignin can be grouped into two main subunits: coniferyl alcohol monomers, which is characteristic of lignin found in softwood trees and the monomer sinapyl which creates syringyl and is found in hardwoods. Wood is composed on average of 25% lignin, 45% cellulose and 25% hemicelluloses [Novaes et al, 2010]. Fig. 1-1 illustrates the tissue that conducts water known as xylem.

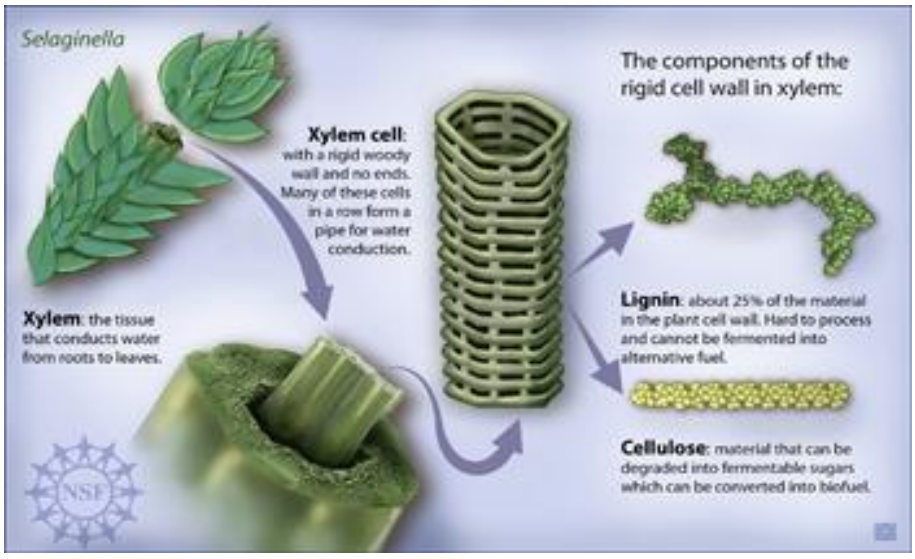

Figure 1-1: Illustration of lignin and cellulose's presence in plant cell structures [Deretsky et al, 2003].

1.3 Processing of Lignin Products

The pretreatment process of biofuel is often viewed as one of the most expensive stages of production costing as high as 30 cents per gallon of ethanol produced [Mosier et al, 2004]. In order for ethanol to be produced the components of lignocellulosic material, cellulose, hemicelluloses and lignin, must be broken apart through pretreatment. Effective pretreatment for biofuel includes breaking the lignin seal and disrupting the crystalline structure of the cellulose in a cost effective manner [Fig. 1-2]. There are several methods of pretreatment ranging from uncatalyzed steam explosion to lime pretreatment. Cellulose is broken down into sugars through enzymatic hydrolysis before being fermented into ethanol [Mosier et al., 2004]. Ethanol is then distilled out of the fermentation broth and the remaining residue consists of lignin and the unreacted polysaccharides.

Separating lignin in wood is a different process since lignocellulosic biomass in wood does work directly through enzymatic hydrolysis [Hu, 2008]. Ball milling is necessary to breakdown the lignin structure after which is mixed with dioxane to produce milled wood lignin (MWL). Another method of processing lignin includes soaking wood chips in acidic calcium bisulfite for 6 to 10 hour cook cycles at 130°. The bisulfite ions react with the lignin polymer to create sulfonated lignin or lignosulfonate and it is this reaction that increases the water solubility of lignin. In the production of calcium lignosulfonate, the calcium ions work to stabilize the

anionic sulfonate. The sulfite content of the lignosulfonate is reduced by evaporating water and impurities are removed through ultrafiltration [Cecilia et al., 2008].

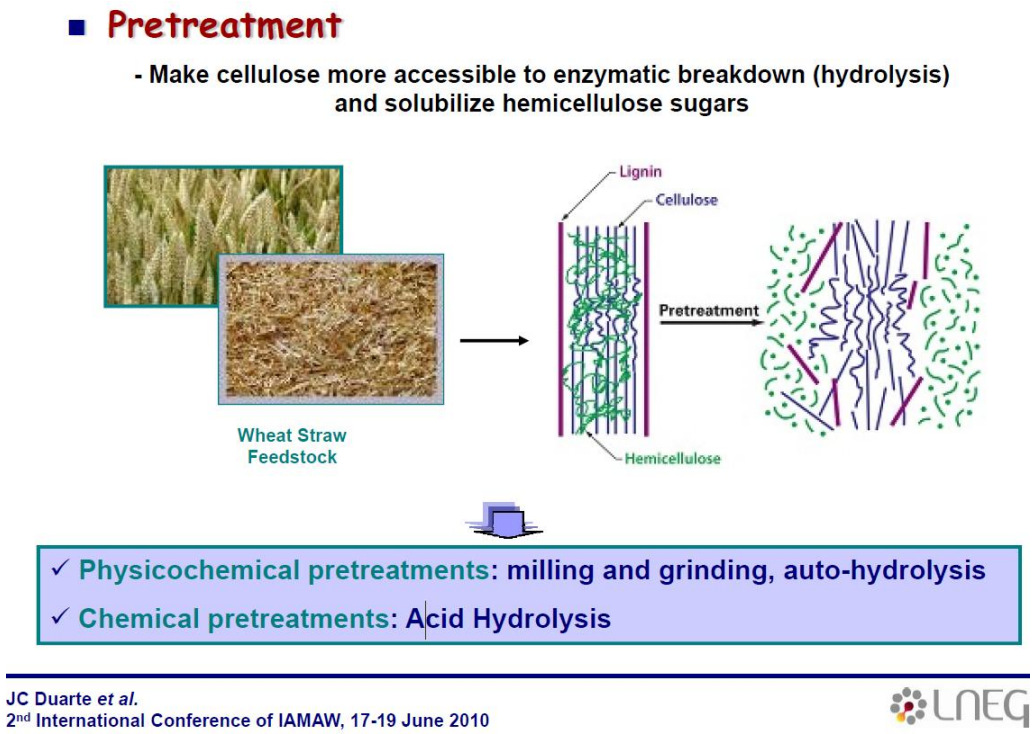

Figure 1-2: Process of breaking down lignocellulosic material [Mosier et al, 2004].

1.4 Previous Work in Lignin Soil Stabilization

1.4.1 Department of Army Headquarters

To determine the effectiveness of the off-the-shelf stabilizers compared to traditional stabilizers, the Department of Army Headquarters conducted research on the effect of different additive quantities on the strength and moisture susceptibility of silty sands. Unconfined compressions testing (UCS) was performed on the soil specimens to determine their strength. For each product six specimens were molded.

The soil used was composed of 34% gravel, 46% sand, and 20% particles passing the No. 200 sieve and classified as silty sand (SM). Compaction curves were generated for soil samples with a 102 millimeter diameter and 152 millimeter height in a Pine Gyratory Compaction machine. Modified Proctor Compaction ASTM 1557 was approximated by a ram pressure of 87 kPa, gyration angle of 1.25°, and 90 revolutions.

The preparation process included blending different soil particle sizes and drying it to a free water moisture content of 2-3%. The lignosulfonate was purchased in powder form and added to the soil in a 30% lignin to water solution. The soil-lignin mix was molded into cylinders of 102 mm diameter to 245 mm height. The soil was placed in the mold in five layers and compacted with a rubber mallet to level off loose particles. A polypropylene membrane was placed on the ends of each soil sample to prevent adhesion to the molding plates. Each specimen was then placed in the Pine Gyratory Compacting machine for one hour to achieve compaction in accordance with ASTM D1557 [Santoni et al, 2001]. After compaction the samples were put in a controlled environment at a constant 22.2°C and 40% relative humidity. The curing method represents field conditions during military construction operations and was the preferred method of the suppliers of the nontraditional additives [Santoni et al, 2001]. The dry soil specimens were those, which were taken out of the controlled environment and tested under unconfined compression immediately. The wet specimens were defined as those which were taken out of the controlled environment and placed on their side in 25.4 mm of water for 15 minutes and then allowed to drain for five minutes prior to testing under unconfined compression. The process showed susceptibility to moisture and strength loss.

Unconfined compression testing was done on an Instron 4208 system. Each sample was subjected to a 4.41 N seating load to ensure proper positioning of the compression piston. Loading was applied at a constant rate of 0.042 mm/s and compressed until the specimen collapsed or until it reached a preset axial strain of 8%. In the end the Lignosulfonate 1 product showed minimal degradation in the wet condition whereas Lignosulfonate 2 began to deteriorate immediately under wet curing and demonstrated no gain in strength. Lignosulfonate 1 did not provide a strength improvement over the control but it did demonstrate potential as a dust control product due to its ability to prevent a loss of fines in the wet samples. It should be noted that the control sample was partially saturated thus deriving its strength from the presence of water. It is because dry soil samples have no uniaxial strength in the absence of confining pressure that they could not be tested in UCS. However, adding lignin and water means the samples could be tested, thus demonstrating that the samples stabilized with lignin have more strength than dry samples.

1.4.2 Buenos Aires Wildlife Refuge

The Central Federal Lands Highway Division (CFLHD) of the Federal Highway Administration conducted two different field studies assessing the stabilization potentials of nonconventional soil additives including lignosulfonates [Surdahl et al, 2005][Woll et al, 2005]. The United States has nearly four million miles of roads and 37% of them are unpaved, and out of that total 613,365 miles of federal roads 86% are unpaved [Surdahl et al, 2005]. Their objective was to rank several products according to the effects on the performance of unpaved roads more specifically they evaluated improvement in bearing capacity and, dust control based on field testing.

In the Buenos Aires National Wildlife Refuge located in south central Arizona, two different lignin products were used: magnesium lignosulfonate and lignosulfonate. According to both AASHTO and ASTM classification methods, soils at the site were classified as A-1-b, SW-SM, and SP-SM [(Fig. 1-3 and Fig. 1-4)]. The stabilizers were applied in windrows, which is blade mixing and compaction with a 12 ton 9-wheel pneumatic roller to the desired depth of six inches [Surdahl et al, 2005]. The process of windrowing involved blading off six inches of soil and pushing it to the side of the roadway. Product was applied to the bladed surface with a water truck. Three inches of the cut soil were placed back on top of the applied surface and also sprayed and rolled again. This was repeated with the remaining three inches of soil. The top of the soil was sprayed and rolled for compaction to complete the application procedure.

Each product was monitored at six month intervals for 24 months to observe its performance over an extended period of time. Monitoring included the visual inspection of dust generation. A two vehicle caravan was used and driven at speeds between 25 to 30 mph. The second car observed the dust generated by the first. Other observations included binding or loss of material, crusting and fragmenting of soil, and impacts to roadside vegetation. An eleven point rating system was designed to measure road quality over time. At each monitoring event a road was arbitrarily chosen as the benchmark to behave as a control for comparison to the other test roads. The benchmark was assigned a rating of five. The vehicle observers independently gave other roads a score above or below five to compare with the benchmark. To prevent bias, a new benchmark was chosen at each monitoring event.

Figure 1-3: Machinery blending soil with stabilizer product in Buenos Aires NWR [Surdahl et al, 2005].

Figure 1-4: Dust Abatement assessment in process in Buenos Aires NWR [Surdahl et al, 2005].

The results indicated that magnesium lignosulfonate's average rating over the 24 months period was consistently above 7.0 for resistance against dust abatement, washboarding, and raveling while its rutting average was 6.1. Lignosulfonate's rating for the same categories were not as high yet still remained above the set benchmark with scores of 6.0, 5.8, 5.8, and 5.4 for dust abatement, washboarding, raveling, and rutting respectively [Surdahl et al 2005]. The cumulative visual inspection rating for both lignosulfonate and magnesium lignosulfonate were 6.5 and 5.6 respectively [Surdahl et al, 2005] thus ranking them second and third out of the six products evaluated.

Objective field testing included nuclear density tests, dynamic cone penetrometer (DCP) readings, soil stiffness and soil modulus testing. Nuclear density gauges were used to measure the compaction level of each product in the field. Readings were taken only during the six month monitoring event because there was no visual evidence of a soft, unsuitable subgrade [Surdahl et al, 2005]. The nuclear gauge measurements were taken in two modes: measuring from a four inch depth and by the backscatter method. The data collected from the nuclear gauge showed compaction levels for magnesium lignosulfonate to be 104% and 96% compaction from the four inch depth and backscatter methods while for lignosulfonate, compaction reached 94% and 69% compaction respectively [Surdahl et al, 2005]. DCP findings were converted into California Bearing Ratio values for analysis and those results state that magnesium lignosulfonate and lignsulfonate had the second and third best performing products with values of 86 and 72 respectively. The silt loading results correspond exactly with subjective dust abatement results with the product called caliber being the best product, magnesium lignosulfonate as second, and lignosulfonate being in the second tier group [Surdahl et al, 2005].

1.4.3 Seedskadee National Wildlife Refuge

Seedskadee National Wildlife Refuge (NWR) is located in southwestern Wyoming and was established in 1965 to provide a wildlife habitat to offset the loss of land caused by reservoir construction [Woll et al, 2008]. The product testing in soil at the Seedskadee NWR occurred subsequent to the Buenos Aires National Wildlife Refuge project and was again undertaken by the Central Federal Lands Highway Division (CFLHD). The objective of the study conducted in Seedskadee was to compare the data on performance of different products' results gathered at

Buenos Aires because of the differences in soil and climatic conditions. The same six products studied in Buenos Aires were also used in Seedskadee except the methods of application were different. At Seedskadee a CMI 650 pulverizer milled the soil to a depth of five inches while a 4,500 gallon distributor truck applied the different products [(Fig. 1-5)]. The CMI pulverizer was again used to grade, process and compact the product treated soil.

Figure 1-5: CMI Pulverizer used to compact and grade soil in Seedskadee NWR [Woll et al, 2008].

The test soil was classified according to AASHTO M 145 as well-graded fine stone fragments, gravel and sand [Woll et al, 2008]. Laboratory tests were conducted on it before and after product treatment to determine its plasticity index, maximum dry density and California Bearing Ratio. Subjective inspections were carried out over two years on four monitoring events. The products were installed in September of 2004 and revisited after 8, 11, 20, and 23 months [Woll et al, 2008]. The events had to be staggered unevenly in order to avoid adverse weather conditions during the unpredictable winter months.

Figure 1-6: Washboarding on unpaved roads in Seedskadee NWR [Woll et al, 2008].

Subjective observations and physical on-site testing were conducted on product performance to assess dust abatement, washboarding (Fig. 1-6), potholing, raveling, and rutting. Visual observers went to the different sites and analyzed the quality of the product-treated roads based on visible suspension of dust caused by vehicle traffic and the resistance of the roads to deterioration. Lignosulfonate stabilized soil performed the best out of the six products tested over the 24 month test period with an overall average of score of 62 based on the average scores of the previously stated assessment criteria. Magnesium lignosulfonate came in second with a score of 60. It was noted that the road surface appeared to have hardened from the 8 month monitoring event to the 11 month [Woll et al., 2008] in the lignosulfonate treated soil. In-situ testing included silt load testing which assessed gradation and dynamic cone penetration (DCP) readings, which were converted to CBR values in order to measure the load bearing capacity of the soil. Over the four monitoring events, lignosulfonate had the highest normalized CBR value of all products at 57, significantly higher than magnesium lignosulfonate which was at 35. With respect to silt loading results, magnesium lignosulfonate and lignosulfonate tied for the highest value with both having normalized ranks of 90. Lignosulfonate's high rankings were attributed

to the fact that it had a plasticity index (PI) of six in the soil whereas other products were nonplastic (NP) [Woll et al, 2008]. No maintenance operations were conducted for 24 months after products application. This time period coincides with duration of the field testing.

1.4.4 Dust Control Performance on Unsurfaced Roadways and Tank Trails

Dust generation has been an ongoing challenge for the military bases at Fort Hood, Texas and Fort Sill, Oklahoma [Gebhart et al., 1996]. Suspended dust is generated by the constant military vehicle traffic and helicopter landing pads. Dust poses a threat to the air quality of the surrounding area endangering both the public and military personnel because it minimizes visibility and is a respiratory irritant [Gebhart et al., 1996]. Dust also damages military equipment by clogging air filters, turbine parts and machine engines. Excessive dust has negative environmental effects when vegetation is coated in it, increasing the leaf temperatures. This hinders a plant's ability to perform photosynthesis and it becomes more prone to disease [Gebhart et al., 1996]. Less roadside vegetation also makes unpaved roads more vulnerable to erosion without strong root networks to hold soil in place.

At Forts Hood and Sill, six 0.3 mile long sections were graded prior to product application to remove unwanted debris from the road surfaces. Then magnetic traffic counters were installed into the roads to measure traffic volume. Calcium lignosulfonate was on the surface applied by tanker trucks at a rate of 0.5 gallons per square yard. Dust control effectiveness was measured by placing oil-coated dust pans on both sides of the roadway to be collected after 24 and 72 hours. After those time periods, the pans were weighed to measure how much dust was generated by vehicle traffic. Video imaging was taken by cameras set up three feet above the road to measure dust suspension caused by controlled traffic traveling at 30 miles per hour [Gebhart et al., 1996].

Data were taken 30, 60, and 100 days subsequent to initial product application. At Fort Hood, lignin reduced dust by 62% in the first 30 days and by 7% during the first 60 days [Gebhart et al., 1996] in comparison to the control. It was around the 60 day point that the signs of potholing and deterioration began to show in the lignin treated road section. At Fort Sill, lignin was found to increase road resistance against dust erosion by 69% during the first 30 days and by 45% over 60 days. Signs of potholing and washboarding were minimal throughout the

100 days of experimentation. Lignin was the cheapest product to apply at Forts Hood and Sill costing $0.28 and $0.30 per square yard, respectively [Gebhart et al., 1996].

1.4.5 A Field Study of LSSM Extracted from Spent Liquor of Straw Pulping in Paper Mills

In recent years, China has been experiencing more severe effects of desertification in areas that were once arable land. The process of land changing into desert is becoming a growing drag on the Chinese economy and a mounting concern for its government. Furthermore pulpwood is scarce in China which is why the country relies heavily on straw pulp as a raw material for paper production [Wang et al, 2005]. Waste produced by the straw pulp mills is often expelled straight in to nearby water ways. Public and government pressure has forced these mills to properly mitigate their pollution however many do not have the funding necessary to solve the contamination problems which may cause many to close, putting people out of work [Wang et al, 2005].

Testing was conducted with the spent liquor generated by the straw pulp mills to study how effective the waste can be at stabilizing sand dunes that are constantly shifting in China's Northwest Ningxia Hui Autonomous Region. The lignin sand stabilization material (LSSM) is extracted from the spent liquor through a chemical process involving evaporation and condensation of the waste liquor which is then spray dried. Field testing consisted of seeding sand dunes with arenaceous plants and then spraying the dunes with different concentrations of LSSM [Wang et al, 2005]. The purpose of the plants was to add further stability to the sand because the seedlings take root, they offer more reinforcement of the soil against wind erosion. Furthermore LSSM is more than 10% nitrogen which is enough soil nutrition for plant to grow [Wang et al, 2005]. The experimental design objective was to determine what concentration of LSSM would provide the best stabilization benefit along with the high rate of plant germination. Plots of land were sorted into two groups: Group I was for soil sprayed with a quantity of 2.5 l/m^2 and Group II had a quantity of 5 l/m^2. In each group three different concentrations of LSSM were tested: 4%, 2% and 1%. Soil and plant seeds sprayed with plain water were also used as a control.

The results of the experiment indicate that a quantity of 2.5 l/m^2 and a concentration of 2% LSSM give the optimum benefit to soil stabilization and plant growth on the sand dunes. Soil

with the concentration of 4% LSSM work the best at creating a hardened shell on the sand dune but plants sprouts had a more difficult time breaking through it whereas the 1% concentrations suffered more from erosion [Wang et al, 2005]. These findings demonstrate that utilizing LSSM on the slopes of sands dunes has the potential to control desertification and keep straw pulping mills open.

1.4.6 Iowa State University Research

Iowa State University conducted research on the ability of biofuel co-products (BCP's) to stabilize soils for the purpose of developing sustainable alternatives to fly ash. Two products were tested: a liquid BCP with a higher lignin content (Co-Product A) and a powder form with a lower lignin content (Co-Product B) [Ceylan et al, 2010]. Dry and wet specimens were prepared to determine the treated soil's resistance to moisture susceptibility. The experimental soil was classified as low plasticity clay (CL) or A-6(8) [Ceylan et al, 2010]. The findings show Co-Product A had the higher resistance against moisture susceptibility and larger unconfined compressive strength results. Different combinations of the two BCP products and fly ash were tested as well and displayed strengths comparable to pure fly ash treatments. Curing was also undertaken by Iowa State where they prepared samples and dried them for 1 and 7 days and the results conclude that curing had more effect on soil-treated with Co-Product A than on Co-Product B [Ceylan et al, 2010].

1.4.7 Environmental Impact of Lignin

The toxicity of lignosulfonate in soil is negligible making it one of the safest chemicals to use for road stabilization. This is due to the fact that impurities such as acetic acid are evaporated away during the manufacturing process [Adams, 1988]. During the purification process of the lignin it was noted that sulfur dioxide (SO_2) was one of the compounds being released resulting in the Environmental Protection Agency conducting tests on dioxins found in paper mill effluents. A seven day composite study was performed on calcium lignosulfonate which resulted in no detectable amounts of the hazardous compounds 2,3,7,8- tetrachloro dibenzofuran or 2,3,7,8- tetrachloro-p-dioxin which are derived from the process of bleaching lignosulfonates [Adams, 1988].

Since lignin is a material applied to soils for stabilization of unpaved roads there is a concern regarding its toxicity towards the surrounding vegetation especially since it would be

applied in such high quantities. To treat a one mile stretch of roadway with lignosulfonate at a depth of six inches requires 2.5 tons to control dust generation [Adams, 1988]. The impact on trees was conducted by spraying a 50% calcium lignosulfonate solution on the ground in a Douglas fir tree plantation in Washington State at three application rates: 21, 42, and 63 tons of solids per acre. These rates were significantly above the typical road application rates which range between 1.3 and 5 tons per acre. Observations of vegetation health were made over a 12 week period after application and the results concluded that woody vegetation was not affected. The application of lignin to unpaved roads raised concerns about contamination of groundwater because of excessive amounts of material permeating through the soil and not having enough time to ferment before it reaches the water table. A study of one time applications of applying 20 to 60 tons per acre of material to soil displayed the lignin's movement and rate of fermentation is not a threat to groundwater meaning standard application rates of 1.3 to 5 tons per acre do not pose a threat [Adams, 1988].

Care has been taken to make sure that lignin is not discarded into waterways containing aquatic life. The wood sugars contained in lignosulfonates are a source of food to microbes which consume dissolved oxygen in the process [Adams, 1988]. The Biochemical Oxygen Demand (BOD_5) of lignosulfonate is 0.23 pounds per pound of solids [Adams, 1988]. Testing was influenced by analysis of laundry detergent because the surfactants present in detergent biodegrades slowly and produces chemical foam when introduced into waterways. Small doses of Norlig A powder were mixed with water from the Wisconsin River and placed for 33 days at room temperature where organic matter content was measured periodically. The results found that 28% of the powder degraded after five days and 43% degraded after 33 days [Adams, 1988]. The percentages corresponded to the carbohydrate content of the product. After 33 days, the remaining 54% was pure lignin.

Chapter 2 - Material Description and Methodology

2.1 Sand Description

The soil used in the research is identified as masonry sand and was donated by Midwest Concrete Materials from their quarry on South Manhattan Avenue in Manhattan, Kansas. Its composition is 90% quartz with 5% to 7% consisting of potassium feldspar common of sands from glacial till [Clark, 2011]. The remaining 1-2% is composed of various opaque material including hematite, magnetite, and ilmenite. A small fraction of the sand is fossil material, a single celled animal called foraminiferans [Clark, 2011]. The sand is typical for the north central United States where glacial ice sheets picked up different rock types and ground them down over time.

The particle size of the sand was determined by sieve analysis according to ASTM D422. Three sieve analyses were performed and results were averaged to give a more representative particle size distribution for the sand. This is clean uniformly graded sand, which is classified as poorly graded sand (SP) according to Unified Soil Classification System. The grain size distribution of the sand is depicted in Fig. 2-1 along with the effective grain size, mean grain size, and coefficients of uniformity and curvature.

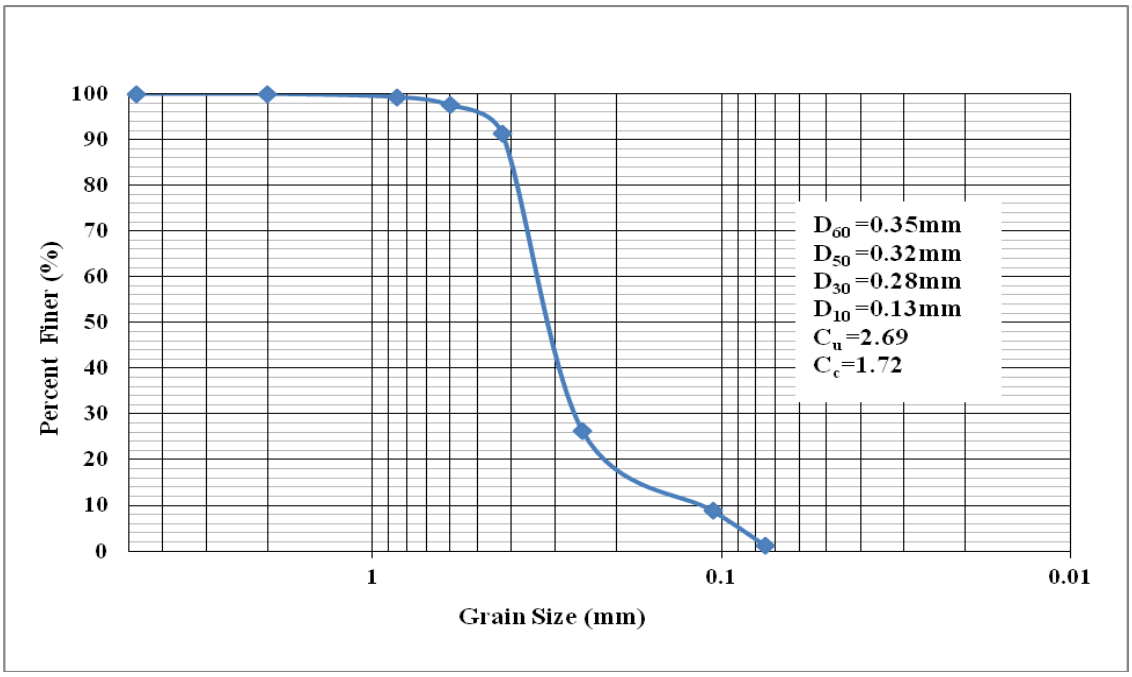

Figure 2-1: Average Grain Size Distribution of the masonry sand.

2.2 Lignosulfonate Description

The lignin product used in this study is a calcium lignosulfonate (CaL) brand called Norlig A powder donated by Borregaard Lignotech USA. Its water content at room temperature is between 3%-8% with a pH and bulk density range of 3.0-4.5 and 0.37-0.56 g/ml respectively. CaL contains a total sulfur content of 5.8% and also has an HPLC sugar content of 17.9%. A macroscopic view of the CaL is shown in Fig. 2-2, while microscopic views are shown in Figs. 2-3 and 2-4.

Figure 2-2: Calcium lignosulfonate in brown powder form.

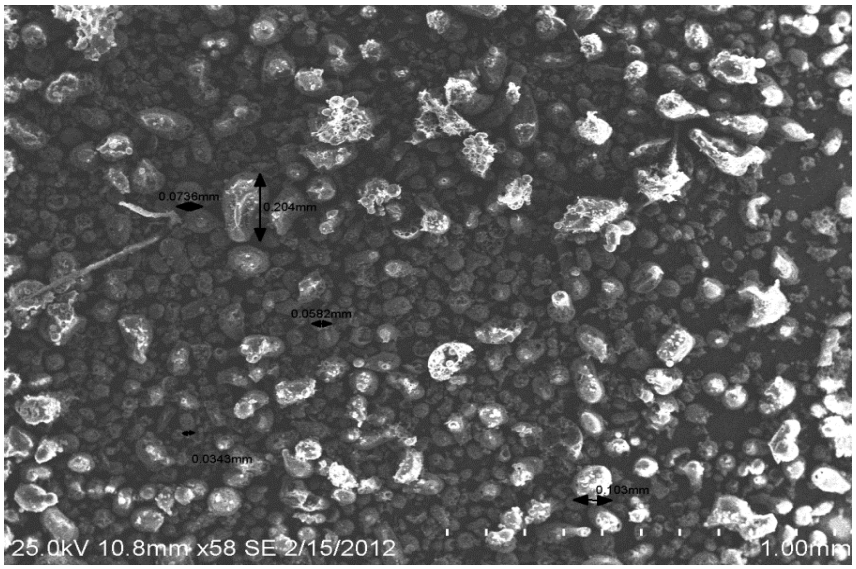

Figure 2-3: Scan Election Microscope view of powdered calcium lignosulfonate in 1 mm scale.

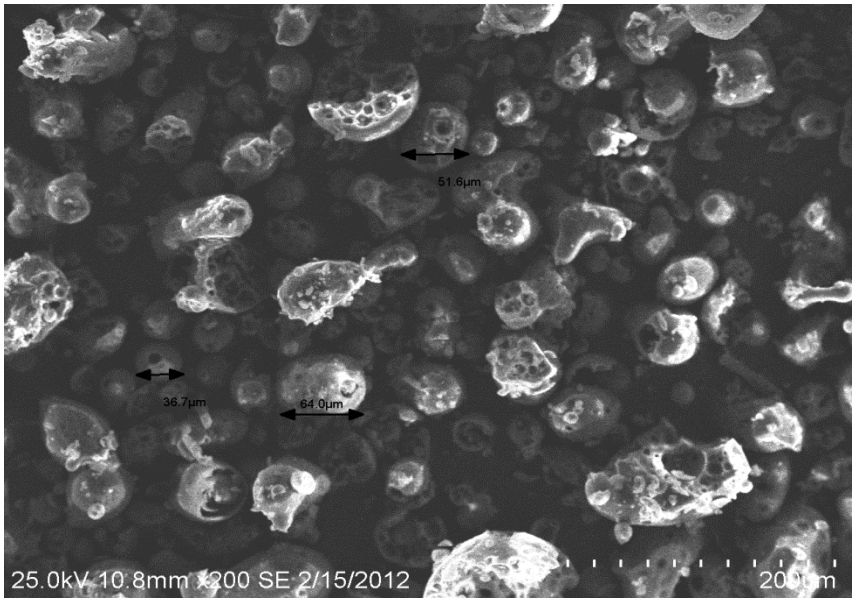

Figure 2-4: Scan Electron Microscope view of calcium lignosulfonate in 200 µm scale.

2.3 Phase Relationships for S-CaL-W mixes

The basic soil mechanics phase relationships were used to interpret changes in volume and moisture. New expressions that reflected the presence of CaL were defined and derived. They are

presented below along with pertinent standard expressions. Fig. 2-5 depicts the corresponding phase diagram.

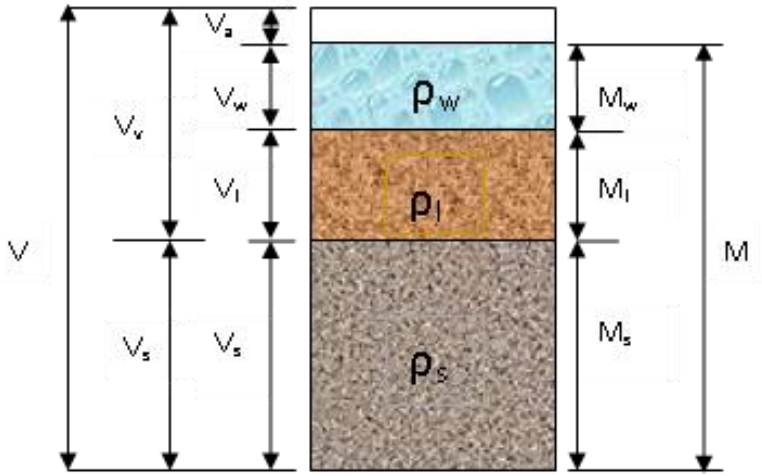

Figure 2-5: Phase relationship of S-CaL-W.

2.3.1 Volume Relationships

2.3.1.1 Void Ratio, e

$$e = \frac{V_v}{V_s} \tag{1}$$

2.3.1.2 Porosity, n

$$n = \frac{V_v}{V} \rightarrow n = \frac{e}{1+e} \quad \text{and} \quad e = \frac{n}{1-n} \tag{2}$$

2.3.1.3 Degree of Water Saturation, S_w

$$S_w = \frac{V_w}{V_v} \tag{3}$$

2.3.1.4 Degree of Lignin Saturation, S_l

$$S_l = \frac{V_l}{V_v} \tag{4}$$

2.3.1.5 Degree of Air Saturation, S_a

$$S_a = \frac{V_a}{V_v} \tag{5}$$

and

$$S_w + S_l + S_a = 1 \rightarrow \left(\frac{V_w + V_l + V_a}{V_v} = 1\right) \tag{6}$$

2.3.2 Mass (or Weight) Relationships

2.3.2.1 Gravimetric Water Content, w

$$w = \frac{M_w}{M_s} \tag{7}$$

2.3.2.2 Gravimetric Lignin Content, χ_l

$$\chi_l = \frac{M_l}{M_s} \tag{8}$$

$$w_{w/l} = \frac{M_w}{M_l} \rightarrow w_{w/l} = \frac{w}{\chi_l} \quad \text{or} \quad w = w_{w/l}\chi_l \tag{9}$$

also

$$w_{w/l} = \frac{1}{G_l}\frac{S_w}{S_l}$$

2.3.2.3 Modified Gravimetric Water Content

$$\underline{w} = \frac{M - M_{dry}}{M_{dry}} = \frac{w}{1+\chi_l} \tag{10}$$

2.3.3 Mass/Volume Relationships

2.3.3.1 Mass Density of Lignin Solids, ρ_l

$$\rho_l = \frac{M_l}{V_l} \tag{11}$$

For this study ρ_l is equal to1.6 g/cm^3 = 99.84 lb/ft^3 according to Lignotech USA Inc.

2.3.3.2 Dry Mass Density, ρ_d

$$\rho_d = \frac{M_s}{V} \tag{12}$$

2.3.3.3 Dry Mass Density of Solids and Lignin, $\rho_{d,s\&l}$

$$\rho_{d,s\&l} = \frac{M_s + M_l}{V} \tag{13}$$

$$\rho_{d\,s\&l} = \frac{(G_s + eS_lG_l)\rho_w}{1+e} \tag{14}$$

2.4 Sample Configurations

Sample configurations for air drying and direct shear testing were selected based on early age results of Standard Proctor and direct shear tests reported by Bartley (2011). Specifically, for each gravimetric lignin content five sample configurations denoted by A, B, C, D and E were selected (Fig 2.5).These five test configurations vary in dry density at optimum water content (A, E, C) and in water content at constant dry density (D,E,B) giving a thorough understanding of how the amount of water and compaction level as well as CaL content affect the strength parameters of the soil. The masses of sand, CaL, and water were calculated to conform to the constant volume of the shear box or the constant initial height of samples. The configurations were labeled with a letter as an abbreviation to denote relative compactions of 100%, 95%, 90% (points A, E, and C respectively) as well as the amount of water with respect to optimum moisture content (B,E,D). Sample configurations having gravimetric lignin contents of 4%, 6%, and 9% were selected for this research. These configurations were selected for this research based on the conclusions about the early age strengths, which states that the optimum cementation benefits were achieved for lignin contents between $\chi = 4\%$ and $\chi=9\%$ [Bartley, 2011].

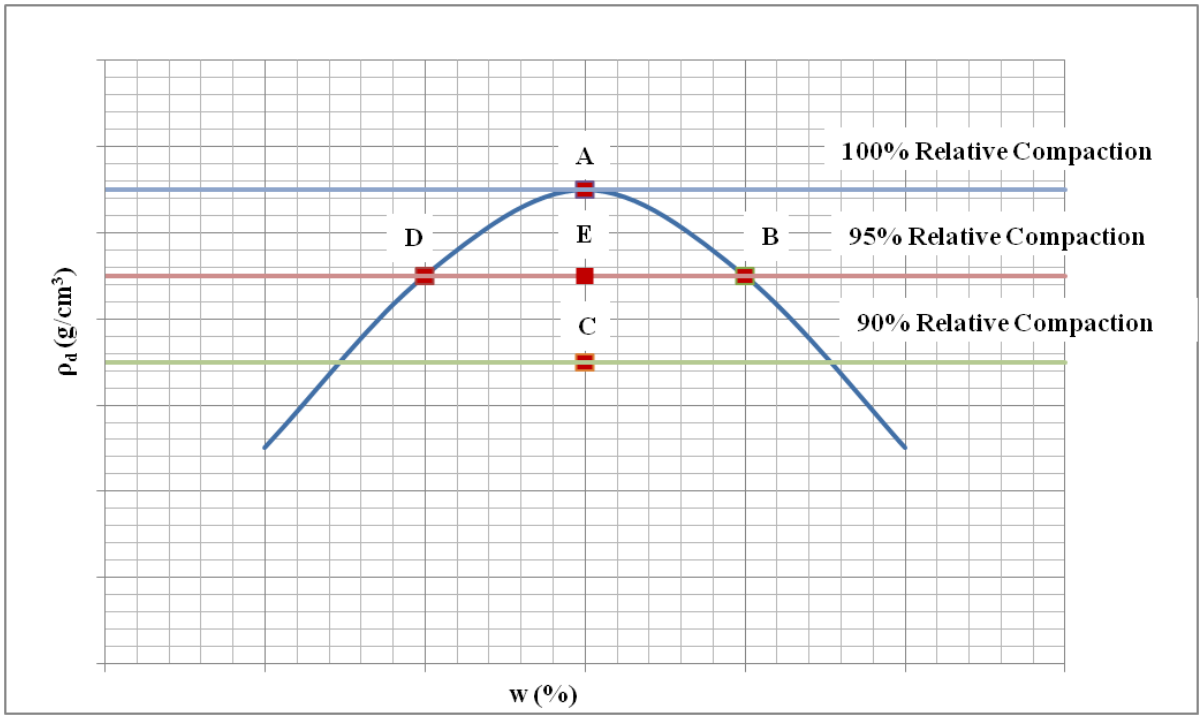

Figure 2-6: A schematic of Standard Proctor Test results depicting selected sample configurations for a given χ_l [Bartley, 2011].

2.5 Standard Proctor Test on Lignin

A Standard Proctor Test was performed on the mix of CaL and water containing no sand to find its compaction curve, thus giving the maximum dry density and the optimum water to CaL ratio. The Standard Proctor Test was performed according to ASTM D698-07. The biggest challenge in the procedure was mixing the water and CaL uniformly. Borregard Lignotech advised mixing 3-5% water by weight of CaL for the first sub-specimen and incrementally adding 3%-5% water for each subsequent sample. A change that occurs in the sub-specimens as water continues to be added was manifested in the change of color from yellow to dark brown (Fig. 2-6 to 2.9). The CaL-water mix was extremely sticky and adheres to the bowls and the mixing utensils. The adhesive properties of the CaL-water mix increased up to the optimum water to CaL ratio before becoming slightly more liquid wet of optimum. Six sub-specimens were ultimately prepared for the compaction tests with CaL to water ratio of about 16% and ending at about 30%. It should also be noted that when water was added to the CaL powder and mixed, heat was generated. The results show CaL reached a maximum density of 0.86g/cm^3 at a CaL to water ratio of 27% (Fig. 2-10).

Figure 2-7: Lignin proctor subspecimen at 5% moisture content.

Figure 2-8: Lignin proctor subspecimen at 15% moisture content.

Figure 2-9: Lignin proctor subspecimen at 20% moisture content.

Figure 2-10: Lignin proctor subspecimen at 25% moisture content.

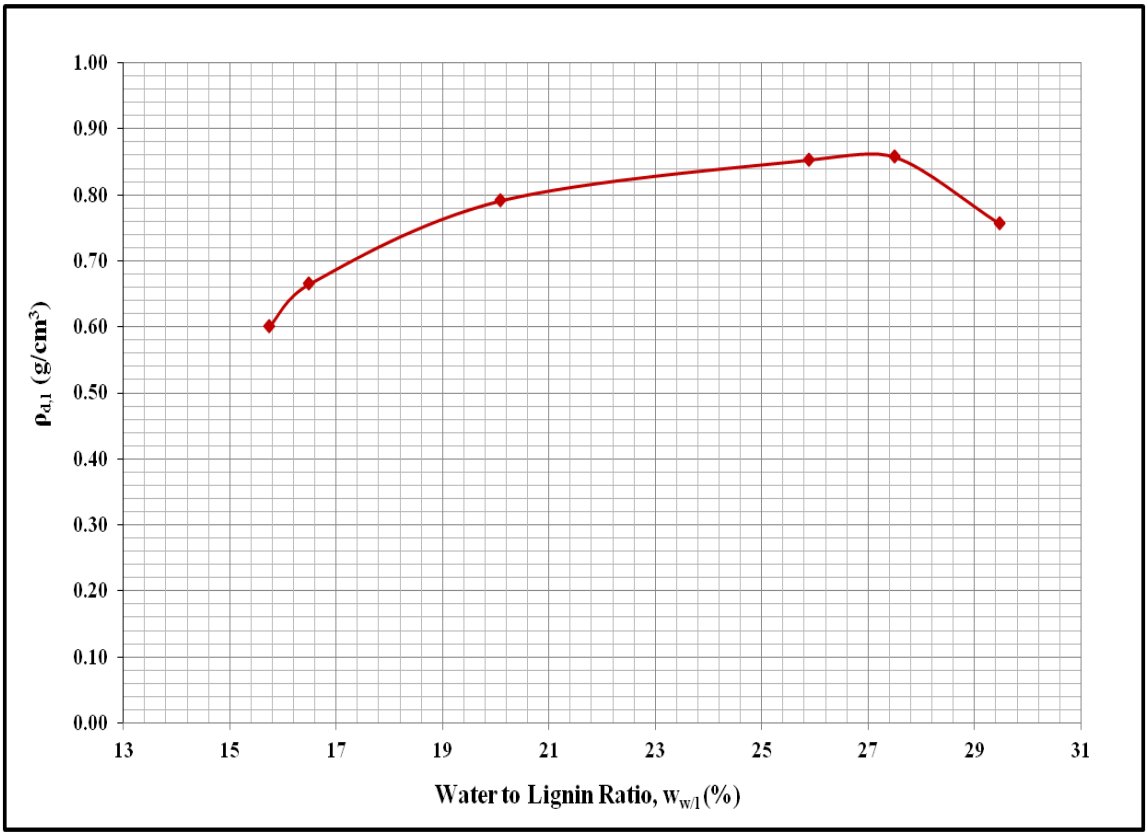

Figure 2-11: Standard Proctor on CaL.

Chapter 3 - Sample Air Drying

Before direct shear testing of the air dried S-CaL-W mixes commenced, time intervals for drying were determined based on measurements taken during the preliminary drying tests. The amount of water in the samples was the most significant determinant as to how long drying would have to take while the compaction level was a secondary factor since the mixes with more air voids take less time to dry than those that are more densely compacted. Preliminary sample drying also revealed that humidity plays a significant role in how much water evaporates out of S-CaL-water mix samples. It became apparent that an environment with a controlled temperature and humidity was necessary.

Initially an incubator was used to dry the samples at a constant temperature and humidity. The incubator contained a sealed chamber, which held a temperature of 71°F and humidity of 27%. A battery powered temperature gauge monitored the incubator's internal environment for more than a week to confirm the consistency of the environment. Samples were then prepared and air dried to measure the change in mass of water versus the elapsed time for each configuration over a period of seven days. Since water was determined to be the only S-CaL-W constituent that changes with time, the samples were weighed at various time increments to deduce the amount of evaporated water.

3.1 Sample Preparation Procedure

Sample preparation before air drying was conducted as follows:

1. Amounts of sand and CaL were measured out in accordance to the results of compaction tests on S-CaL-W and mixed thoroughly for two minutes using a stop watch.
2. Water was measured next and mixed with the CaL and sand for an additional two minutes.
3. After mixing the S-CaL-W mix was placed in the shear box in three lifts with a spoon. Each lift was slighlty compacted with a wooden tamper and its surface scarcified.
4. A porous stone and dry filter paper were placed on the top and bottom of the samples within the shear box to prevent loss of fines.
5. After all the material is placed, the shear box was set on hydraulic sample extruder and was compacted down to its designated height of 24 mm.

6. After compaction, the top half of the shear box was removed. The sample (still connected with bottom half of the box) was gently placed on top of a narrow cylinder whereby the shear box was "settled" downward while the cylinder elevated the sample on the bottom metal plate, thus separating it from the bottom part of the shear box. (Fig. 3-1).
7. The samples were then placed on porous stones, weighed and placed in an incubator to dry. Each sample was turned upside down during the middle of its designated drying period to allow the bottom to dry. Since these lignin-sand samples tended to dry from the outside inward and from the top downward, turning the samples over allowed for more uniform drying.

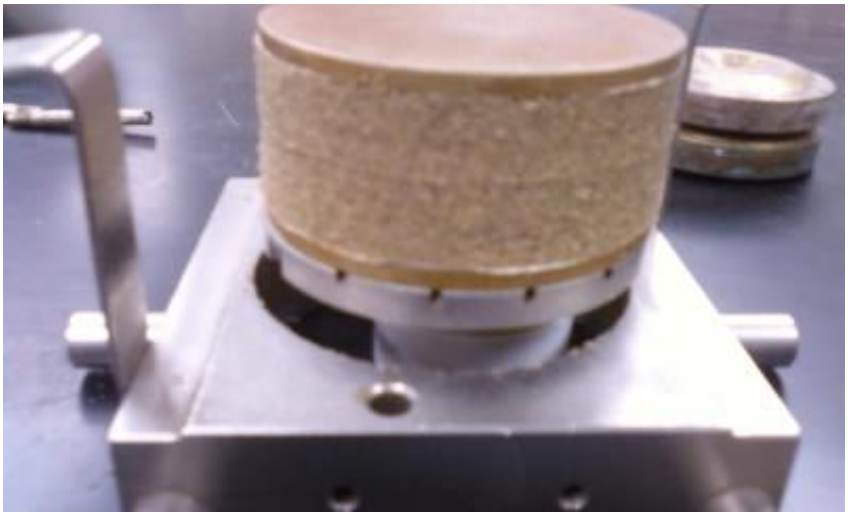

Figure 3-1: Soil Sample extruded from shear box.

It is noted that the samples for direct shear testing were air dried following the above outlined procedure for a predetermined amount of time, which is discussed in the upcoming sections. In addition, the final mass change measurement was performed immediately before mounting the samples inside the direct shear apparatus for strength testing.

3.2 Drying Interval Determination

Samples were prepared (Fig. 3-1) for the purpose of being placed in the incubator for seven days and recording the change in weight at various time intervals. Each sample configuration was weighed after the following time periods in hours: time (t) = 0, 0.25, 0.5, 1, 2, 4, 8, 24, 48 etc. until seven days had passed. The masses of the samples were used to calculate the change in

moisture content versus time which was graphed, thus creating drying curves. They were created for 4%, 6%, and 9% lignin sample configurations. Drying curves are presented in Figs. 3-2 through 3-22.

3.2.1 Drying Curves for χ_l = 4%

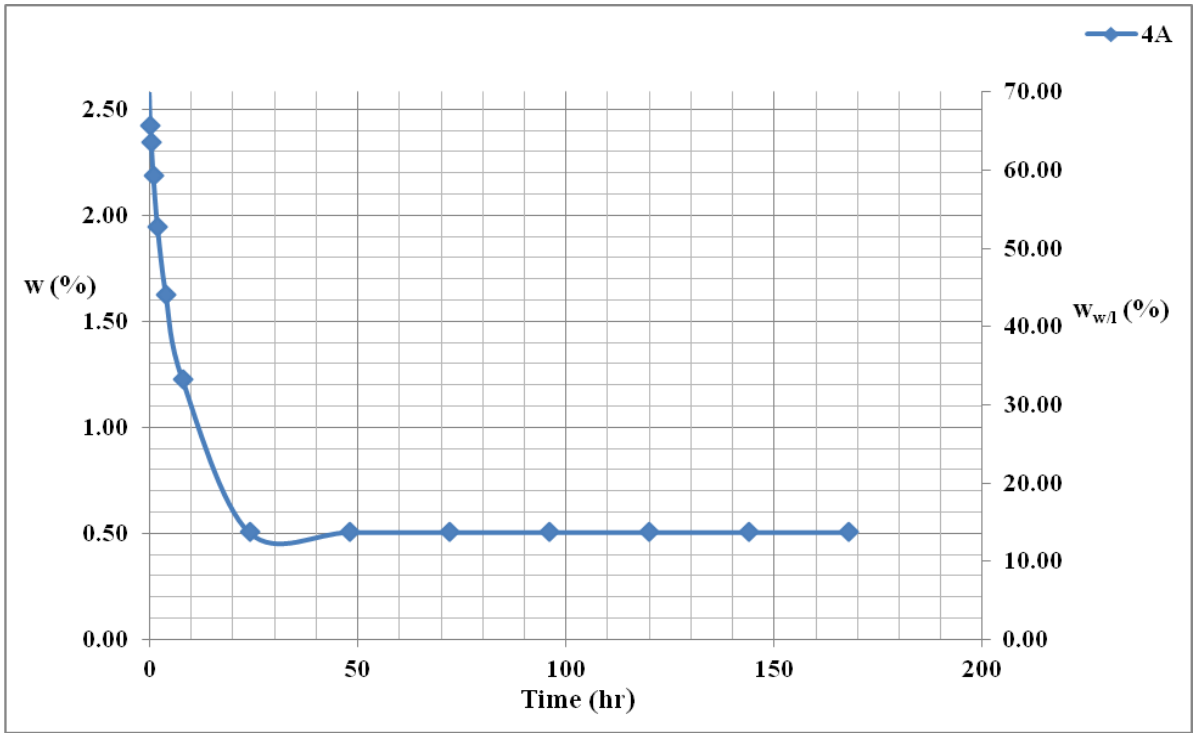

Figure 3-2: Moisture content and water/CaL ratio vs. time. (4A)

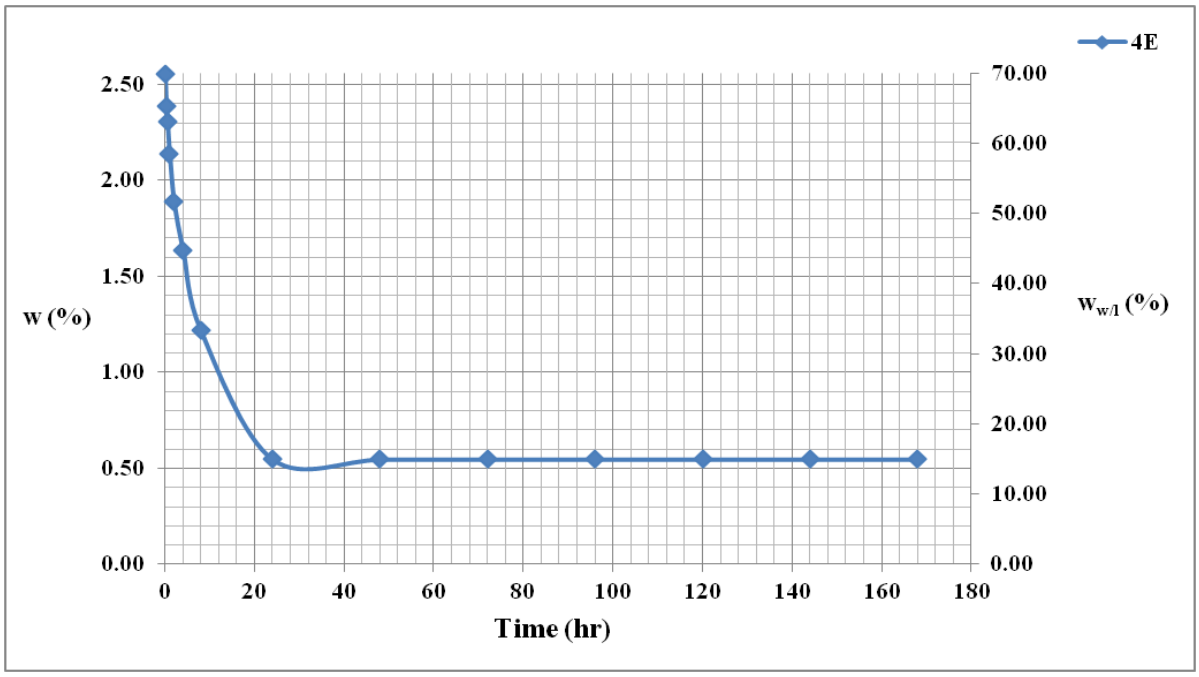

Figure 3-3: Moisture content and water/CaL ratio vs. time. (4E)

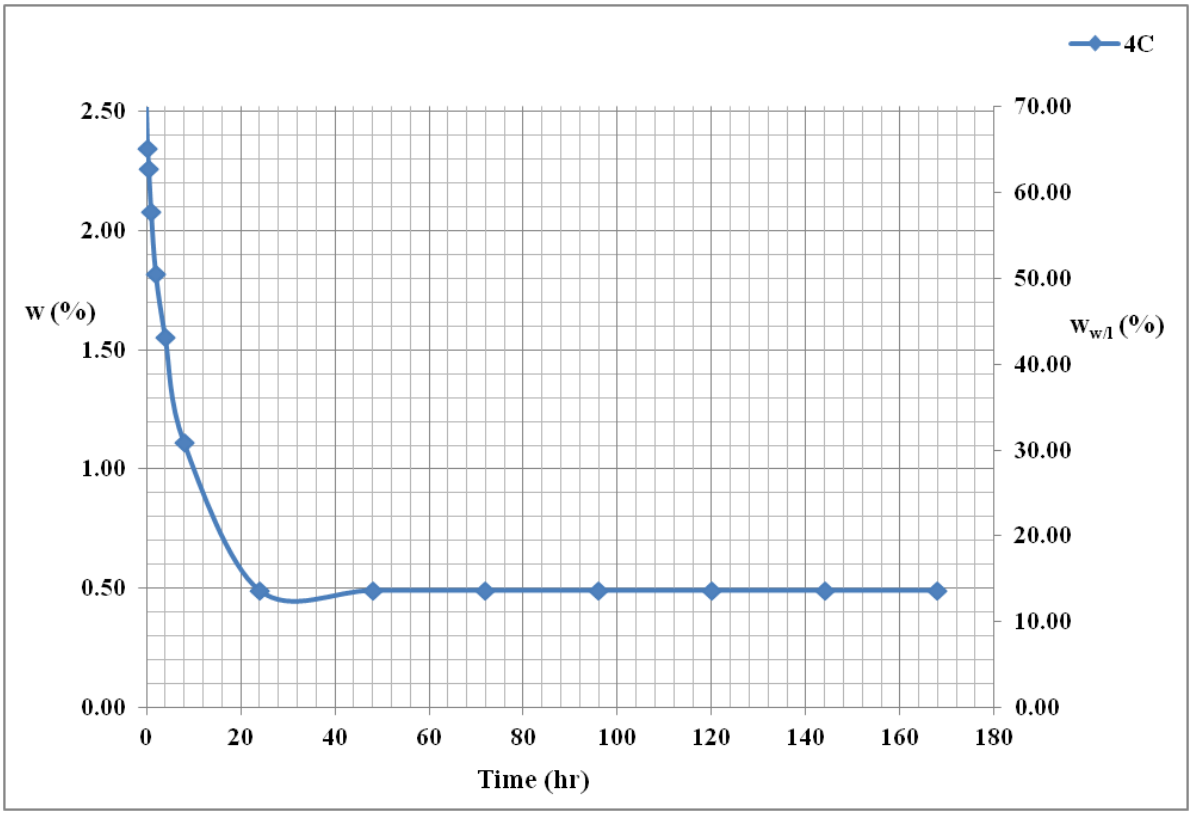

Figure 3-4: Moisture content and water/CaL ratio vs. time. (4C)

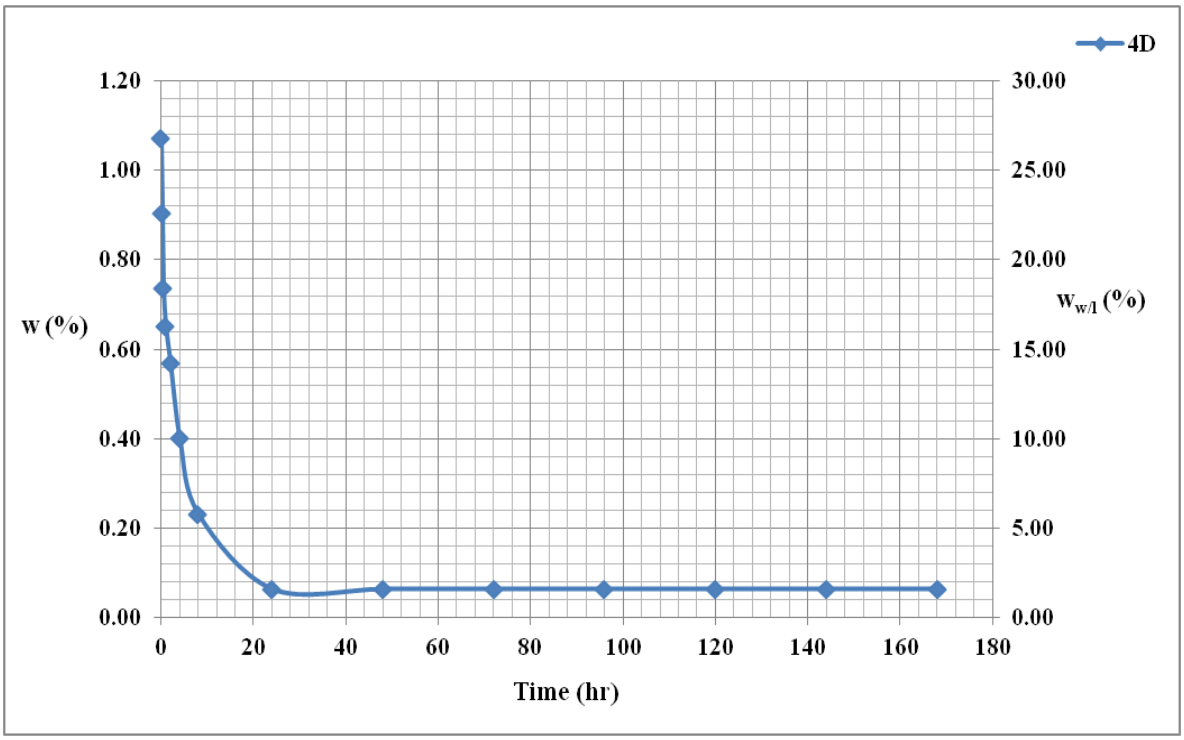

Figure 3-5: Moisture content and water/CaL ratio vs. time. (4D)

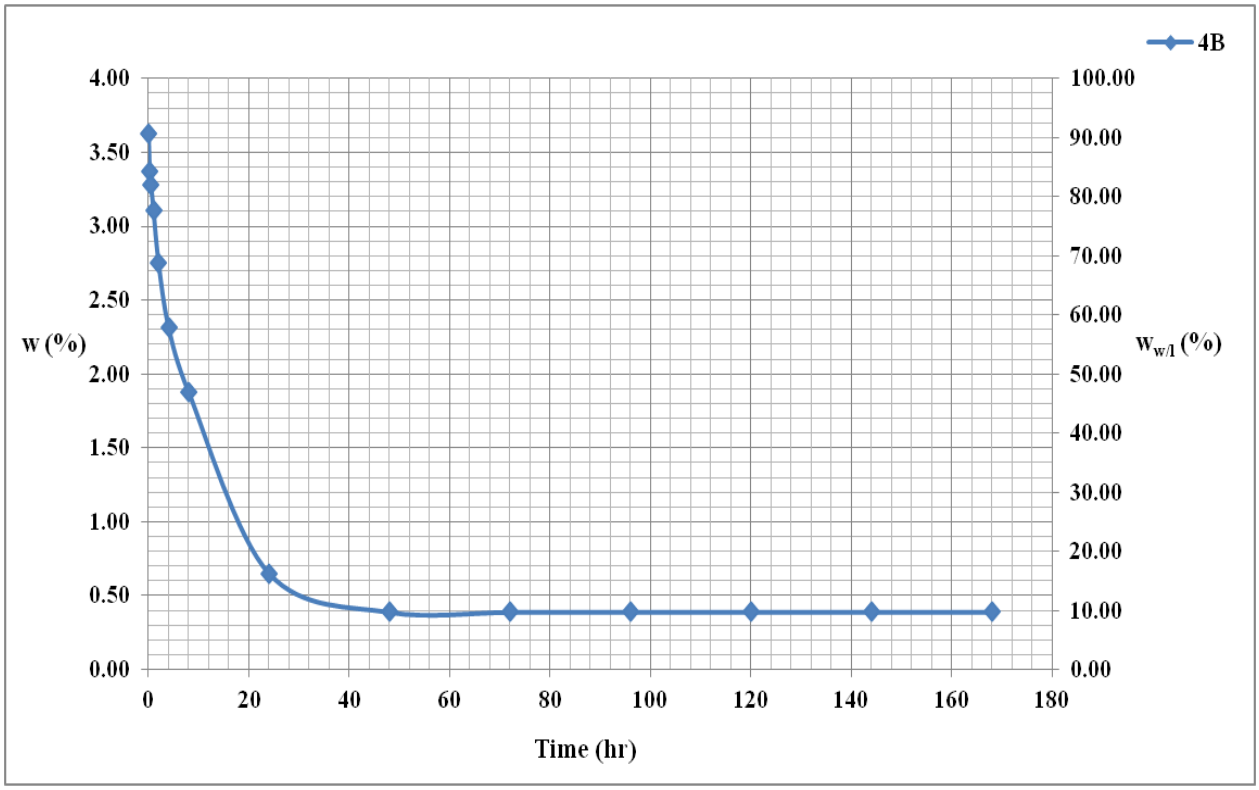

Figure 3-6: Moisture content and water/CaL ratio vs. time. (4B)

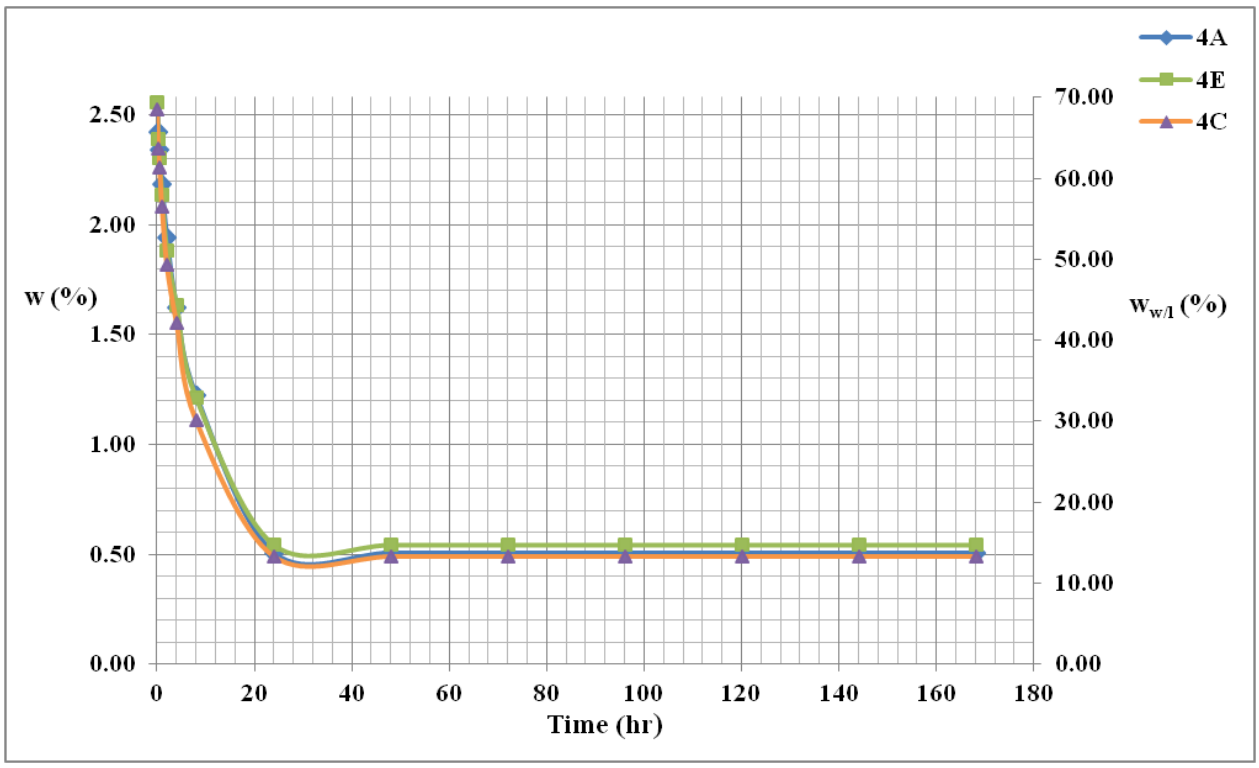

Figure 3-7: Moisture content and water/CaL ratio vs. time. (4A, 4E, 4C)

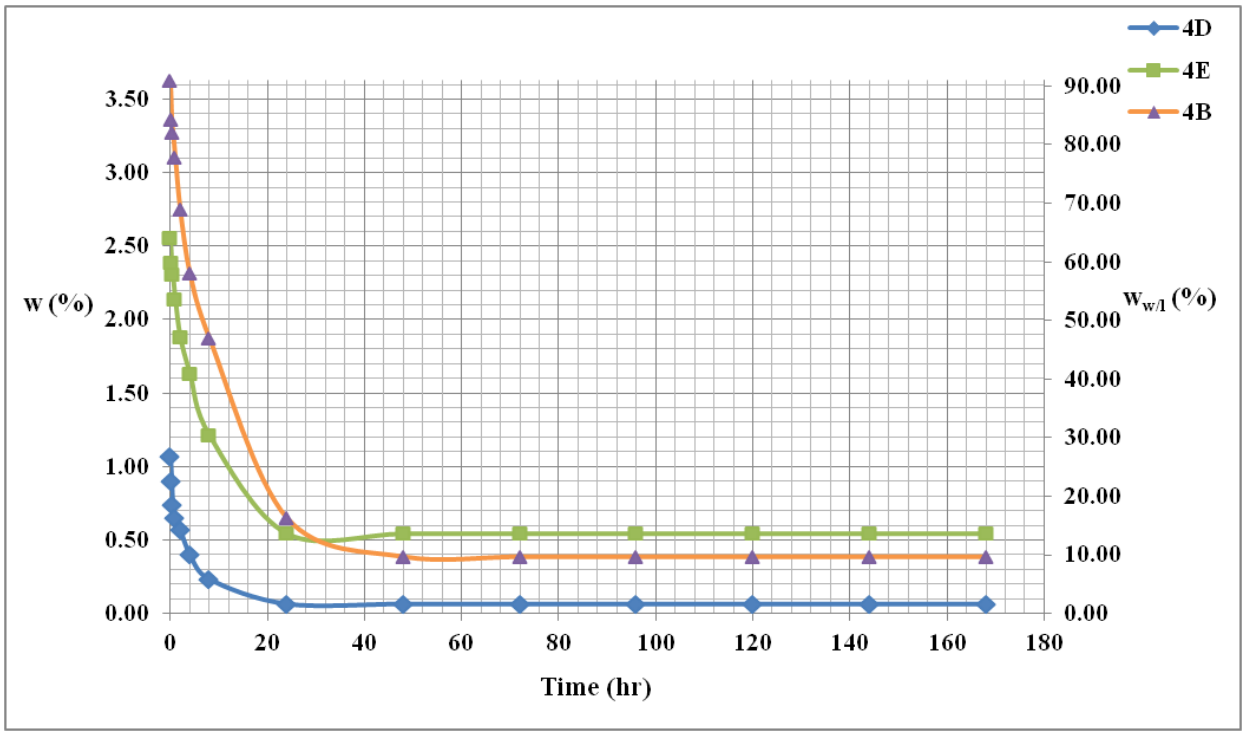

Figure 3-8: Moisture content and water/CaL ratio vs. time. (4D, 4E, 4B)

3.2.2 Drying Curves for $\chi_l = 6\%$

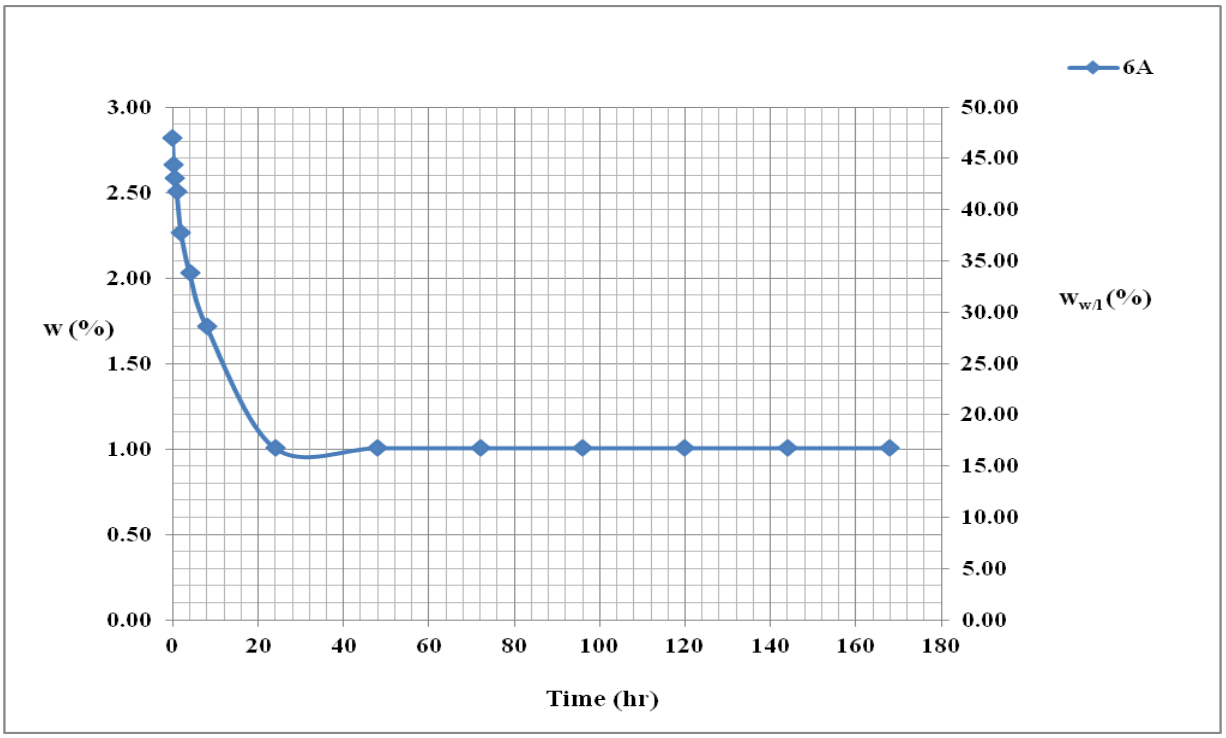

Figure 3-9: Moisture content and water/CaL ratio vs. time. (6A)

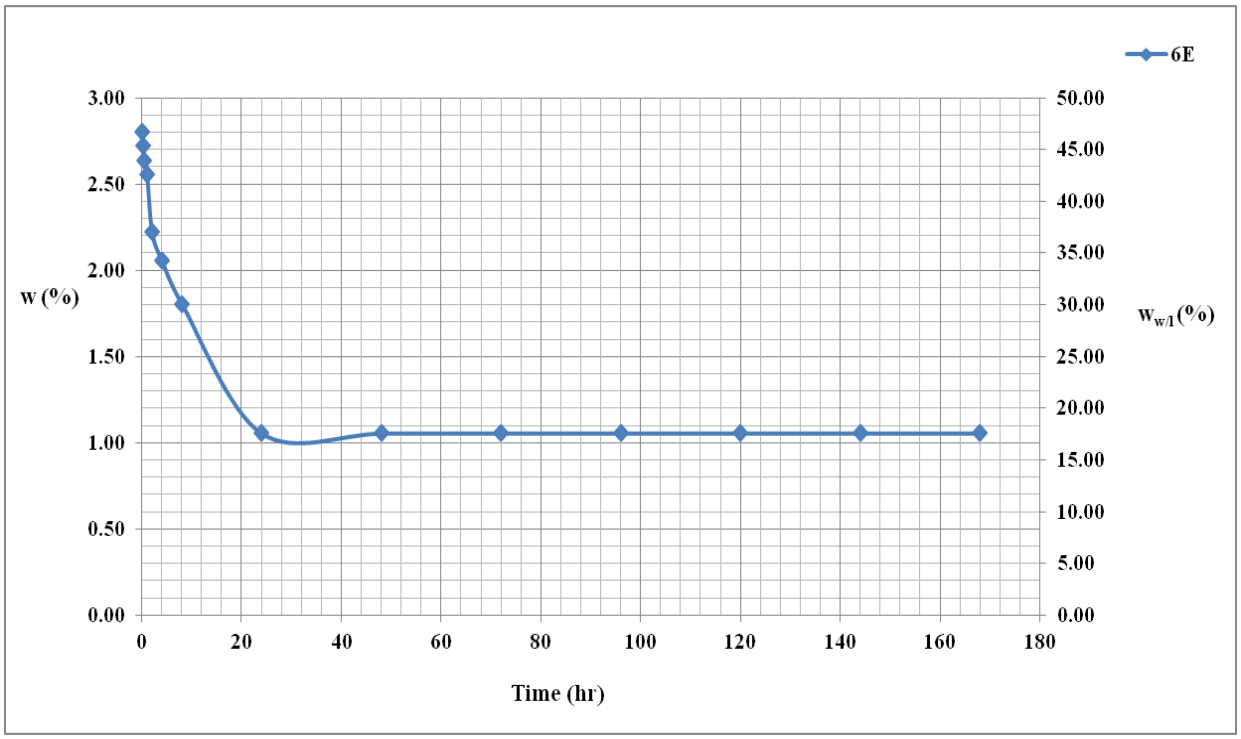

Figure 3-10: Moisture content and water/CaL ratio vs. time. (6E)

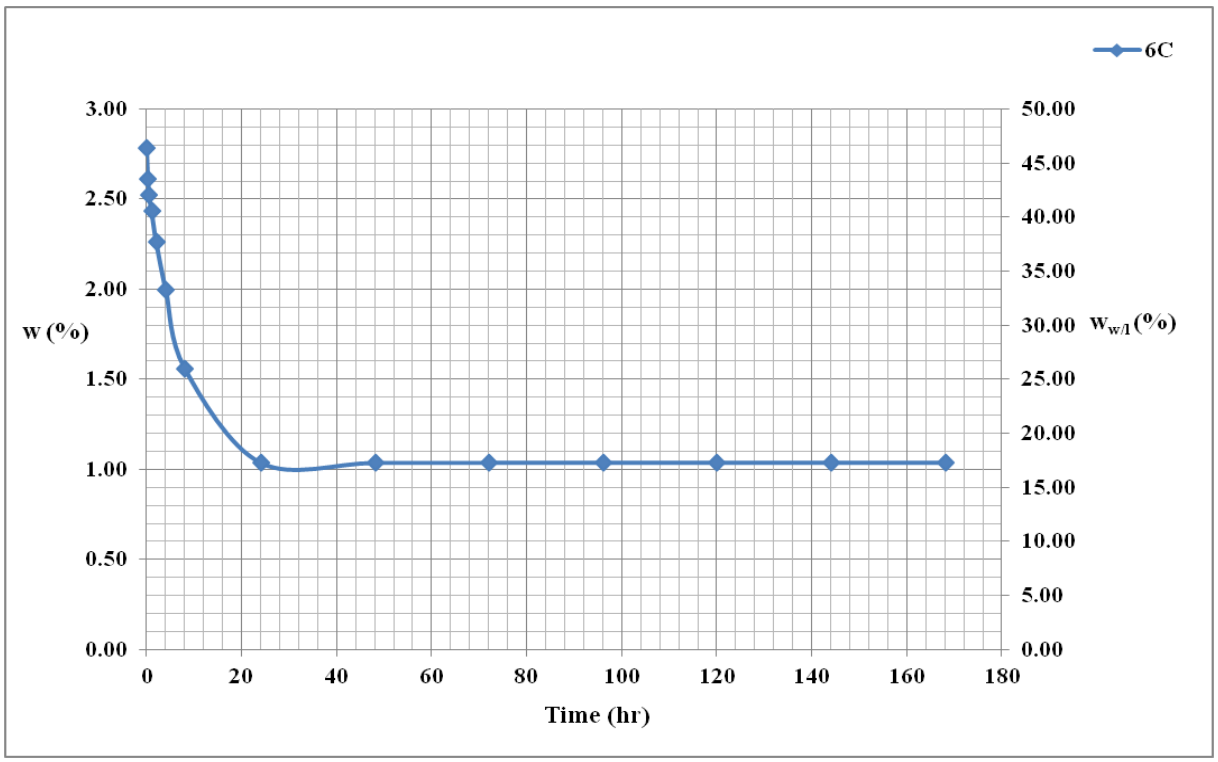

Figure 3-11: Moisture content and water/CaL ratio vs. time. (6C)

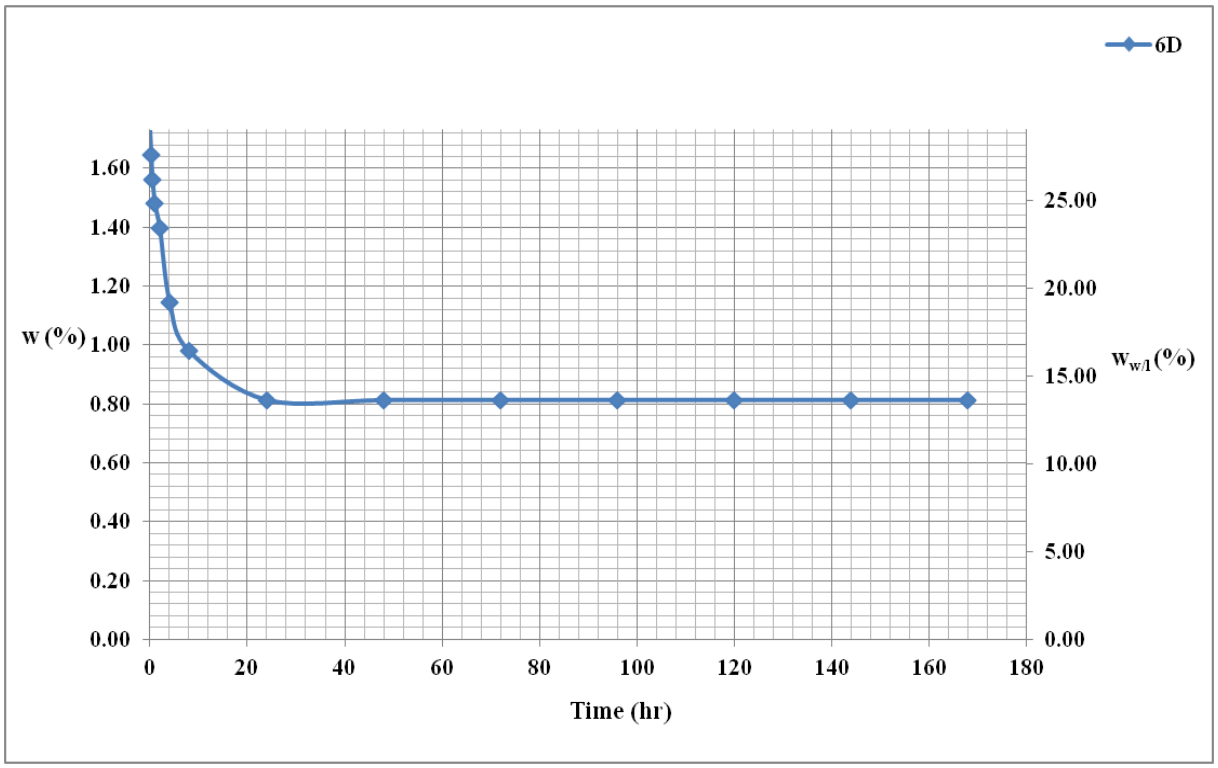

Figure 3-12: Moisture content and water/CaL ratio vs. time. (6D)

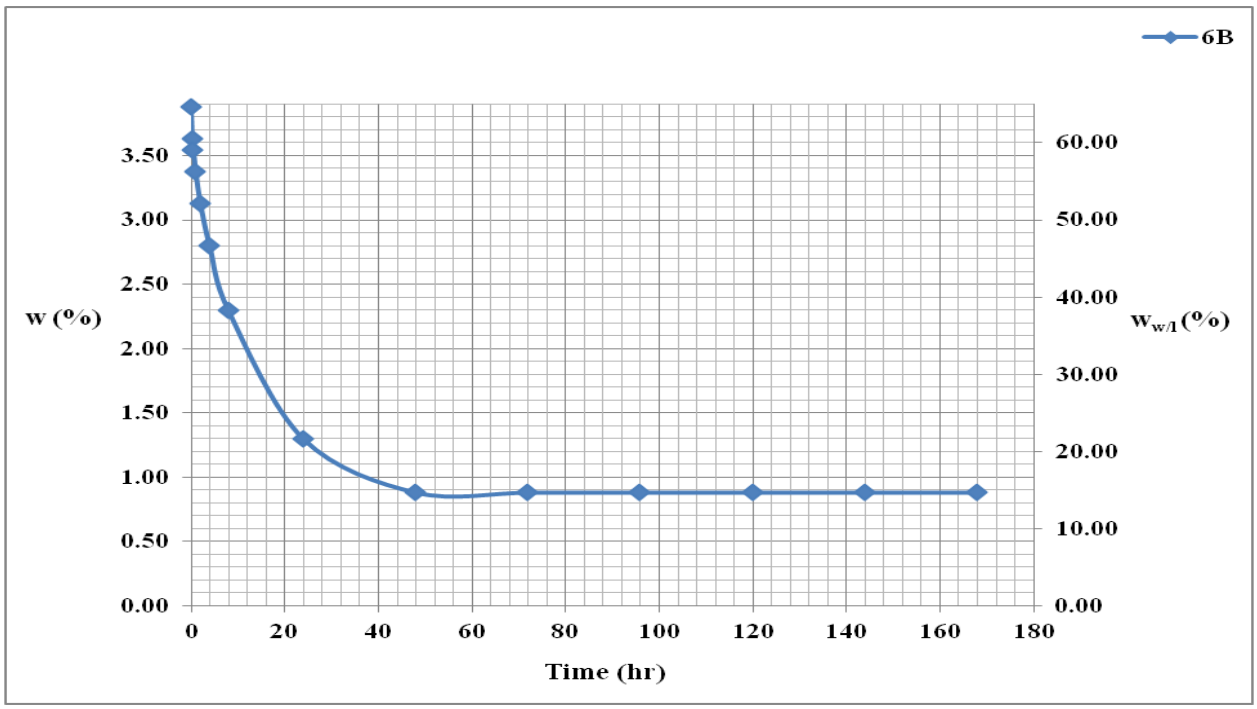

Figure 3-13: Moisture content and water/CaL ratio vs. time. (6B)

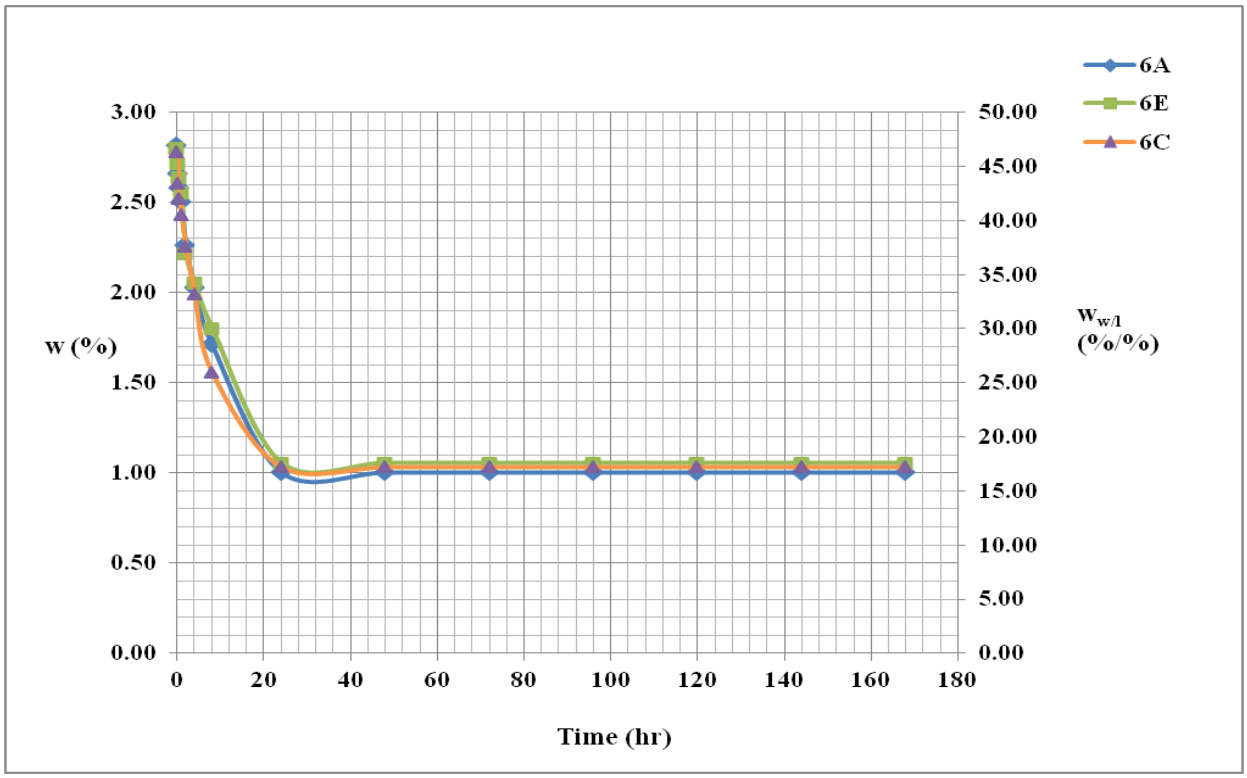

Figure 3-14: Moisture content and water/CaL ratio vs. time. (6A, 6E, 6C)

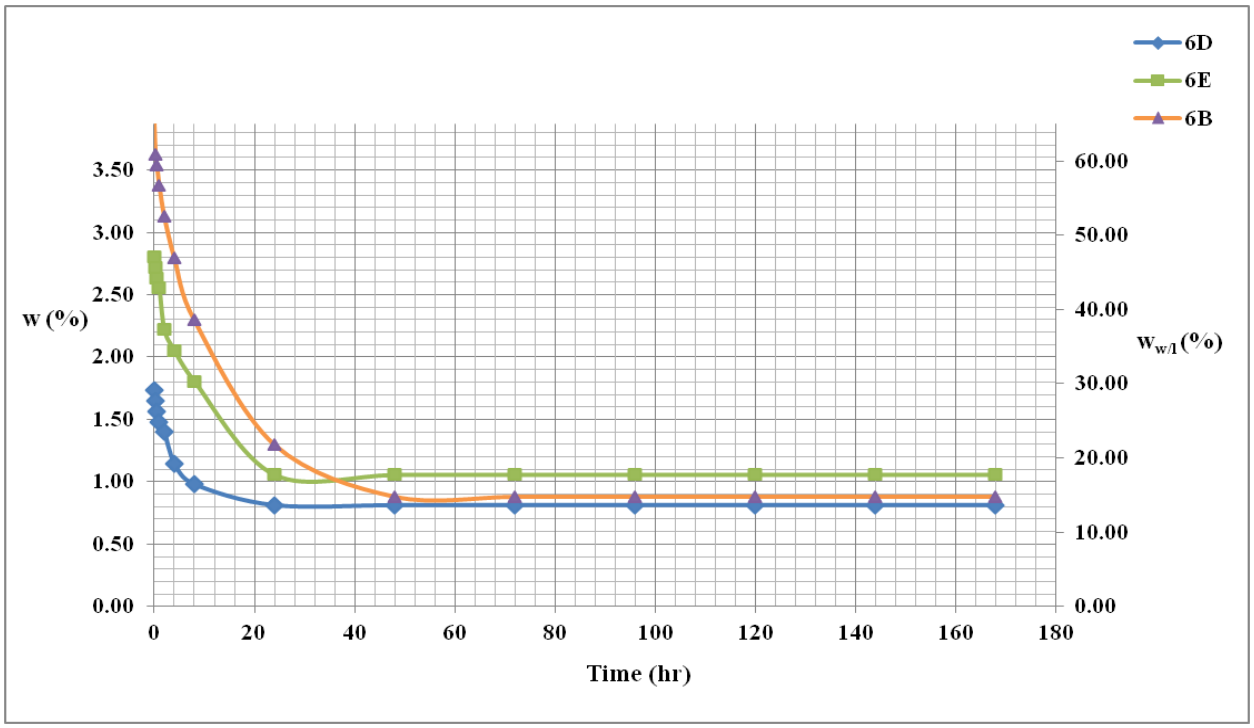

Figure 3-15: Water content and water/CaL ratio vs. time. (6D, 6E, 6B)

3.2.3 Drying Curves for χ_l = 9%

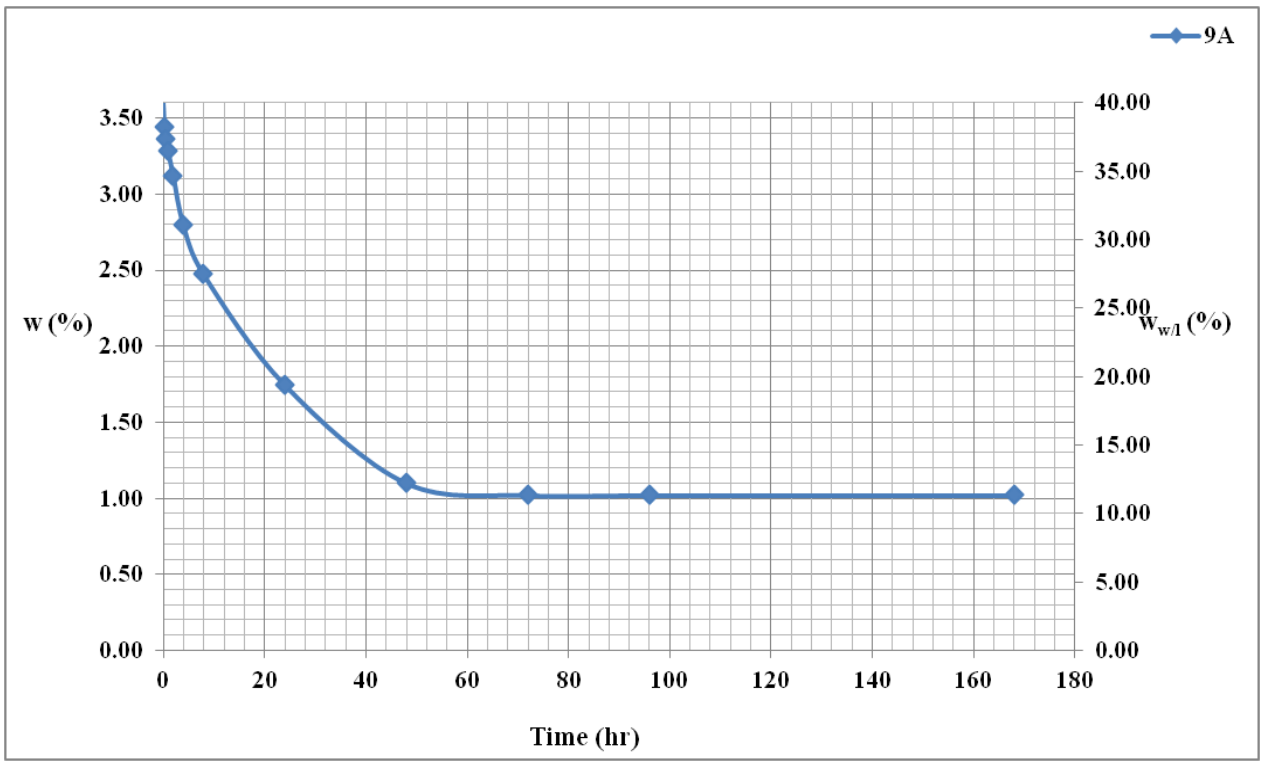

Figure 3-16: Moisture content and water/CaL to lignin ratio vs. time. (9A)

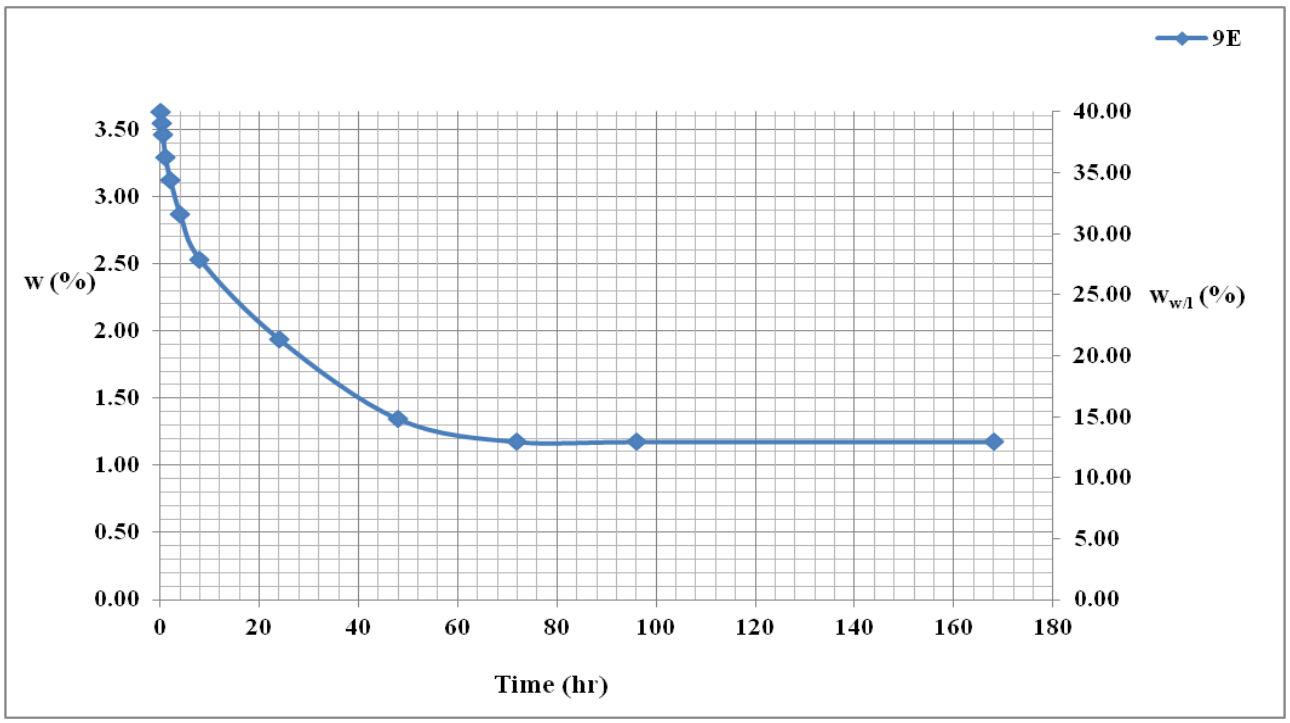

Figure 3-17: Moisture content and water/CaL ratio vs. time. (9E)

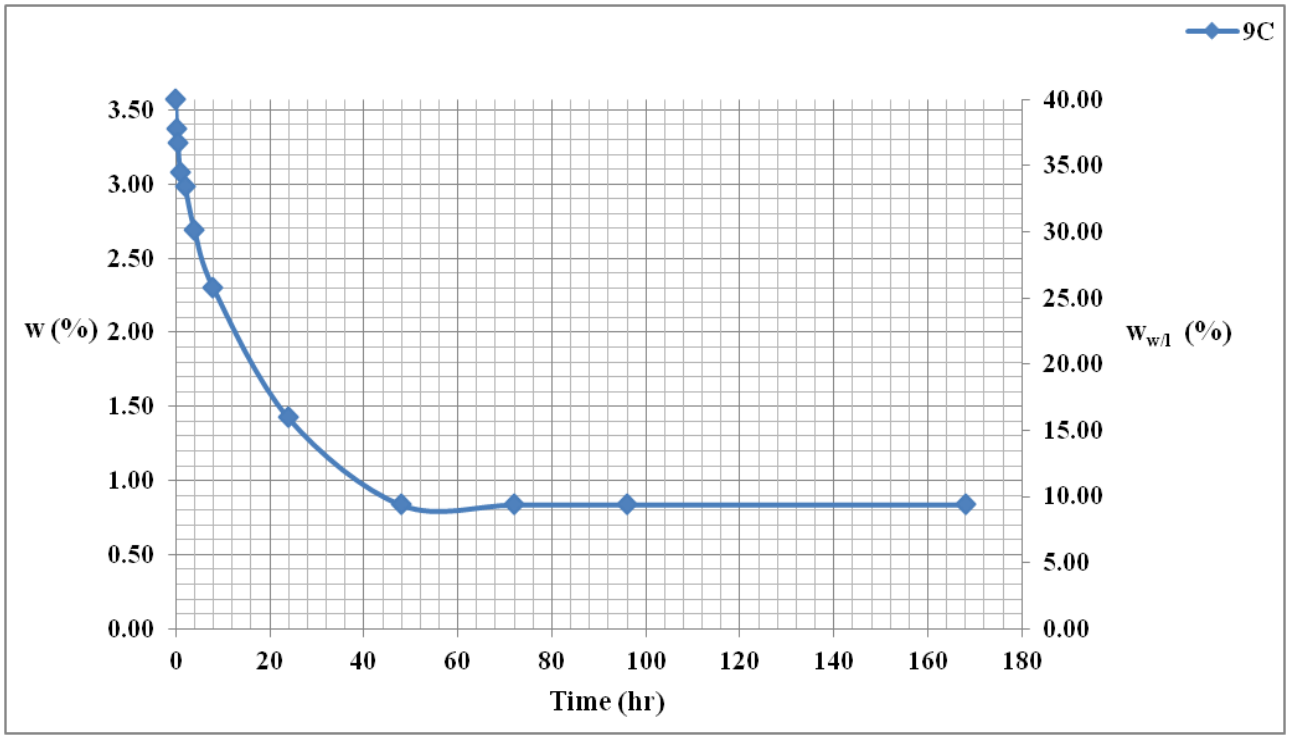

Figure 3-18: Moisture content and water/CaL ratio vs. time. (9C)

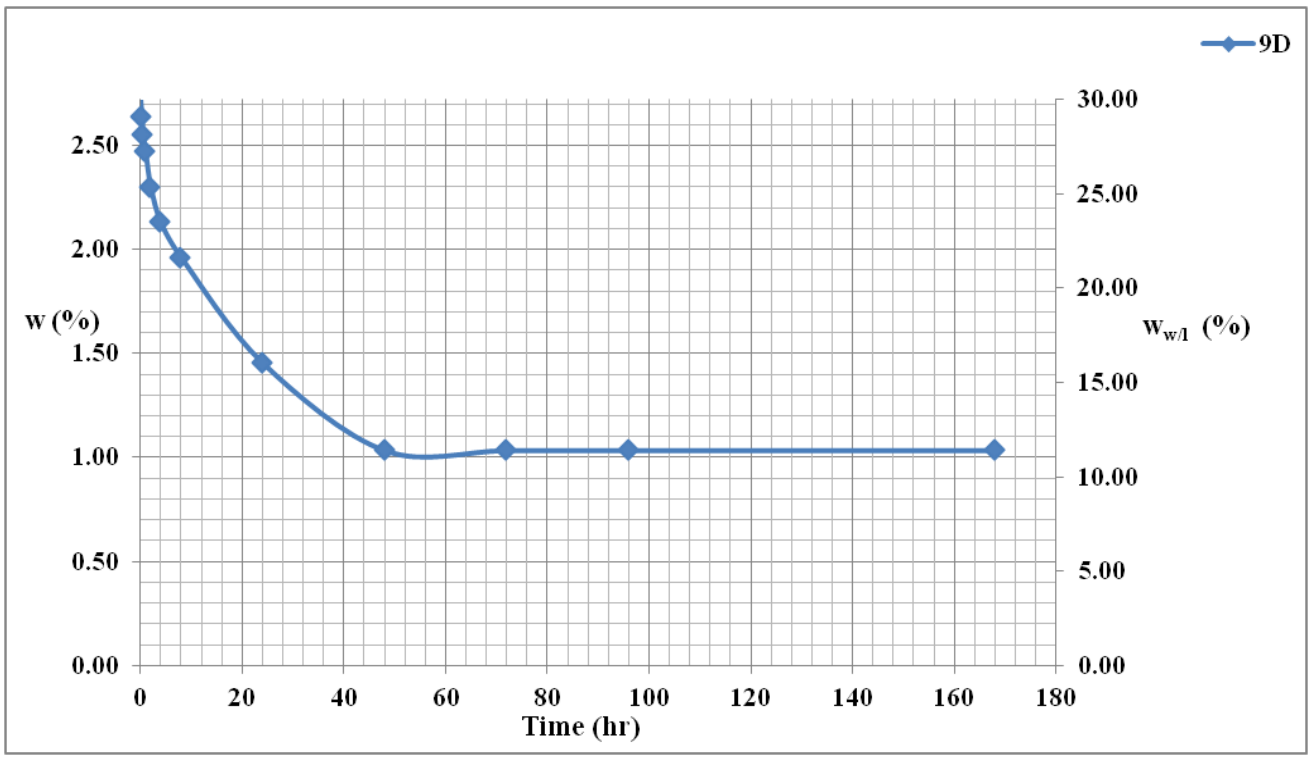

Figure 3-19: Moisture content and water/CaL ratio vs. time. (9D)

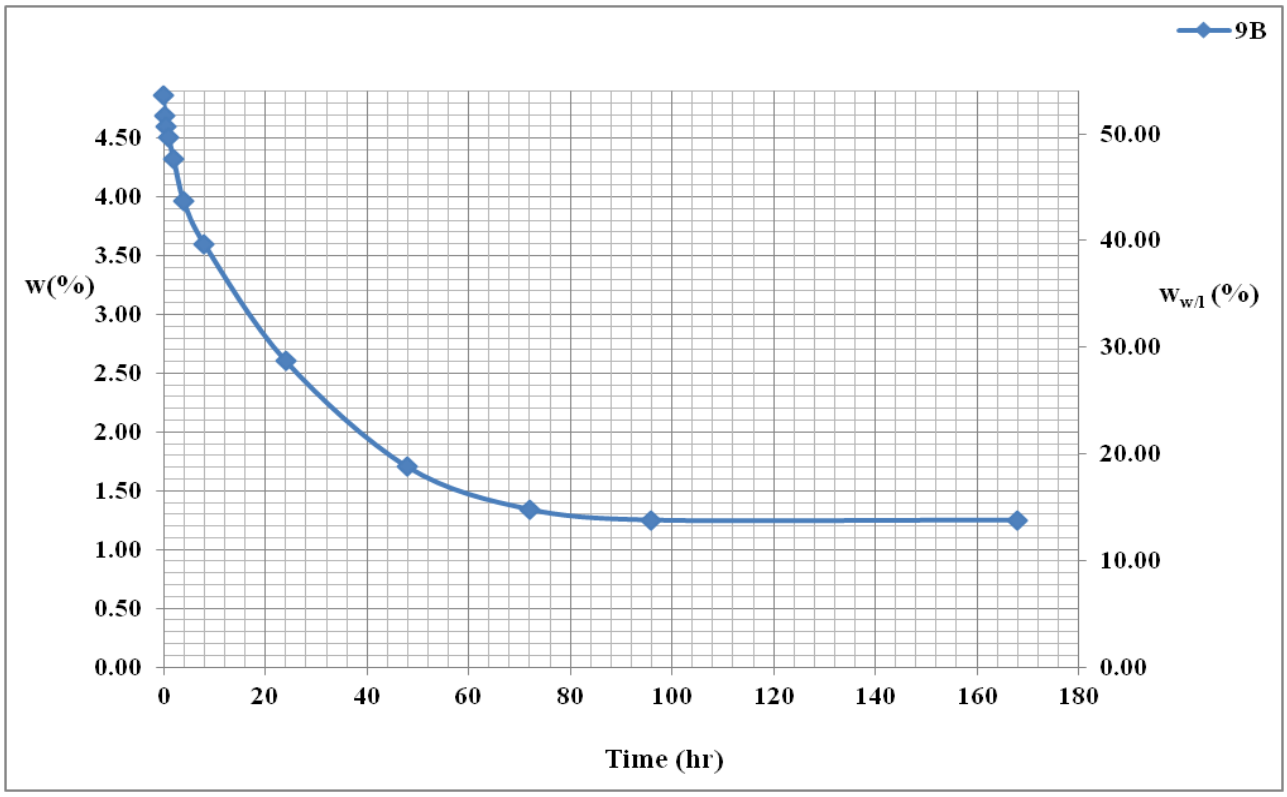

Figure 3-20: Moisture content and water/CaL ratio vs. time. (9B)

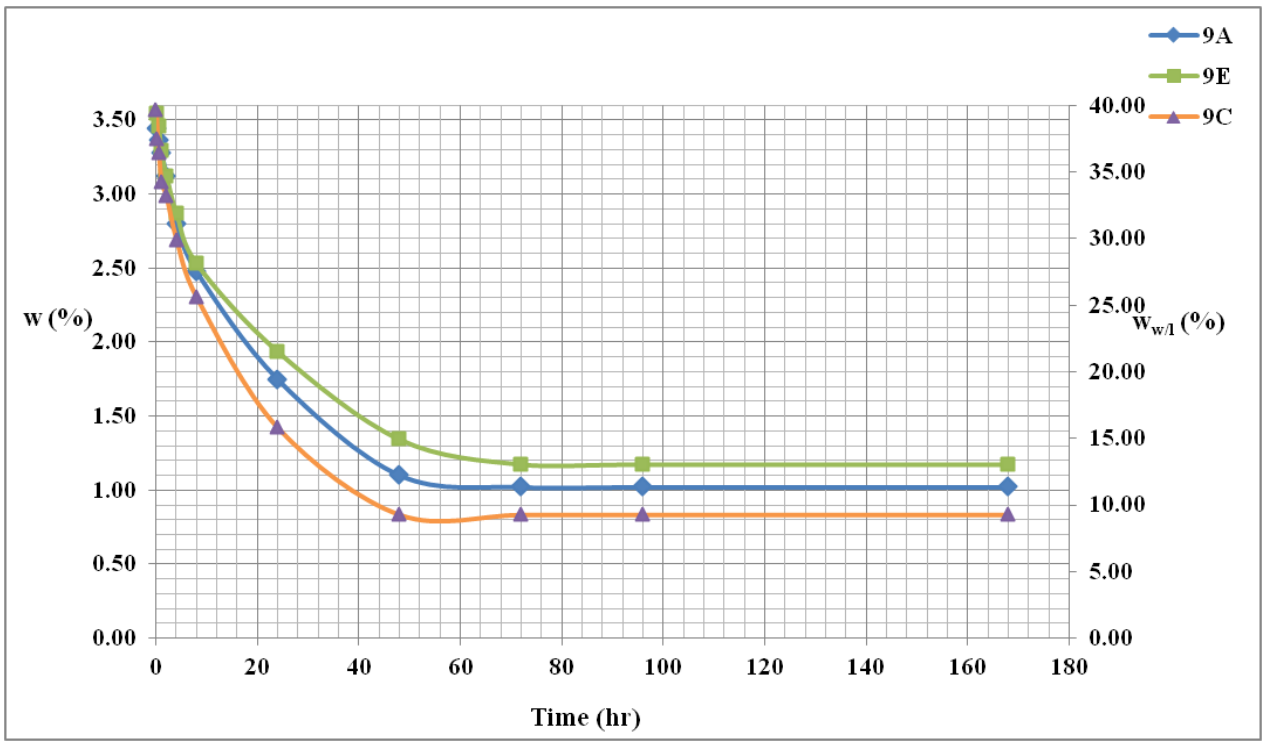

Figure 3-21: Water content and water/CaL ratio vs. time. (9A, 9E, 9C)

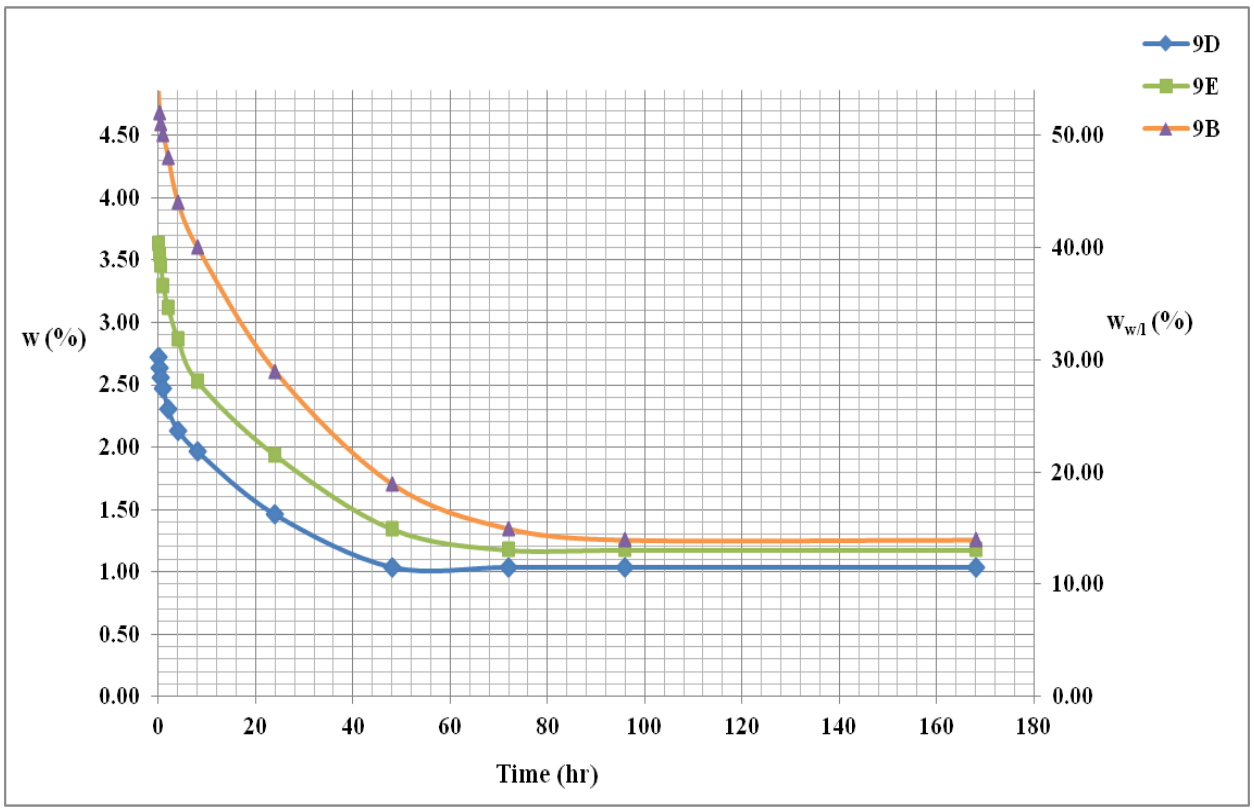

Figure 3-22: Water content and water/CaL ratio vs. time (9D, 9E, 9B)

3.3 Phase Diagrams

This section (Fig 3-23 to Fig 3-25) presents the composition of air dried samples at time t_3.

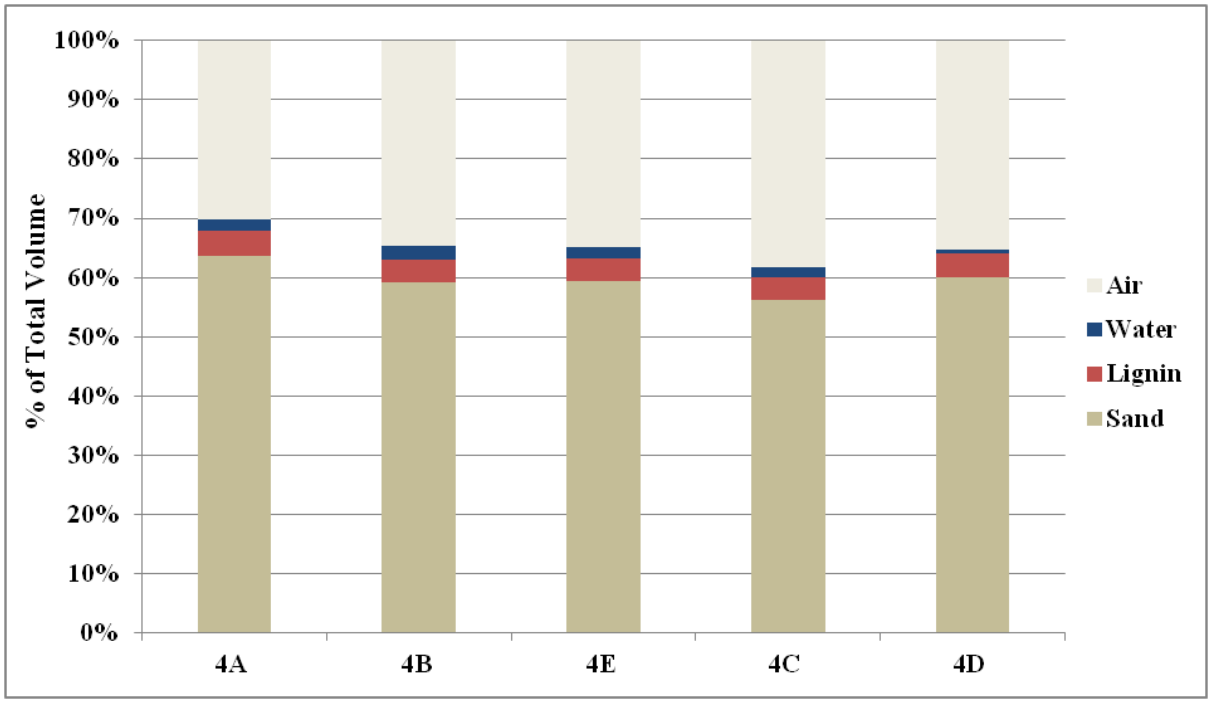

Figure 3-23: Phase relationships for χ_l =4% at t_3.

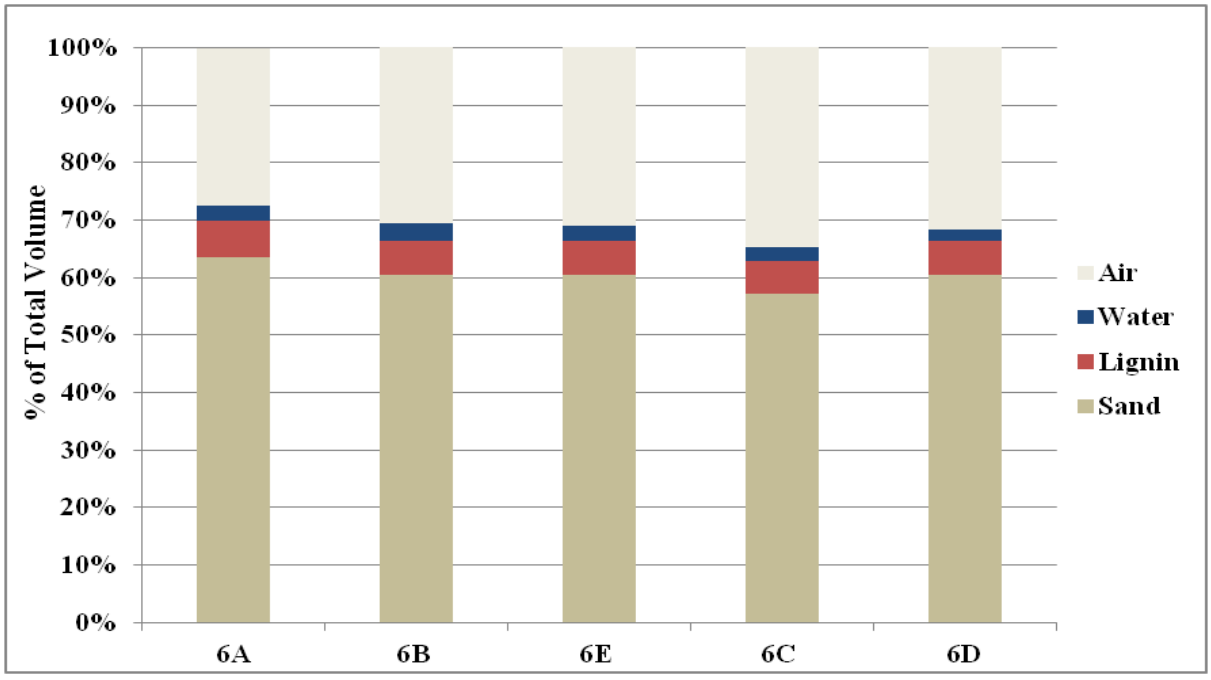

Figure 3-24: Phase relationships for χ_l =6% at t_3.

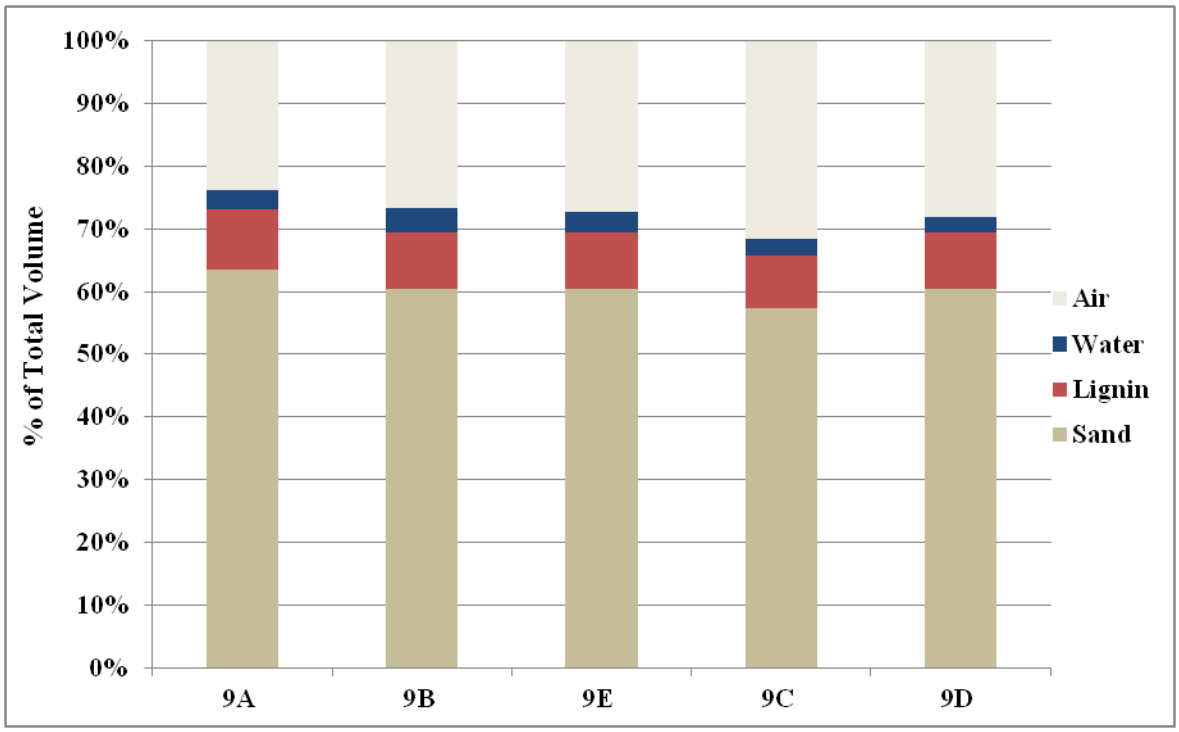

Figure 3-25: Phase relationships for χ_l =9% at t_3.

It can be seen from Figs. 3-2 to Fig. 3-22 that all specimens eventually reached equilibrium water content beyond which no water evaporated at the given temperature and relative humidity. Thus, it was decided to conduct shear strength testing at water contents corresponding to one third, one half, and two thirds of the ultimate decrease in the water content as well as at the final equilibrium state. The corresponding water contents are denoted as w_1, w_2, w_3 and w_f, respectively. The times that corresponded to those water contents were obtained from the drying curve graphs and labeled t_1, t_2, t_3 and t_f respectively. Drying curves are further quantified in Tables 3-1 through 3-3.

Table 3-1: Moisture contents and corresponding time intervals of χ_l = 4%.

Configuration	w_o(%)	w_f(%)	Δw(%)	w_1	w_2	w_3	t_1	t_2	t_3	t_f
4A	2.58	0.51	2.07	1.89	1.55	1.20	2	4	8	24
4E	2.52	0.49	2.03	1.84	1.51	1.17	2	4	7	24
4C	2.56	0.54	2.02	1.89	1.55	1.21	2	4	6	24
4D	1.07	0.06	1.01	0.73	0.57	0.40	0.5	2	4	24
4B	3.63	0.39	3.24	2.55	2.01	1.47	3.5	7	12	48

Table 3-2: Moisture contents and corresponding time intervals of χ_l = 6%.

Configuration	w_o(%)	w_f(%)	Δw(%)	w_1	w_2	w_3	t_1	t_2	t_3	t_f
6A	2.82	1	1.82	2.21	1.91	1.61	2	5	10	24
6E	2.8	1.05	1.75	2.22	1.93	1.63	2	6	11	24
6C	2.79	1.03	1.76	2.20	1.91	1.62	2	5	7	24
6D	1.73	0.81	0.92	1.42	1.27	1.12	2	3	4.5	24
6B	3.87	0.88	2.99	2.87	2.38	1.88	3.5	7	13	48

Table 3-3: Moisture contents and corresponding time intervals of χ_l = 9%.

Configuration	w_o(%)	w_f(%)	Δw(%)	w_1	w_2	w_3	t_1	t_2	t_3	t_f
9A	3.6	1.02	2.58	2.74	2.31	1.88	4	12	20	72
9E	3.63	1.17	2.46	2.81	2.40	1.99	4	10	21	72
9C	3.57	0.87	2.7	2.67	2.22	1.77	4	16	17	48
9D	2.72	1.03	1.69	2.16	1.88	1.59	3.5	9	18	48
9B	4.86	1.25	3.61	3.66	3.06	2.45	8	16	28	96

3.3.1 Times from the Drying Curves

Initial direct shear testing began on samples at $w_{1.}$ However the results were inconsistent. Upon further inspection it was noticed that samples were non-uniform due to too short drying time. In particular, the outsides dried quickly and gave the illusion of a rigid structure yet the

interiors remained moist and plastic. At the other end of the spectrum, specimens tested during the t_f intervals were too rigid making the direct shear motor unable to shear through the sample without getting stuck. In addition, these samples were extremely brittle, and thus very sensitive to material imperfections, thus often causing premature failure. It is noted that material inhomogeneity or material imperfections play more a significant role in smaller specimens and more brittle materials. It was decided to conduct shear strength testing on specimens dried for a time period t_3 corresponding to a 2/3 of a total decrease in the water content.

3.4 Challenges with Sample Drying

It was in the middle of testing that an unexpected challenge was encountered. The incubator (Fig. 2-23) no longer was holding the required temperature and humidity for experimentation. It turned out the chamber was not completely sealed from the outside. During the winter months the internal chamber's environment held constant but during the transition from winter to spring, its humidity increased significantly from 27% to as high as 53%. At this time samples containing 4% of CaL were being dried and high humidity which coincided with the intense rainfall occurring outside, made it impossible for the soil samples to dry properly. The sensitivity of CaL to atmospheric moisture is due the presence of polysaccharides or sugar molecules within its composition. These compounds are hydrophilic and bond to the hydrogen found in water. It is the same mechanism the turns the powder into paste; however, when the excess water is present in the air the water cannot be driven out to allow the paste to dry. It is the effect of drying the required paste that gives the soil samples their increased strength.

Alternative methods of drying were attempted in order to create the appropriate drying conditions to resume testing. Some samples lost the required amount of water because the humidity decreased enough while other others sat for days without reaching their moisture content. The hydrated salt, magnesium chloride was used as a means of regulating the humidity. This particular salt has the ability to hold the relative humidity of an environment at a constant 33% at a temperature of 20°C. Initial experimentation of the product showed promising results. A layer of the salt was spread on the bottom of a five gallon bucket (Fig. 3-24). A temperature and humidity gauge was placed inside and the lid to the bucket sealed the environment from the outside atmosphere. Temperature readings were taken over a two day period with the results

showing the humidity staying at or near 33% relative humidity. The sample configuration containing 9% CaL at 90% relative compaction, (9C), was mixed with the intention of drying it in the hydrated salt environment. Five samples were prepared with the humidity reading 31% as the first sample was placed into the bucket. At the end of the drying interval, 17 hours later, the bucket was unsealed to commence the direct shear test process and it was noted that the humidity had increased to 56%. The bucket was resealed to allow a time to pass and see if there was a change. After another seven hours, the gauge was checked again revealing the humidity had changed to 52%. These findings confirmed the hydrated salt was not a suitable method for drying soil samples. The reasoning behind the sudden changes in the humidity with addition of samples is that at 33% samples began evaporating the water that had nowhere to go in the seal bucket causing the humidity to increase. It became apparent the necessary equipment to continue drying samples was not available. Thus, the target water content for direct shear testing could only be produced for samples containing 6% of CaL.

Figure 3-26: Drying incubator for soil samples.

Figure 3-27 Five gallon bucket, magnesium chloride salt, and humidity gauge.

Chapter 4 - Direct Shear Results and Analysis

4.1 Direct Shear Test Results

Strength testing of the sand-lignin specimens was conducted in the laboratory on the direct shear device. The samples were placed within the apparatus, compressed to a desired normal stress and sheared to failure. Further details about of direct shear device were provided by Bartley (2011). For each sample configuration, five soil samples were prepared and tested at the following normal stresses: 62.0 kPa, 92.9 kPa, 123.9 kPa, 185.9 kPa, and 247.8 kPa. The DS7 software recorded and displayed the shear stress and vertical displacement of the samples each with respect to horizontal displacement as shown below for the configuration containing 6% of CaL dry of optimum moisture at 95% relative compaction (Fig. 4-1 and 4-2). The Mohr-Coulomb strength parameters were determined by plotting the peak shear stress versus the corresponding normal stress (Fig. 4-3). Additional direct shear response graphs and peak shear stresses versus normal stress for the remaining test configurations can be found in Appendix A.

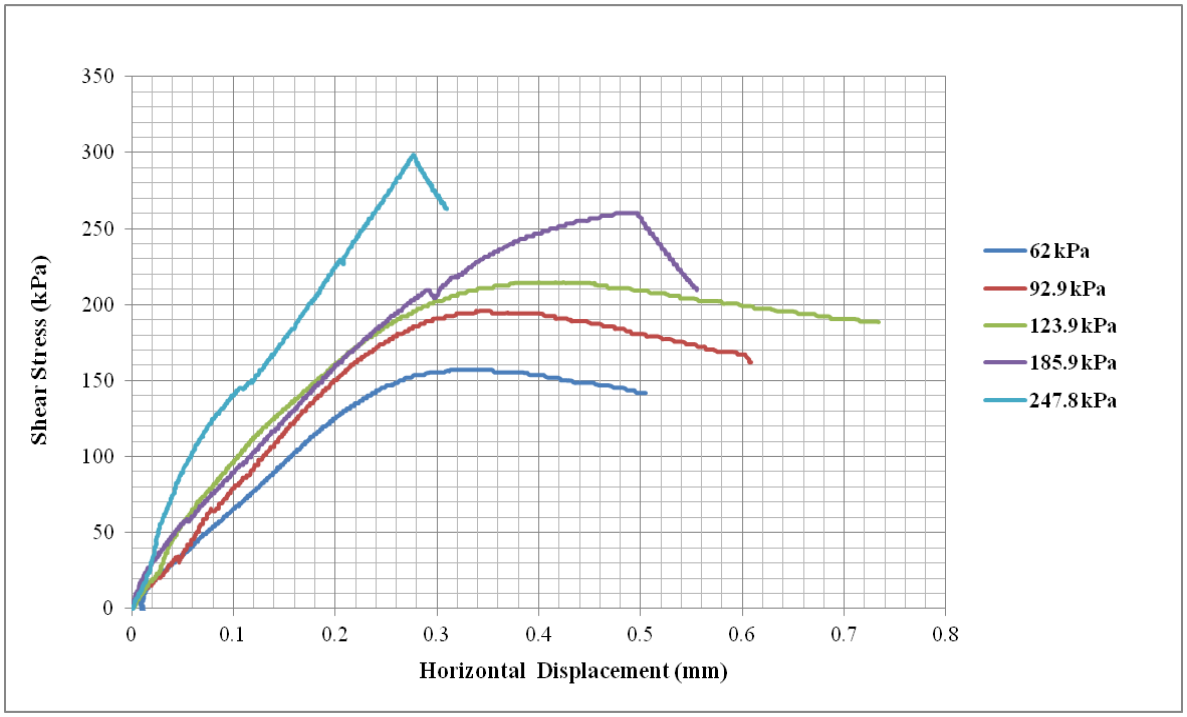

Figure 4-1: Shear stress vs. horizontal displacement (6D)

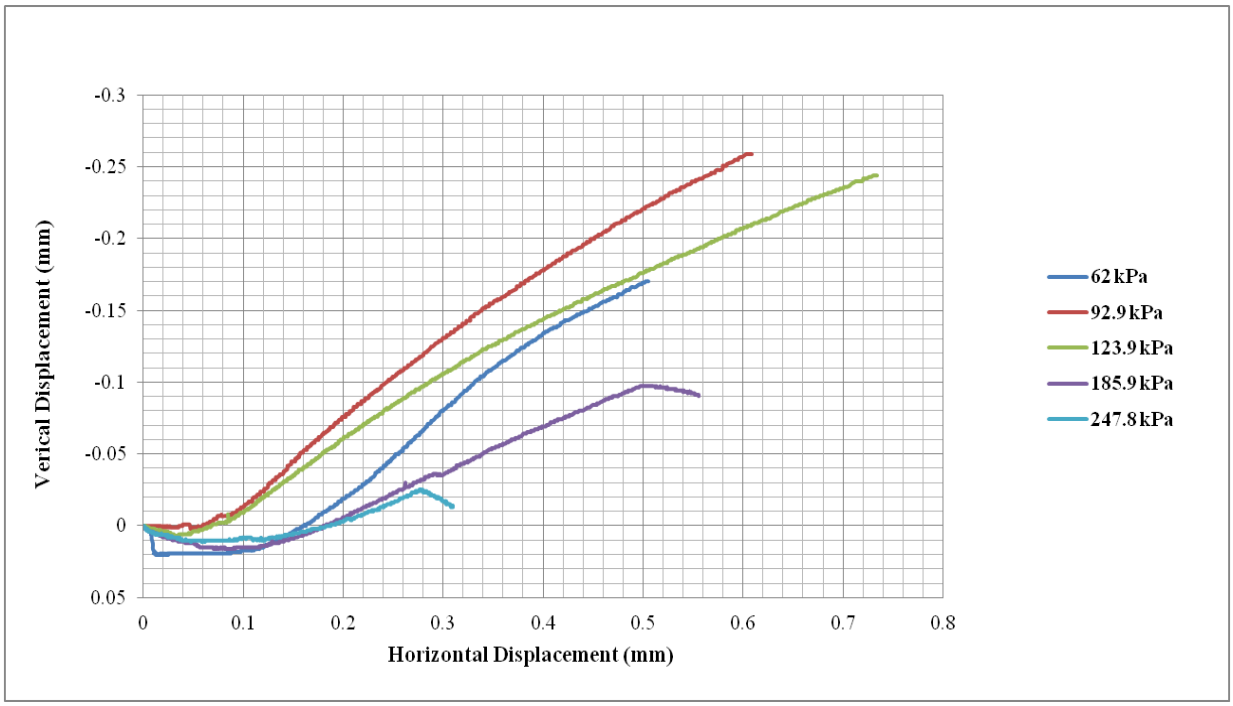

Figure 4-2: Vertical displacement vs. horizontal displacement (6D)

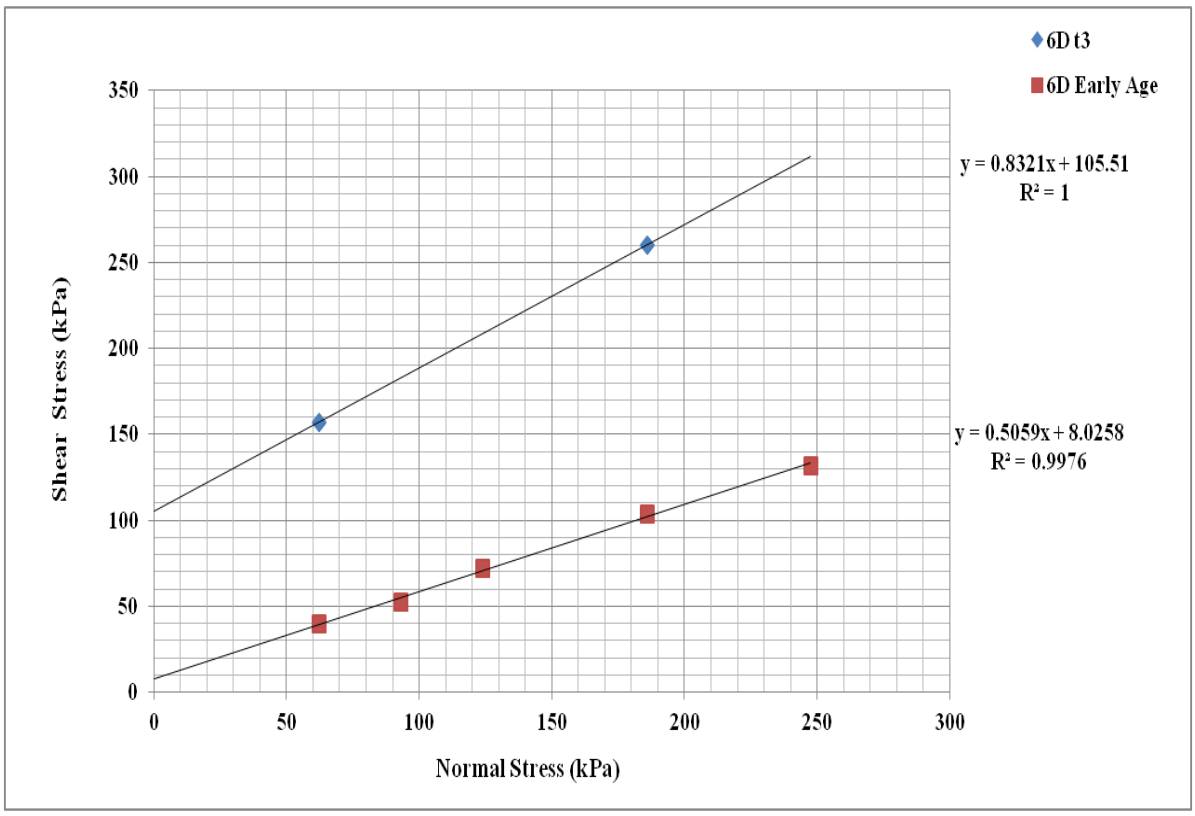

Figure 4-3: Peak shear stress vs. normal stress (6D)

Figure 4-3 is the plot of the peak shear stress with respect to the applied normal stress. Although five samples were prepared and tested at five different normal stresses for each sample configuration not all of them were used for determination of cohesion and angle of internal friction. Certain tests were eliminated carefully by considering the response across the full range of normal stresses. In particular, the tests that did not fit in the overall pattern of magnitudes of peak shear stresses, initial stiffness and dilatancy were not considered. These deviations are expected because of the increased brittleness of the S-CaL-W mixes caused by drying. Specifically, drying caused more significant imperfection sensitivity leading to premature failure, which was further exaggerated due to the small sample size. The data points for early age tests are also included in the graphs to better illustrate the significant strength gains caused by air drying.

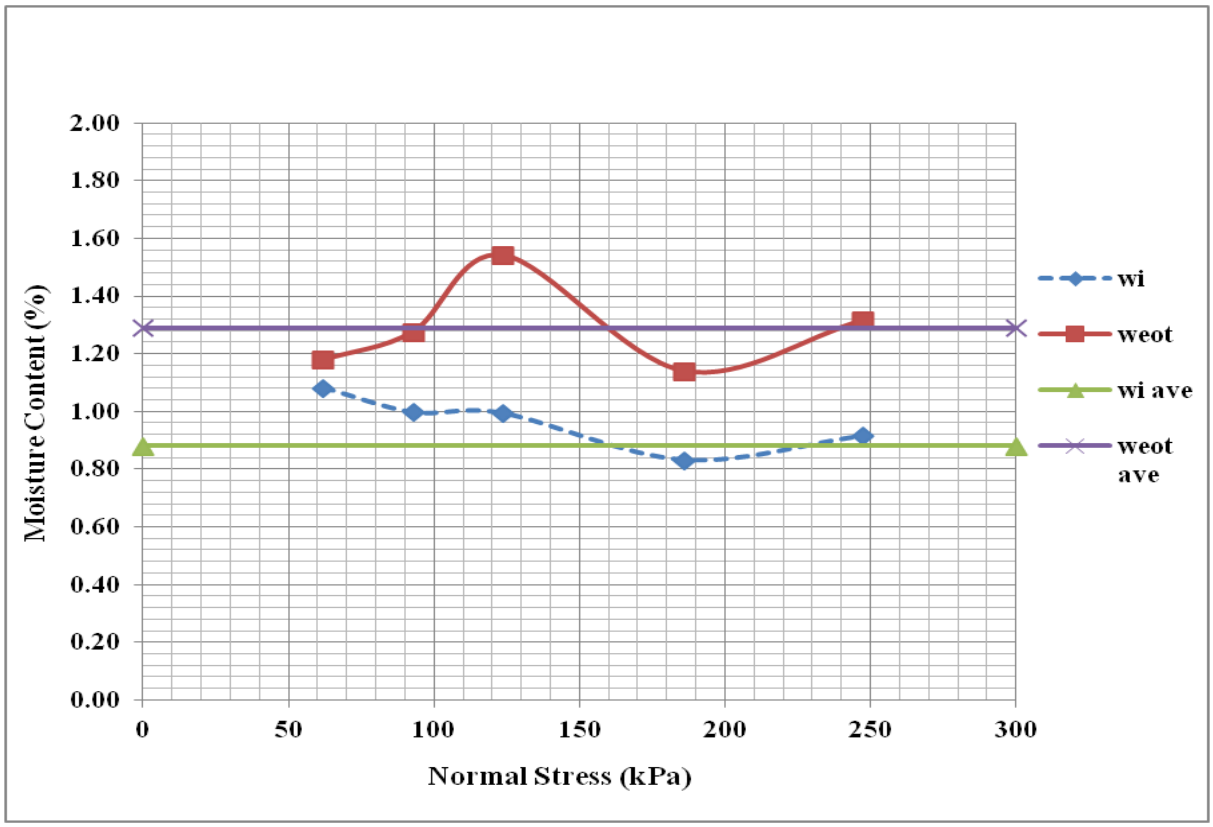

Figure 4-4: Normal Stress vs. Moisture Content. (6D)

The moisture content of the soils samples was tracked throughout the experimental process. Initial moisture content was added to the soil samples in the same manner as in the early age tests. The samples were placed in the incubator for their drying time, taken out, and weighed to record how much water evaporated. Equation (15) defines the moisture content after the drying stage whereas Equation (16) is the moisture content at the end of the direct shear test.

$$w_i = \frac{w_0 - (1+\chi_l)\overline{w_i}}{1+\overline{w_i}} \tag{15}$$

$$w_{eot} = \overline{\overline{w_{eot}}}(1+\chi_l) \tag{16}$$

$$\overline{\overline{w_{eot}}} = \frac{M_{eot} - M_{ao}}{M_{ao}} \tag{17}$$

The objective of recording the moisture content at these stages is to observe whether there is a correlation between the moisture content and the strength of the soil particularly among the five samples within each sample configuration. In Figure 4-4, w_i and w_{eot} were plotted for 6D versus normal stress. The average values of w_i and w_{eot} were calculated as benchmarks for comparison to observe if the points that deviated furthest from the average had irregular peak shear strengths. Figure 4-5 simply shows the difference in the moisture contents with respect to their average values. Additional figures depicting the moisture contents for other sample configurations containing 6 % CaL are included in Appendix A.

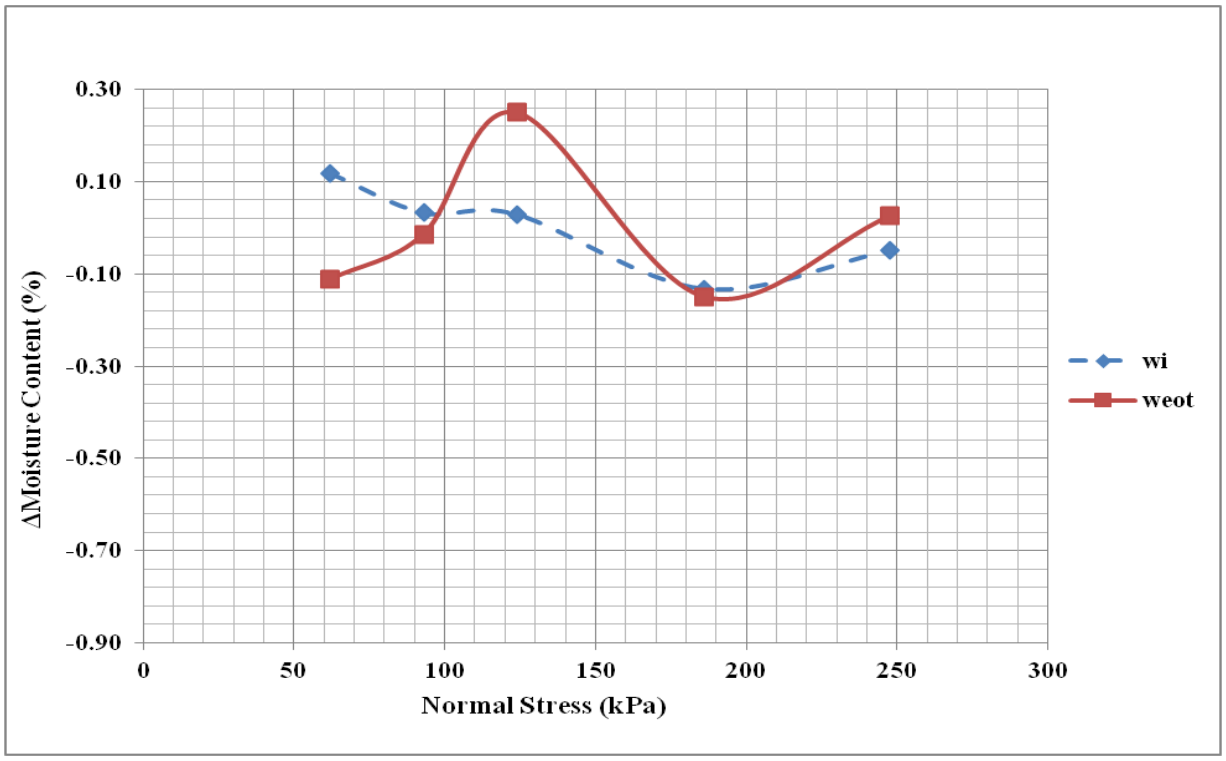

Figure 4-5: Normal stress vs. Change in moisture content. (6D)

The shear strength parameters for sample configurations containing 6 % CaL are listed in Table 4-1.

Table 4-1: Cohesion and Angle of Friction for χ_l = 6%

χ_l	c (kPa)	ϕ (°)
A	**136.8**	**31.6**
E	**115.1**	**44.7**
C	**101.8**	**46**
D	**105.5**	**39.8**
B	**122.8**	**42.9**

Additional analysis was conducted to further investigate the relationships between amounts of CaL, water, and void ratio to gain a deeper insight into the experimental data. Equations were derived to interpret the effect of CaL, water, and void ratio on the strength gain upon air drying. The analysis continues to build upon the data collected by Bartley (2011) who quantified the portion of the cross-sectional area of the sample occupied by CaL and water. Fig 4-6 depicts the normalized area ratio as a function of water to CaL ratio for both, early age sample configurations and after air drying for duration t_3. It is seen that the ranges of x-axis and y-axis variables decrease upon drying.

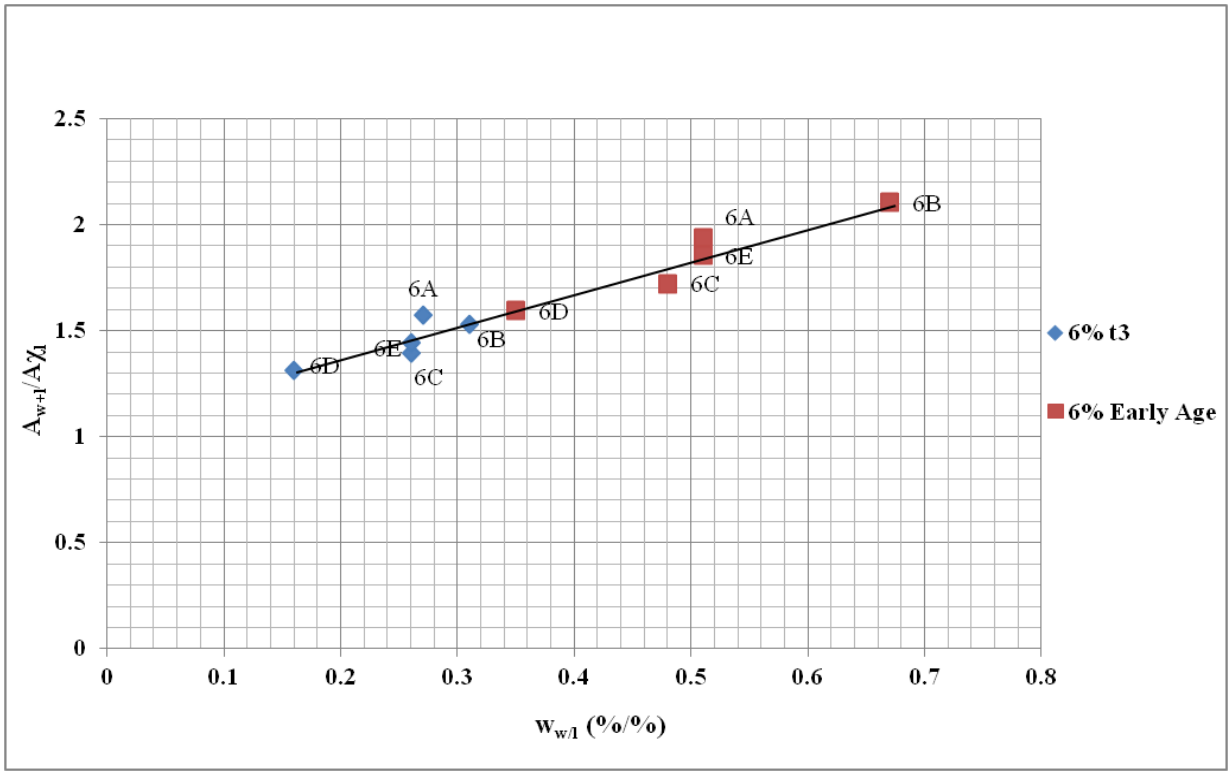

Figure 4-6: Water to lignin ration vs. Normalized area ratio.

The ratio of the portion of the cross sectional area occupied by water and CaL with respect to the total cross sectional area of the soil sample was given by Bartley (2011) as:

$$\frac{A_{w+l}}{A} = \frac{A_w}{A} + \frac{A_l}{A} = \frac{G_s}{1+e}(w + \frac{\chi_l}{G_l}) \tag{18}$$

The normalized area ratio is defined as the area ratio given in Eqn. (18) divided by the amount of CaL present. This gives the contribution of each individual percent of CaL to the area ratio. It is expressed as:

$$\frac{A_{w+l}}{A\chi_l} = \frac{G_s}{1+e}(w_{w/l} + \frac{1}{G_l}) \tag{19}$$

The updated void ratio accounts for the volume change encountered during the initial compression phase in the direct shear device. It is given by:

$$e_1 = e_o - \frac{\Delta H_{avg}}{H_O}(1+e_o) \tag{20}$$

All area ratios are calculated by using the updated void ratios, which are provided in Table 4-2.

Table 4-2: Changes in Height and Void Ratio.

χ_l(%)	Pt.	e_0	ΔH_{avg} (mm)	e_1
6	**A**	**0.571**	**1.067**	**0.501**
6	**E**	**0.654**	**0.962**	**0.588**
6	**C**	**0.746**	**0.981**	**0.675**
6	**D**	**0.654**	**1.004**	**0.585**
6	**B**	**0.654**	**0.55**	**0.616**

As can be seen from Eqn. (19) there is a one to one relationship between the normalized area ratio and water to CaL ratio for a given void ratio (Fig. 4-6). Namely, points D,E, and B remain on the same straight line after drying because void ratio is unaffected by drying (Fig. 4-6). Moreover, these points remain arranged in the same pattern. In addition, points A at early age

and after air drying, and points C at early age and after air drying define the lines that are parallel to the line defined by points B,E, and D.

4.1.1 Strength Parameter Relationships

Figures 4-7 illustrates that there is a direct relationship between an increase in cohesion and a decrease in water content. The latter causes the shift to the left in the water to CaL ratios and in normalized area ratios of the air dried test configurations with respect to the early age configurations.

Fig. 4-14 and 4-15 depict normalized cohesion versus void ratio indicating that there is an influence of the void ratio on the normalized cohesion which remains in effect even after air drying. Fig. 4-8 through 4-13 show change in normalized cohesion and friction versus the change in normalized area ratio.

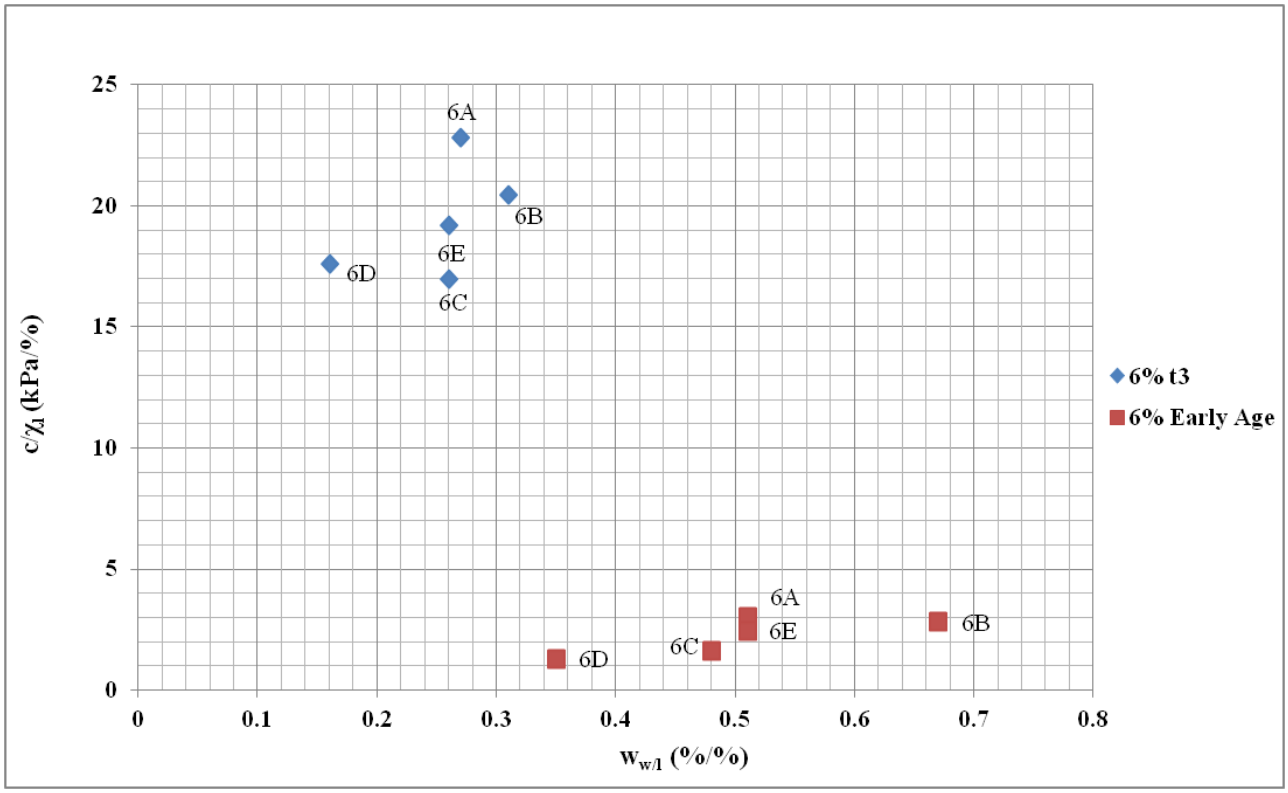

Figure 4-7: Normalized cohesion vs. water/CaL ratio.

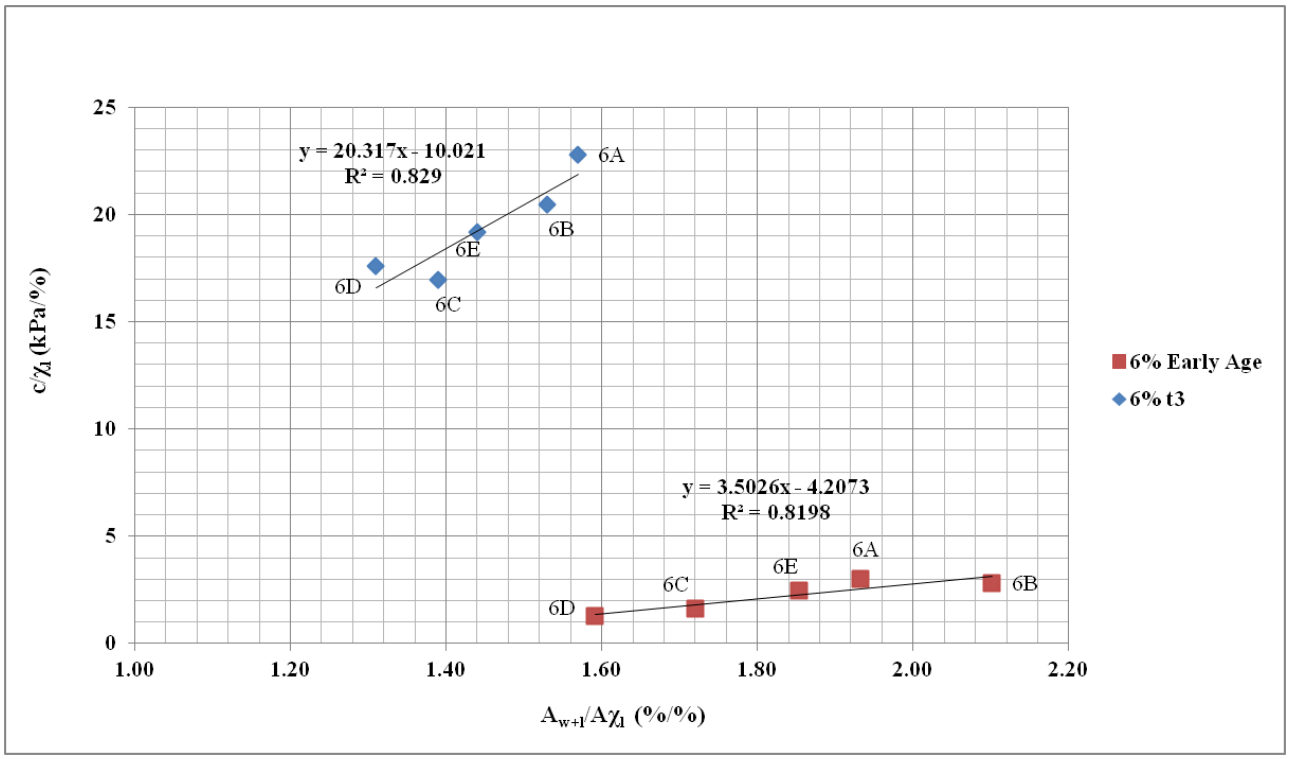

Figure 4-8: Normalized cohesion vs. normalized area ratio.

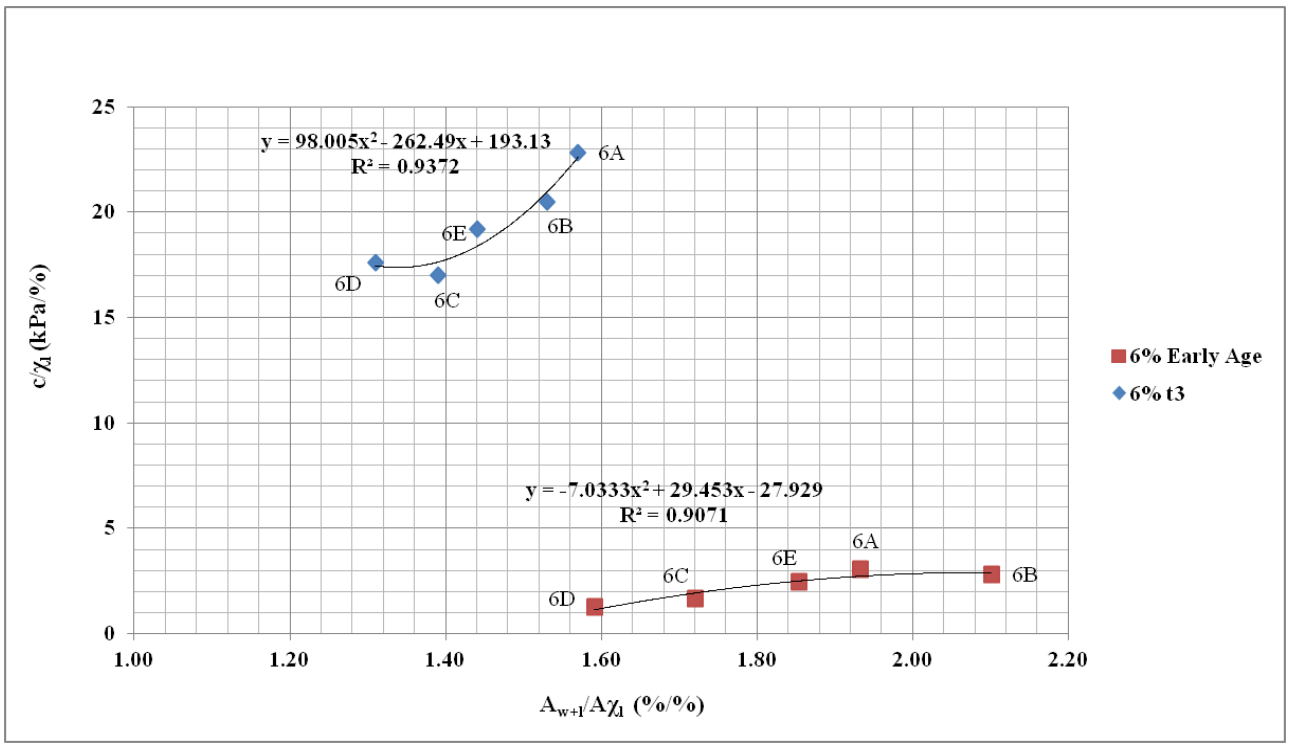

Figure 4-9: Normalized cohesion vs. normalized area ratio.

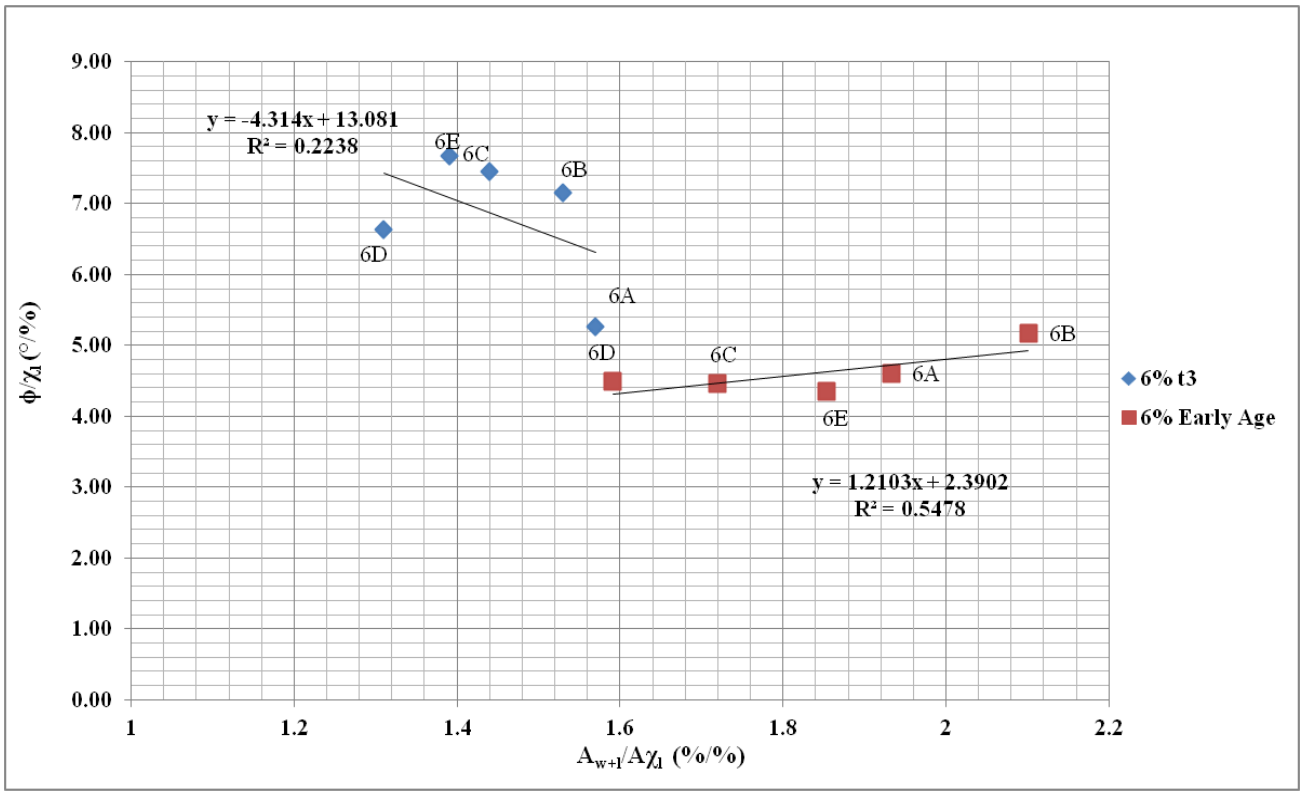

Figure 4-10: Normalized friction vs. normalized area ratio.

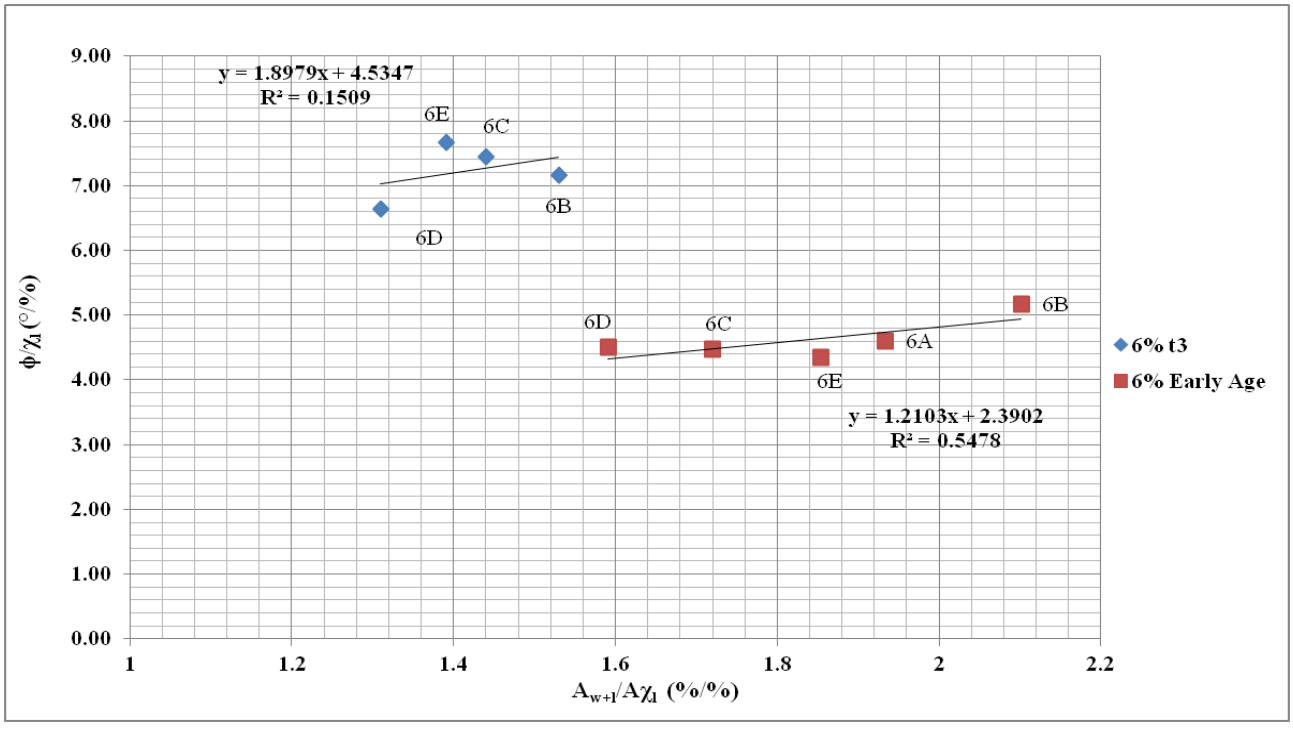

Figure 4-11: Normalized friction vs. normalized area ratio without 6A.

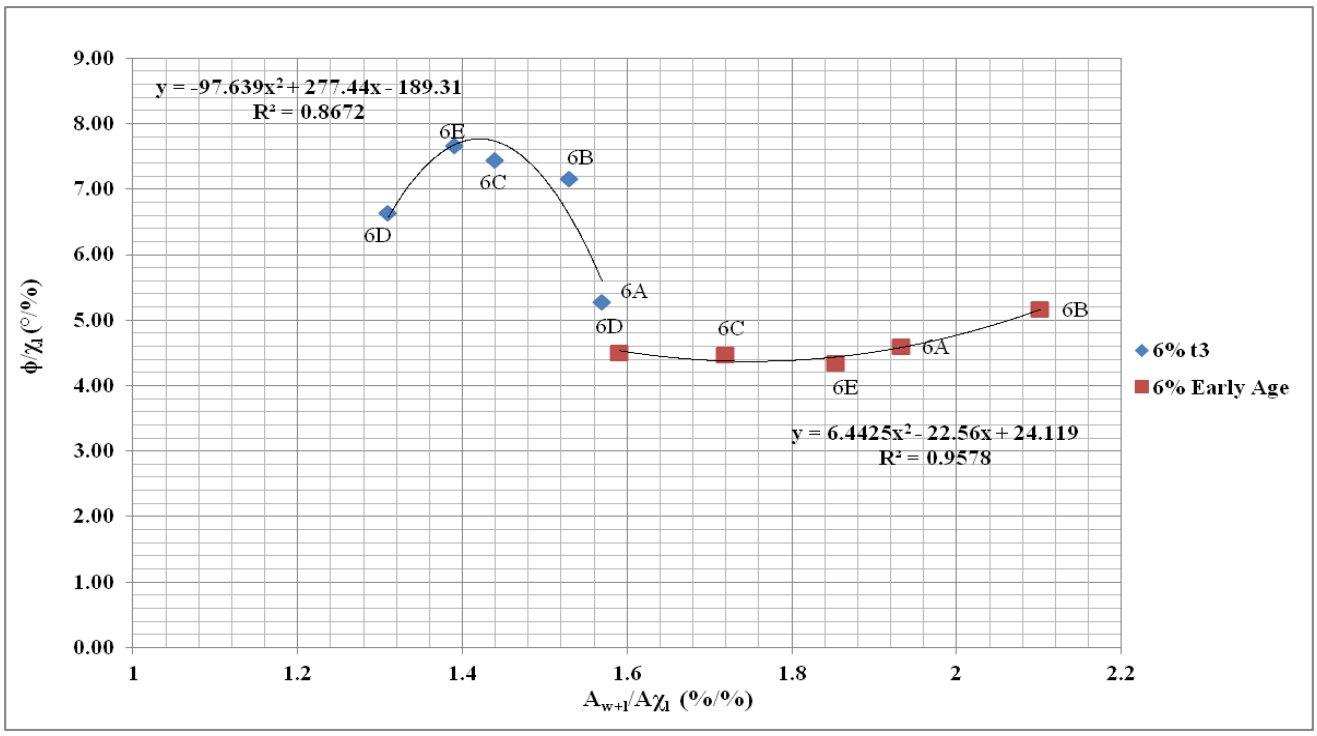

Figure 4-12: Normalized friction vs. normalized area ratio.

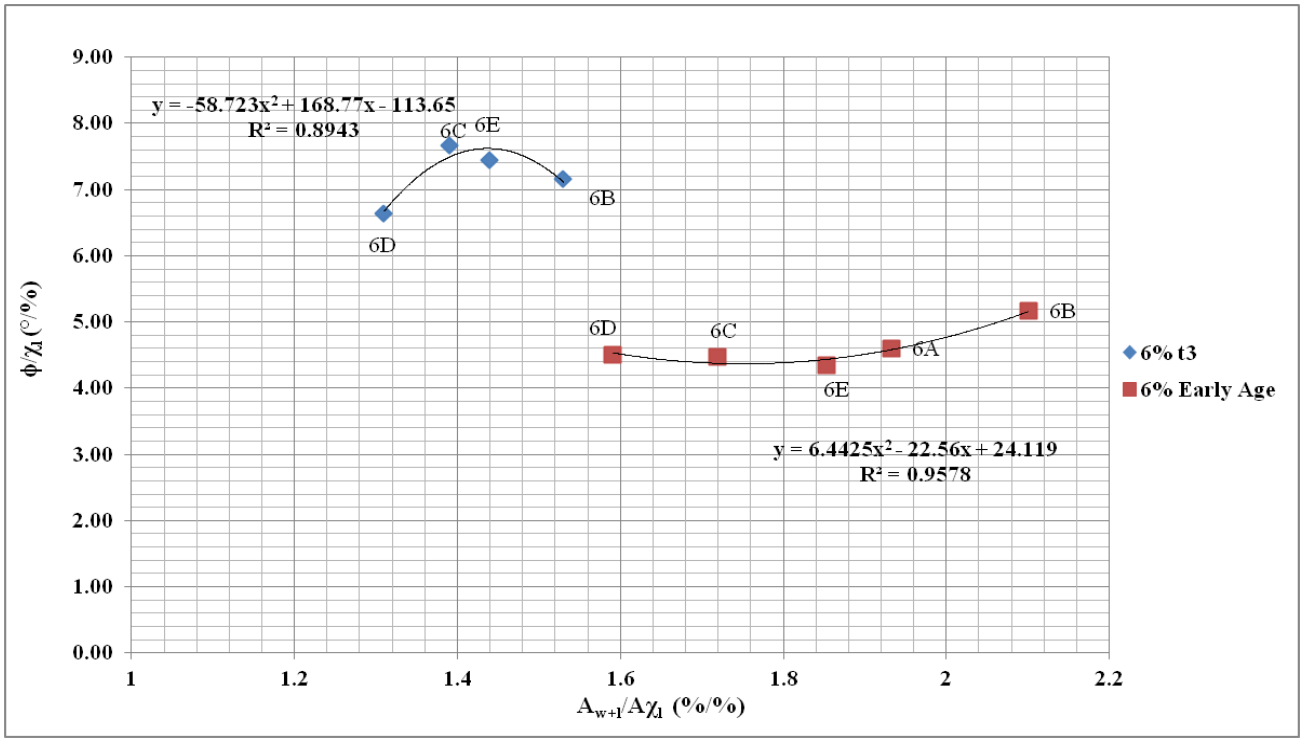

Figure 4-13: Normalized friction vs. normalized area ratio without 6A.

Figs. 4-8 and 4-13 show that there is a significant increase in normalized cohesion and friction with air drying. While both the normalized cohesion and normalized friction still increase approximately linearly with the increase in normalized area ratio, the rate of increase is higher after air drying. Specifically, normalized cohesion increases 5.80 times faster with increase in normalized area ratio for air dried samples than at early age. The internal friction angle increases 1.57 times faster after air drying if the point A is not considered. This implies that strength benefits of each added single percent of CaL increase with air drying. It seems that the points with lowest early age strengths (C and D) benefit the most through the air drying process. This may be due to the fact that sample configurations at higher void ratios can dry more efficiently than those at lower void ratios. This may be further substantiated by Fig. 4-19, depicting the phase diagrams after the initial compression stage in the direct shear apparatus. This also might be the explanation for lower friction angle at point A after air drying as compared to other sample configurations. It is also noted that friction angles increased significantly and all their values after air drying are higher than the friction angles of dry sand at the corresponding dry mass densities Finally it is noted that the water to CaL ratio at points A, E, and C after air drying reached exactly the optimum water to CaL ratio based on the Standard Proctor Test conducted on CaL-W mix. The water to CaL ratio at point B was higher than the optimum while it was lower than optimum at point C.

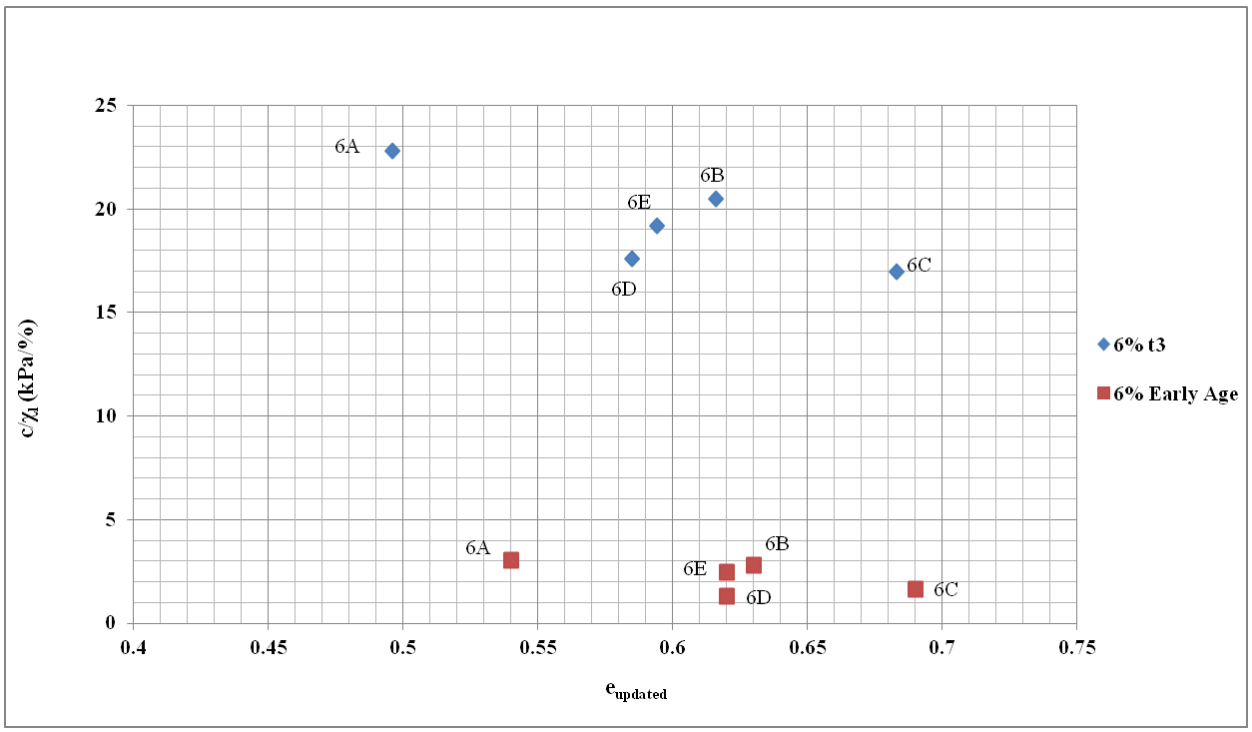

Figure 4-14: Normalized cohesion vs. updated void ratio.

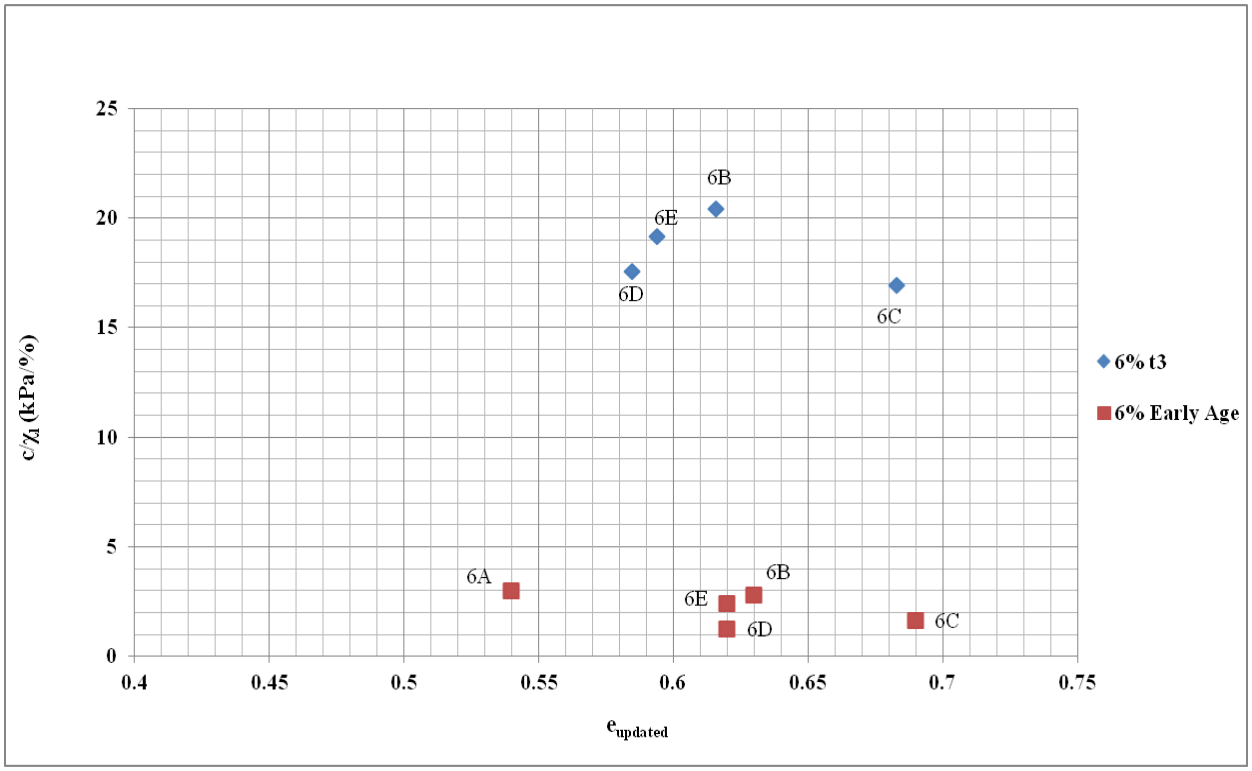

Figure 4-15: Normalized cohesion vs. updated void ratio without 6A.

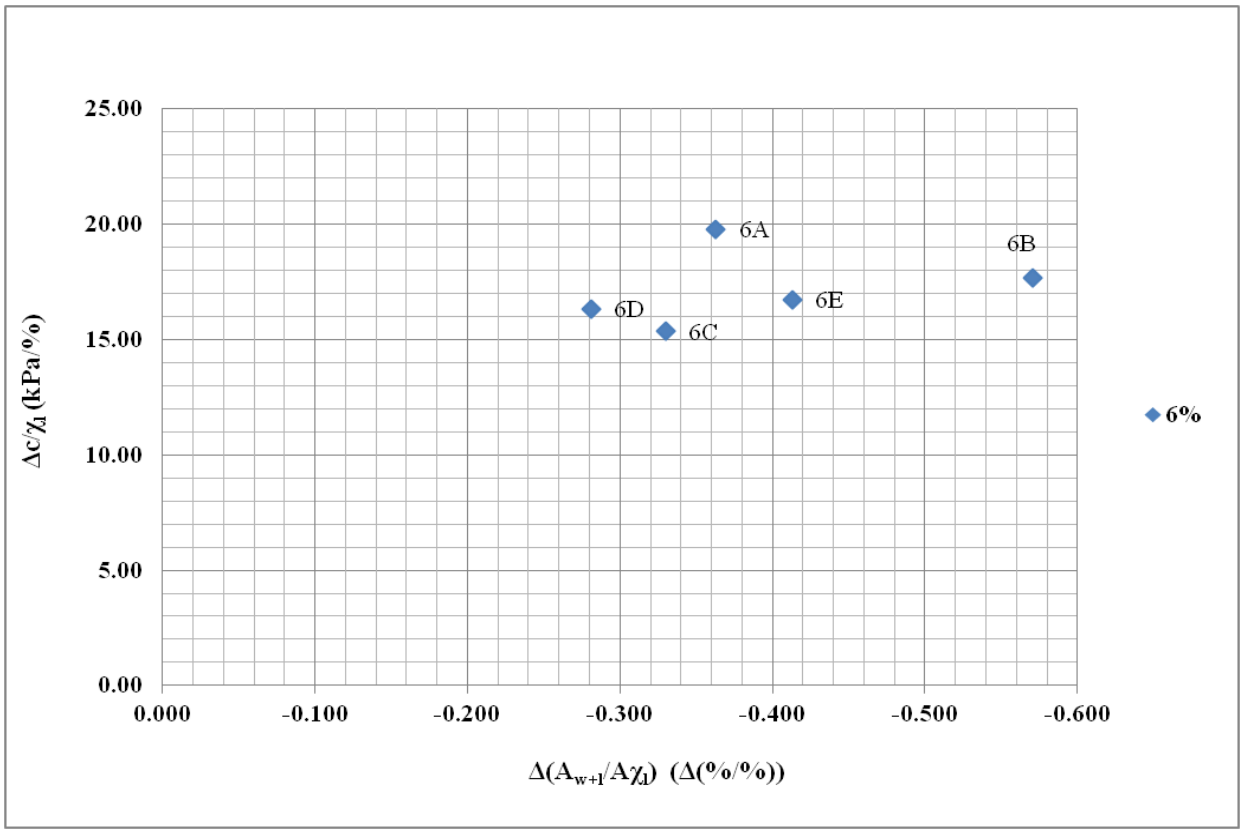

Figure 4-16: Change in normalized cohesion vs. change in normalized area ratio.

In Figure 4-16, the x and y axes represent differences between subsequent and initial normalized area ratios, and differences between subsequent and initial cohesions respectively whereby subsequent refers to values after air drying while initial refers to early age values. For example, in configuration 6D, the cohesion ratio demonstrates that the cohesion has increased nearly 16 with respect to the early age magnitude. The corresponding normalized area ratio has decreased by 0.28. Similarly Fig. 4-17 depicts the ratio of subsequent and initial cohesion versus the ratio of subsequent to initial normalized area ratio. Fig. 4-18 shows the ratio of subsequent and initial friction angle versus the ratio of subsequent to initial normalized area ratio. Finally, Fig 4-19 shows the phase diagrams of the sample configurations for 6% after consolidation.

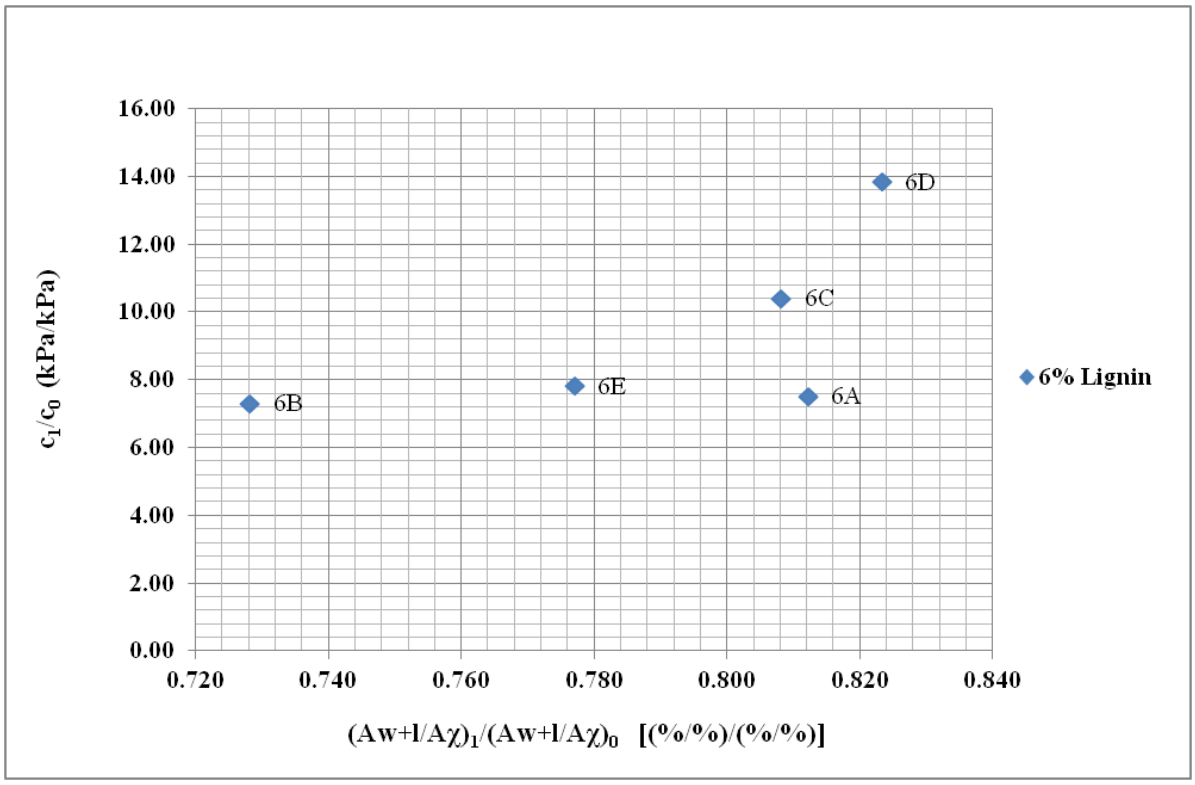

Figure 4-17: Cohesion and normalized area ratio relationships.

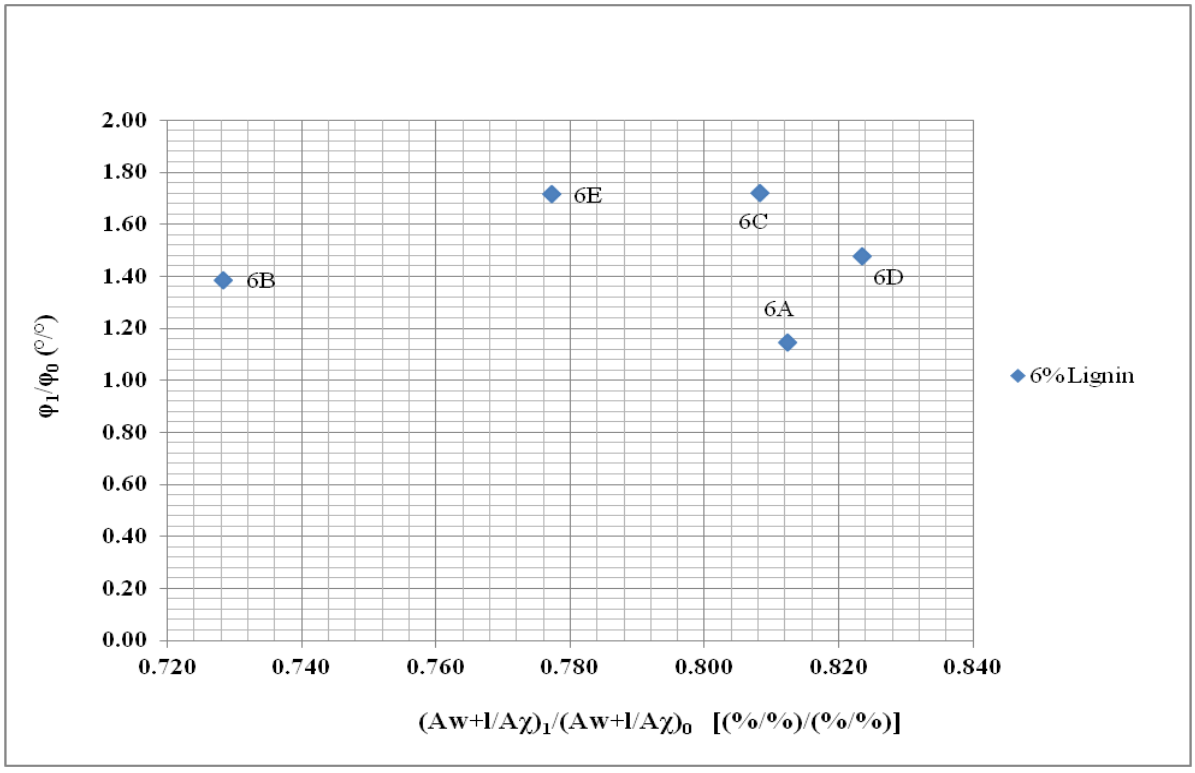

Figure 4-18: Angle of friction relationship vs. formalized area ratio relationship.

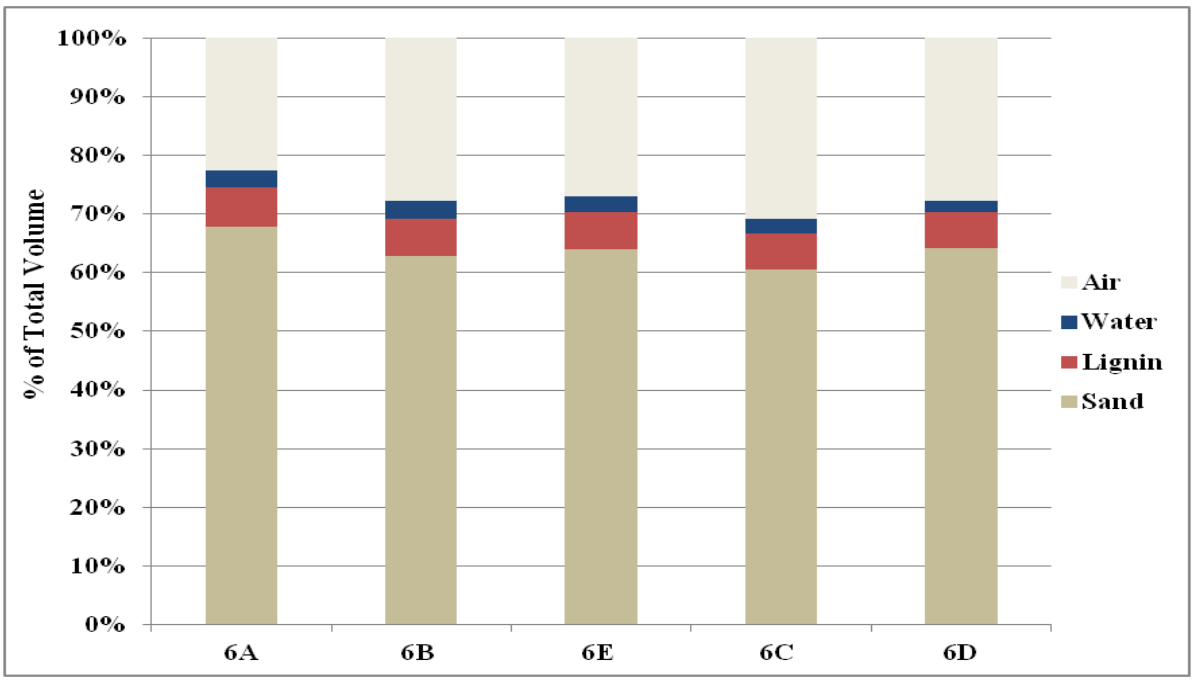

Figure 4-19: Updated Phase relationships for χ_l =6% at t_3 reflecting values after the initial compression in direct shear apparatus.

Chapter 5 - Conclusions and Recommendations

The research produced several conclusions based of the data collected by comparing air dried samples with those that were tested for strength immediately upon mixing. The results provide useful preliminary data for the broader investigation of the effects of air drying on the rapid strength gain of S-CaL-W mixes and the feasibility of the use of CaL as a soil stabilizer.

5.1 Conclusions

1. There is a significant increase in the cohesion and angle of internal friction of S-CaL-W mixes with respect to the corresponding early age values due to drying. This is caused by the evaporation of water, and thus a decrease in the water to CaL ratio. This process improves the quality of binder, thus increasing the inter-particle bonding, but it also makes these bonds more brittle. These characteristics are what make CaL potentially viable as an application product to unpaved roads to improve structural integrity against weathering.

2. Changes in humidity levels have a substantial impact on the drying capabilities of S-CaL-W mixes and the subsequent strength gains that follow.
3. Mixing CaL and water causes an exothermal reaction as noted in the description of Standard Proctor performed on CaL and water only (without sand). Heat generation was only apparent when large amounts of CaL powder and water were mixed. For S-CaL-W mixes sand and very small quantities of lignin were thoroughly mixed first while water was added subsequently. The latter mixing process did not exhibit readily observable exothermal reaction.

5.2 Recommendations

1. Preliminary uniaxial strength testing on large samples having a height to diameter ratio of 2:1 to prevent the risk of premature failures due to the pronounced imperfection sensitivity of small brittle samples. Ultimately conventional triaxial test program should be carried on the S-CaL-W mixes to gain deeper insight into stress-strain and volume change response, thus enabling fundamental knowledge advances.
2. Strength testing on the samples after 7 days and 28 days of air drying to understand whether there are any longer term effects of air drying.
3. Study on the effects of moisture susceptibility of the S-CaL-W mixes and its relationship to the strength.

References

Adams, J. (1988). *Environmental Effects of Applying Lignosulfonate to Roads* (U05-01R). Research and Development. Daishowa Chemicals Inc.

Abdullah, A., Kiousis, P. (1997). *Behavior of Cemented Sands – I. Testing.* International Journal for Numerical and Analytical Methods in Geomechanics. Vol. 21, pp. 533-547.

Bartley, P. (2011). *Experimental Investigation of the Sand-Stabilization Potential of a Plant-Derived Biomass.* M.S. Thesis. Kansas State University.

Ceylan, H., Gopalakrishnan, K., Kim, S. (2010). *Biofuel Co-Product Uses for Pavement Geo-Materials Stabilization.* Technical Report No. IHRB Project TR-582. InTrans. Project 08-316.

Cecilia, M., Toledo, F., Kuznesof, P. (2008). *Calicum Lignosulfonate (40-65).* FAO JECFA Monographs 5. 69th JECFA.

Clark, G.R. (2011).. Department of Geology, Kansas State University, Private communication.

Davis, L. (2009). Department of Biochemistry. Kansas State University. Private communication.

Davis, L. (2012) Department of Biochemistry. Kansas State University. Private communication.

Deretsky, Z., Weng, J., Chapple, C., Bergjan, Wout, R., John. Baucher, M. (2003). National Science Foundation. Purdue University. Annual Review of Plant Biology. Vol. 54, pp. 519-546.

Gebhart, D. Hale, T. Michaels-Busch, K. (1996). *Dust Control Material Performance on Unsurfaced Roadways and Tank Trails.* U.S. Army Environmental Center.

Hodges, F. M. (2003). *The promised planet: Alliances and struggles of the gerontocracy in American television science fiction of the 1960s.* The Aging Male, pp. 175-182.

Hu, T. (2008). *Characterization of Lignocellulosic Materials.* Blackwell Publishing Ltd.

James, N. E. (1988). Two *sides of paradise: The Eden myth according to Kirk and Spock. In D. Palumbo (Ed.), Spectrum of the fantastic* pp. 219-223.

Mosier, N., Wyman, C., Dale, B., Elander, R., Lee, Y.Y. Holtzapple, Mark. Ladisch, Michael. (2004). *Features of Promising Technologies of Pretreament of Lignocellulosic Biomass,* Bioresource Technology 96, pp 673-686.

Mohanty, A., Misra, M., Drzal, L. (2005). *Natural Fibers, Biopolymers, and Biocomposites. CRC Press.* Taylor & Francis Group, LLC.

Novaes, E., Kirst, M., Chiang, V. (2010). *Lignin and Biomass: A Negative Correlation for Wood Formation and Lignin Content in Trees.* Plant Physiology Vol. 154, pp. 555-561.

Onyango, M. (2009). Department of Civil Engineering, University of Tennessee Chattanooga. Private Communication.

Santoni, R. Tingle, J., Webster, S. (2002). *Stabilization of Silty Sand with Nontraditional Additives.* Transportation Research Record, No. 1787, pp 61-70.

Sharma, M.S. Ravi., Baxter, C., Moran, K., Vaziri, H., Narayanasamy, R. (2011). *Strength of Weakly Cemented Sands from Drained Multistage Triaxial Tests.* Journal of Geotechnical and Geoenvironmental Engineering.

Surdahl, R. W. Woll, J.H. Marqez, R. (2005). *Road Stabilizer Product Performance: Buenos Aires National Wildlife Refuge.* Technical Report No. FHWA-CFL/TD-05-011.

Wang, H-J., Li, J., Lu, X-Z., Jin, Y. (2005). *A field experimental study of lignin sand stabilizing material (LSSM) extracted from spent liquor of straw pulping mills.* Journal of Environmental Sciences, Vol. 17, No.4, pp. 650-654.

Woll, J.H. Surdahl, R.W. Everett, R. Anderson, R. (2008). *Road Stabilizer Product Performance: Seedskadee National Wildlife Refuge.* Technical Report No. FHWA-CFL/TD-08-005.

Appendix A - Additional Data Plots

A.1 6% Lignin Configuration Shear Responses

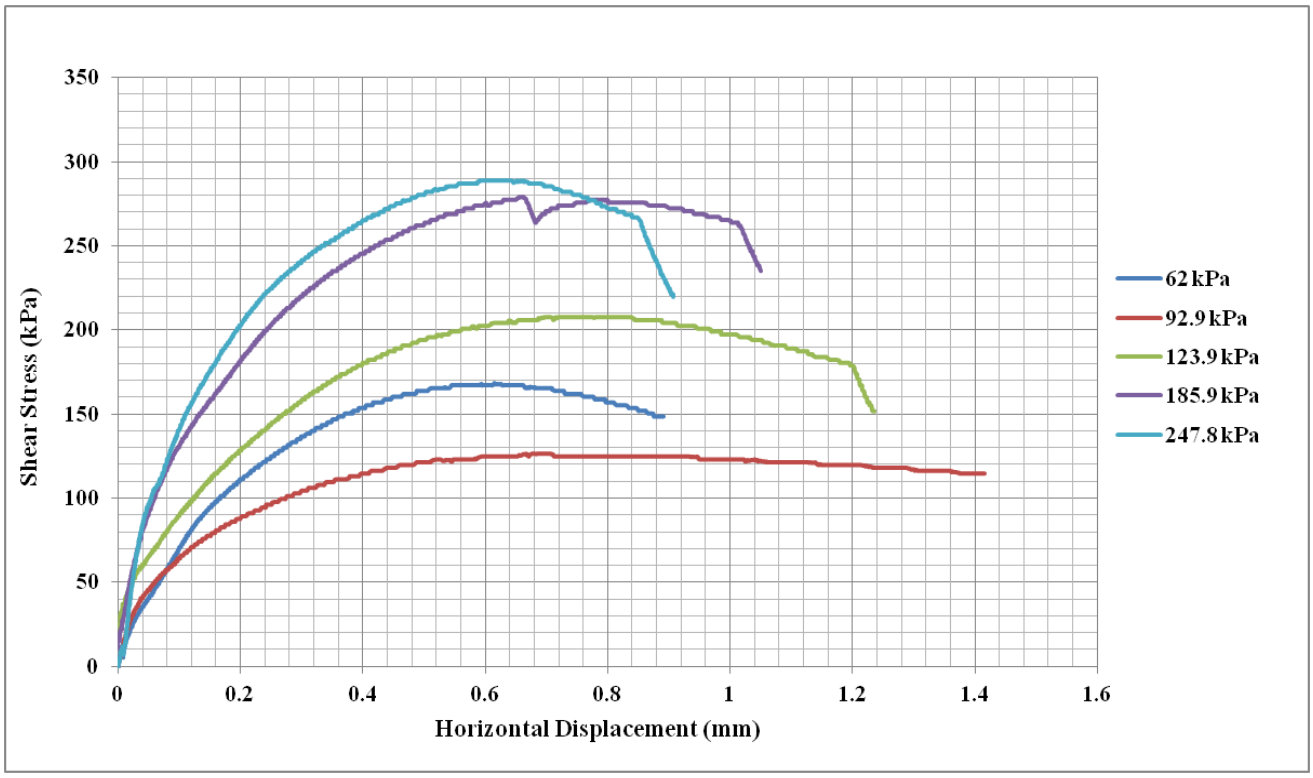

Figure A-1: Peak shear stress vs. normal Stress. (6A)

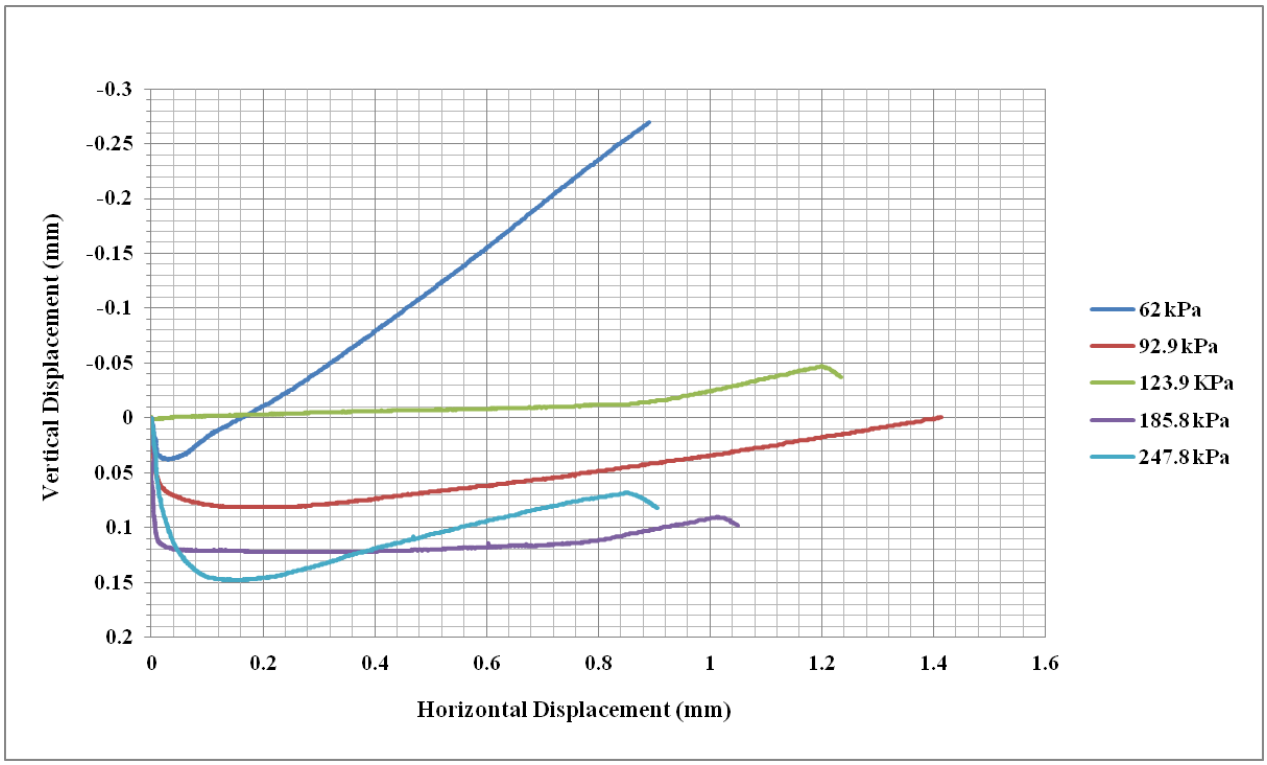

Figure A-2: Vertical displacement vs. horizontal displacement. (6A)

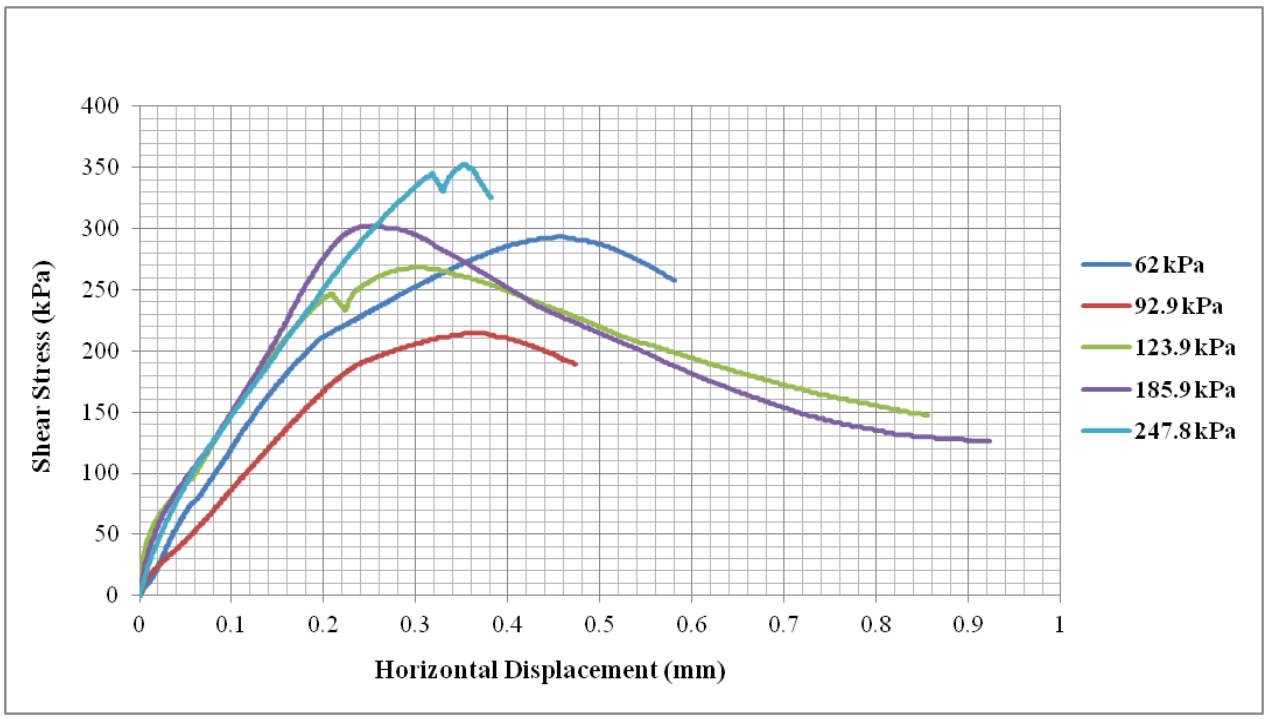

Figure A-3: Peak shear stress vs. horizontal displacement. (6E)

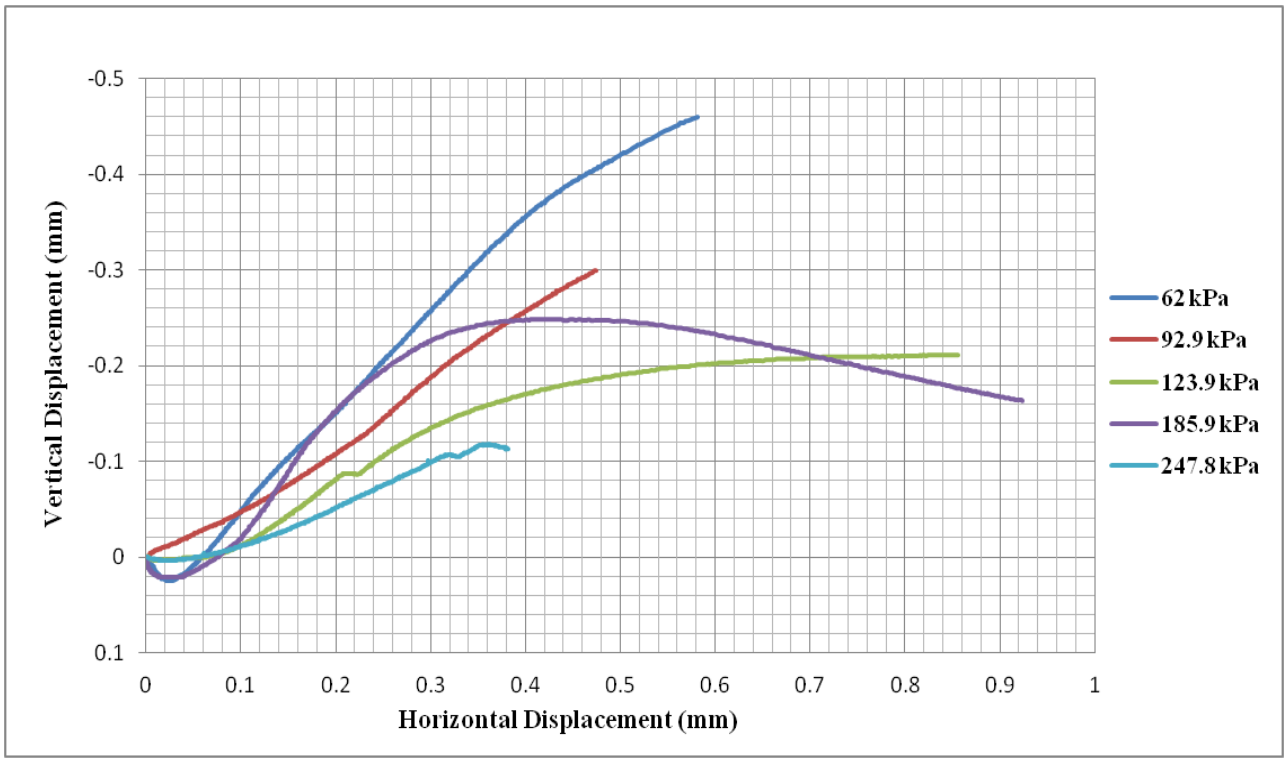

Figure A-4: Vertical displacement vs. horizontal displacement. (6E)

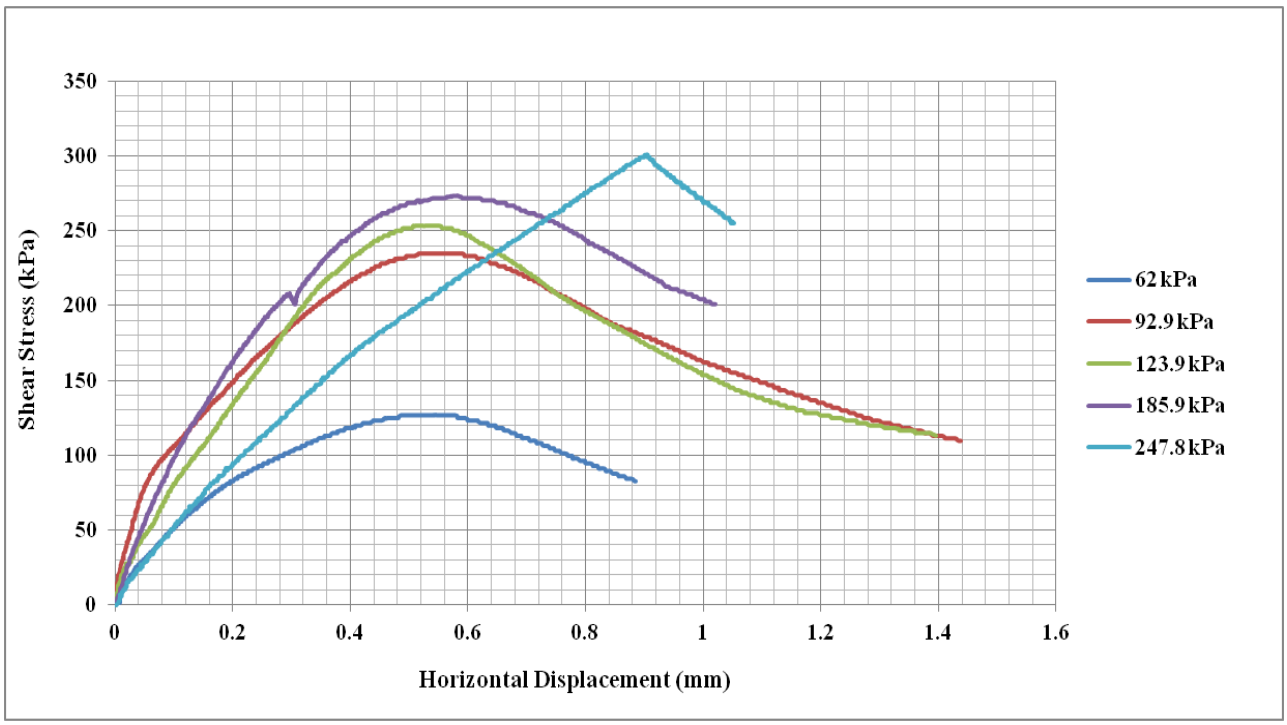

Figure A-5: Peak shear stress vs. horizontal displacement. (6C)

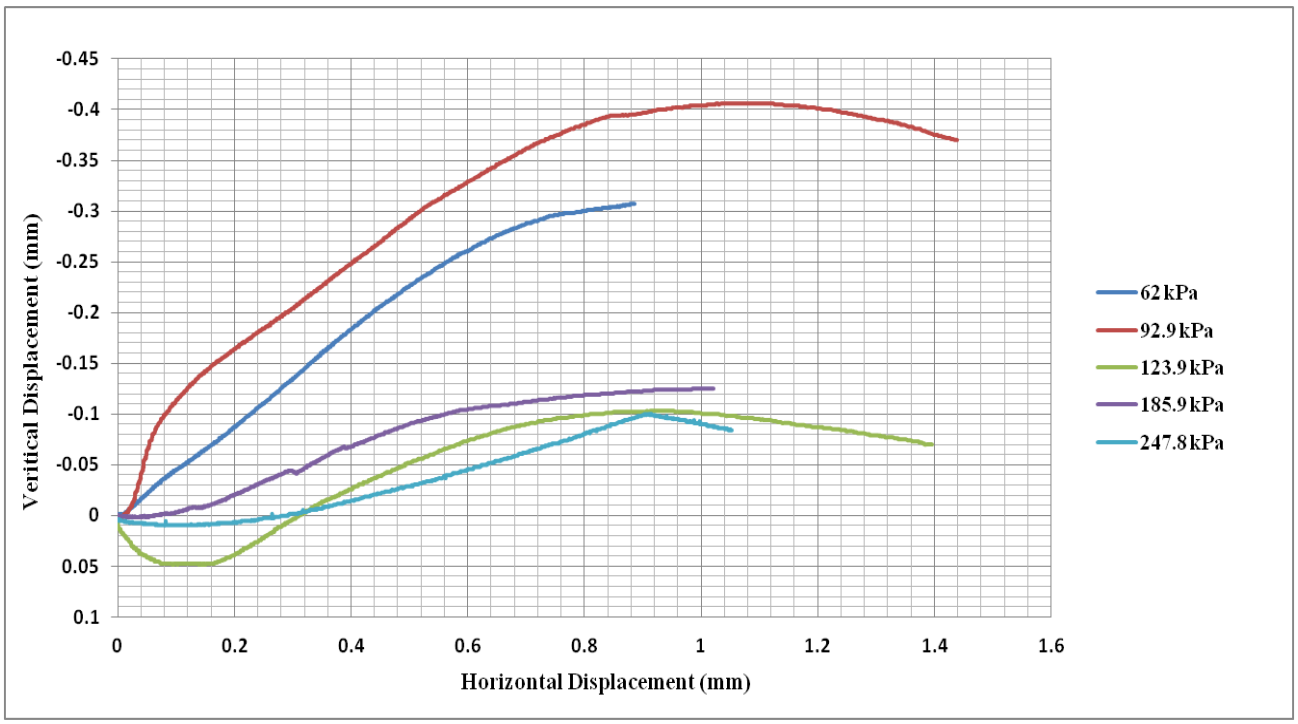

Figure A-6: Vertical displacement vs. horizontal displacement. (6C)

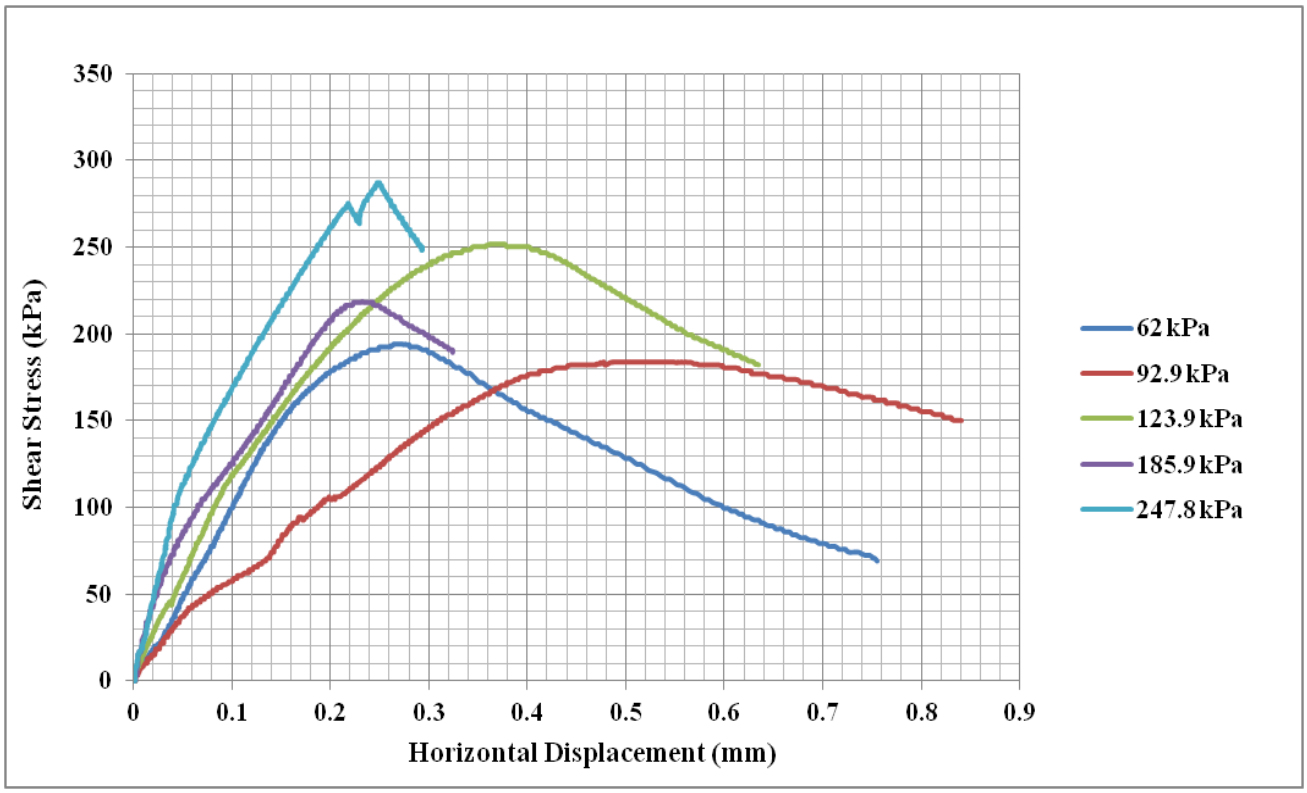

Figure A-7: Peak shear stress vs. horizontal displacement. (6B)

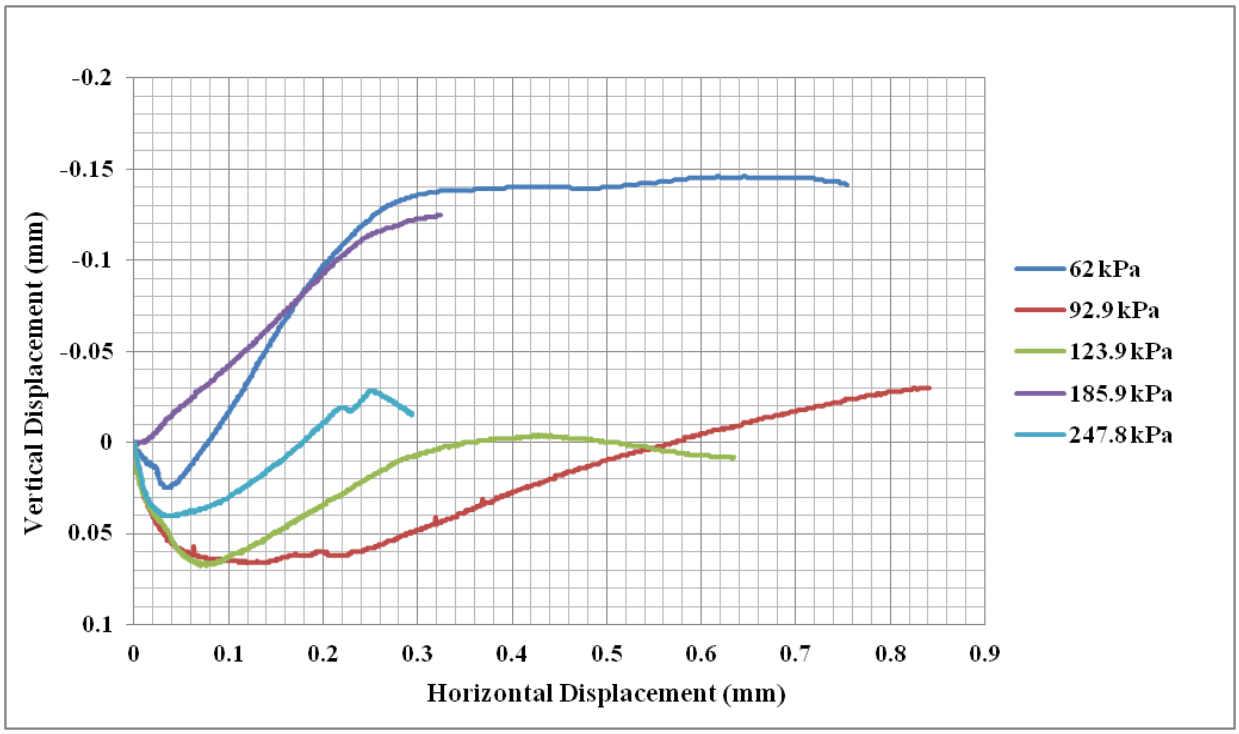

Figure A-8: Vertical displacement vs. horizontal displacement. (6B)

A.2 Additional Normal Stress vs. Shear Stress Plots

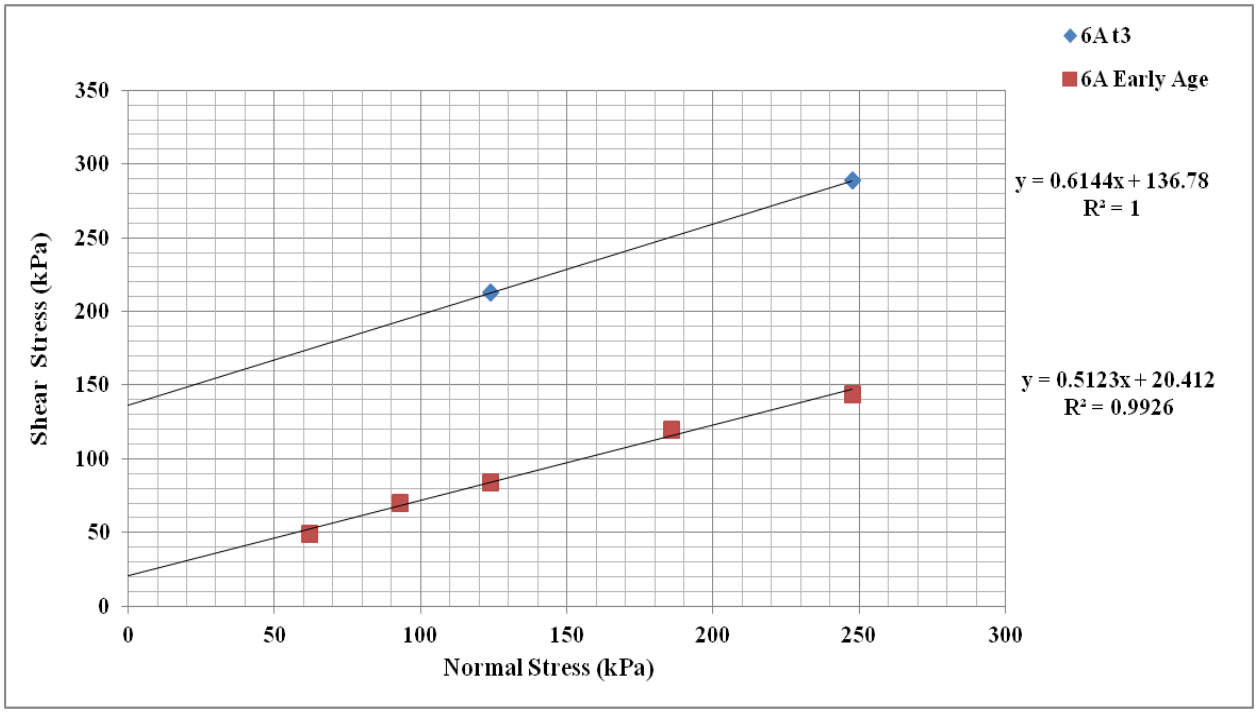

Figure A-9: Shear stress vs. normal stress. (6A)

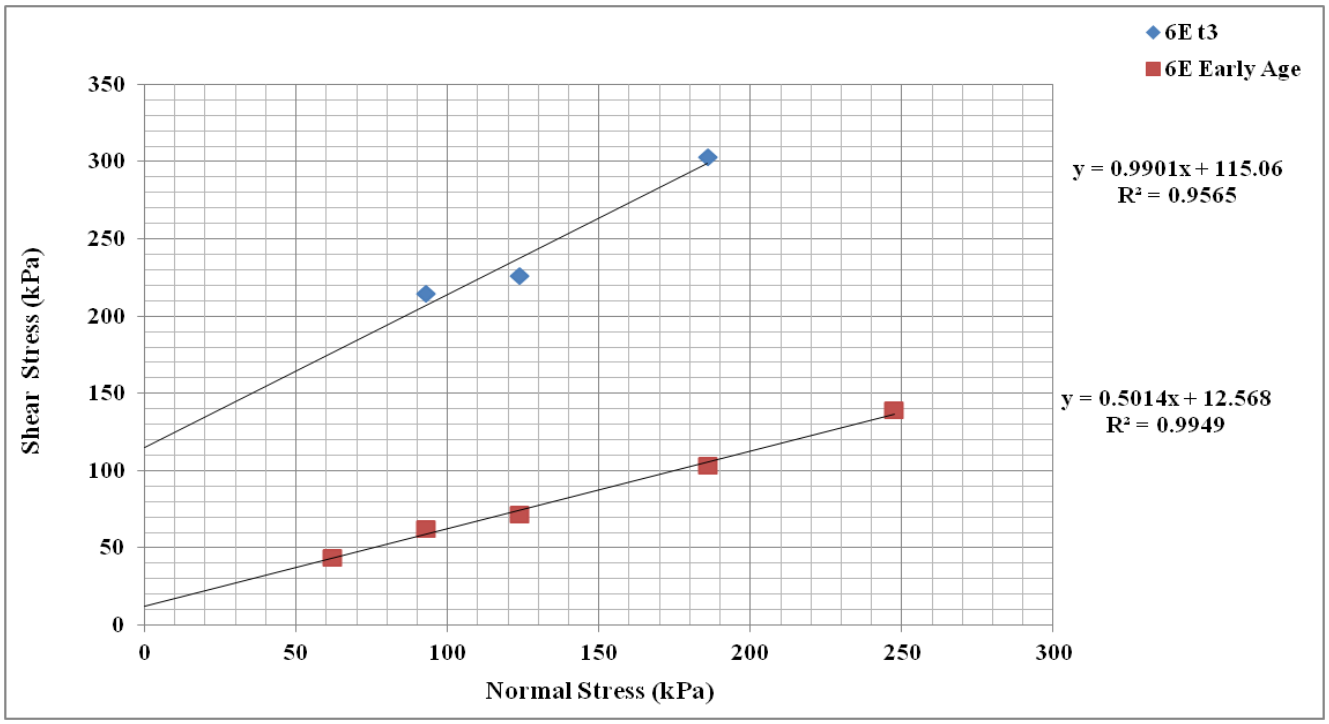

Figure A-10: Shear stress vs. normal stress. (6E)

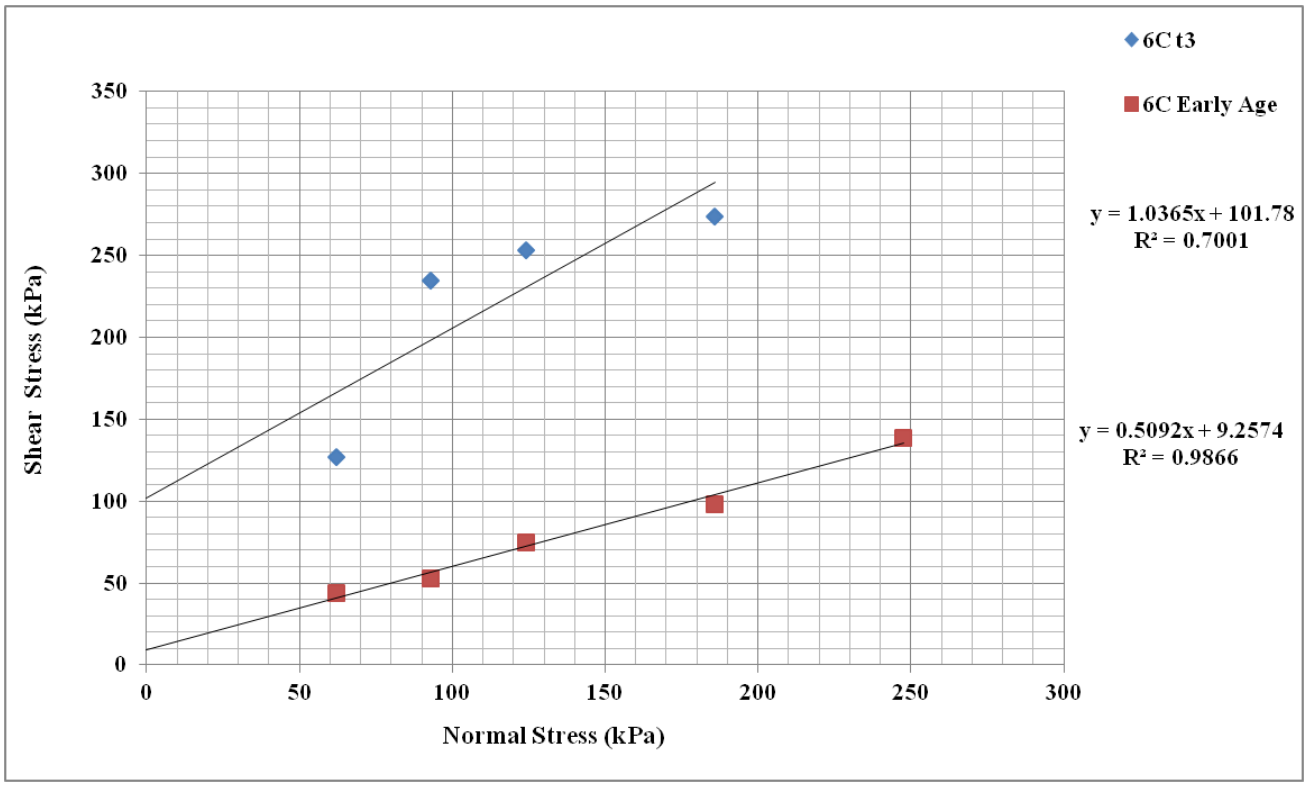

Figure A-11: Shear stress vs. normal stress (6C)

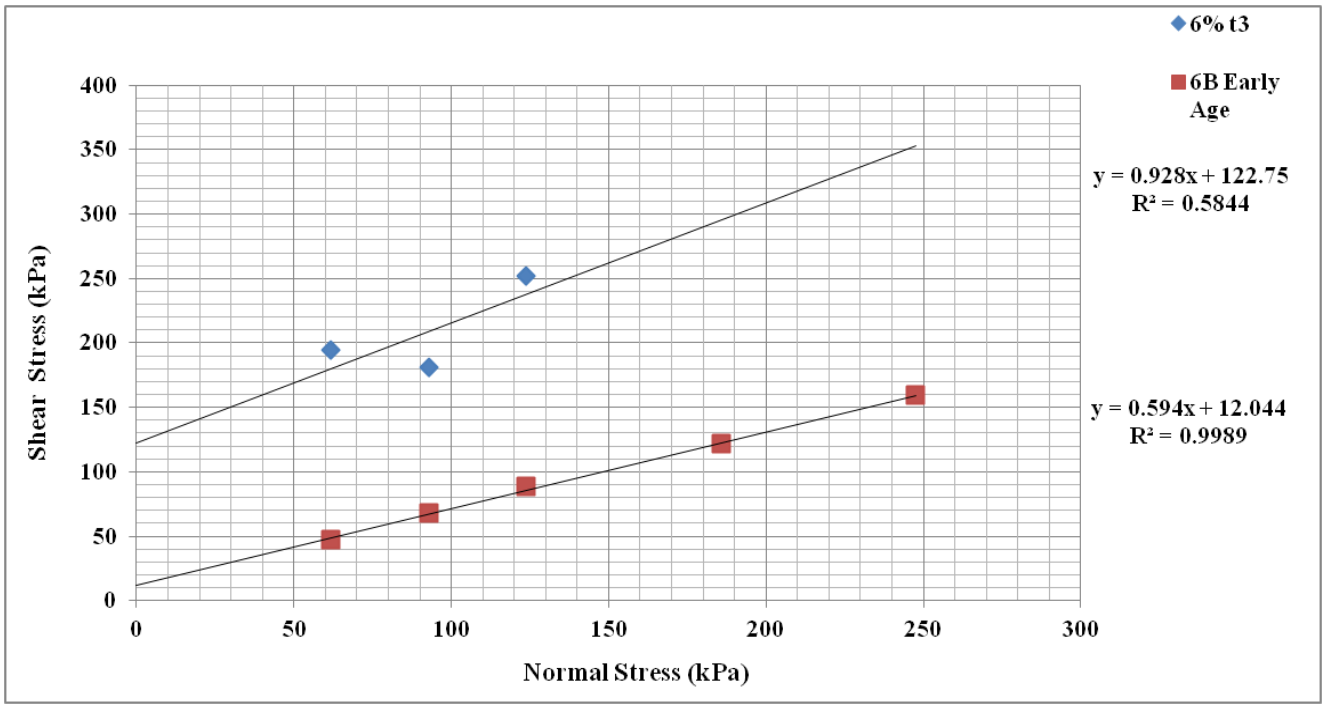

Figure A-12: Normal stress vs. shear stress (6B)

A.3 Additional Moisture Content Plots

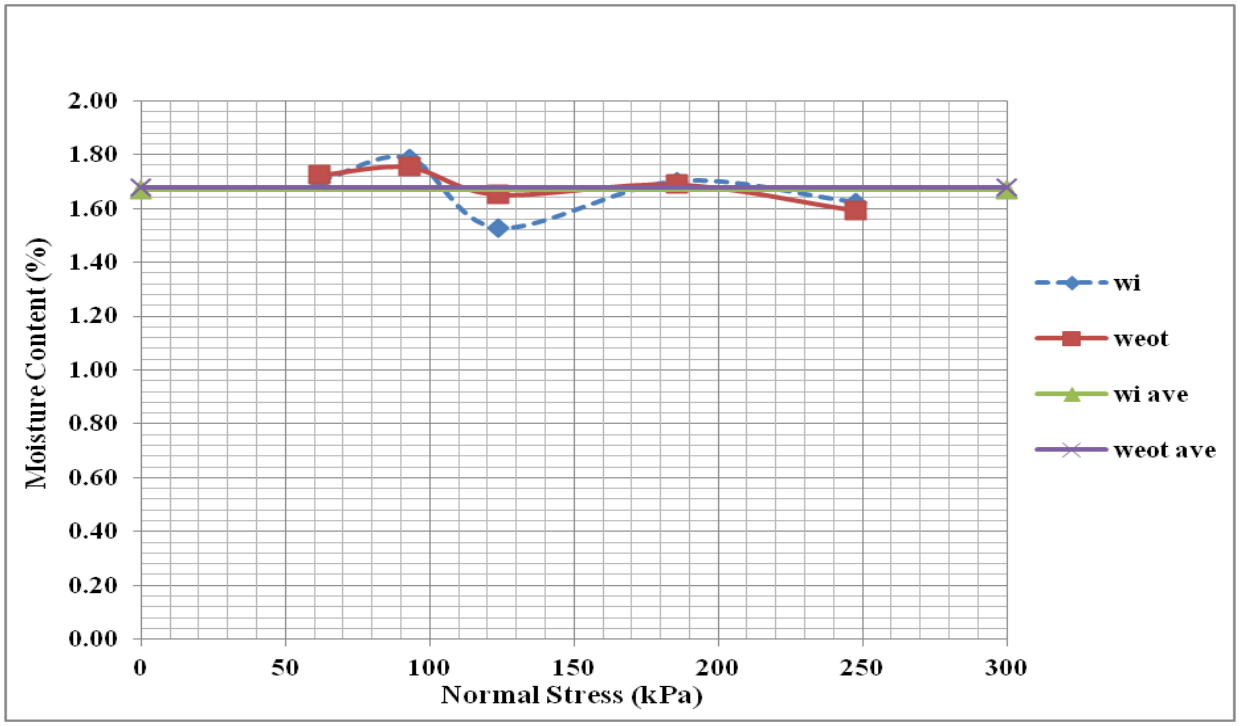

Figure A-13: Moisture content vs. normal stress. (6A)

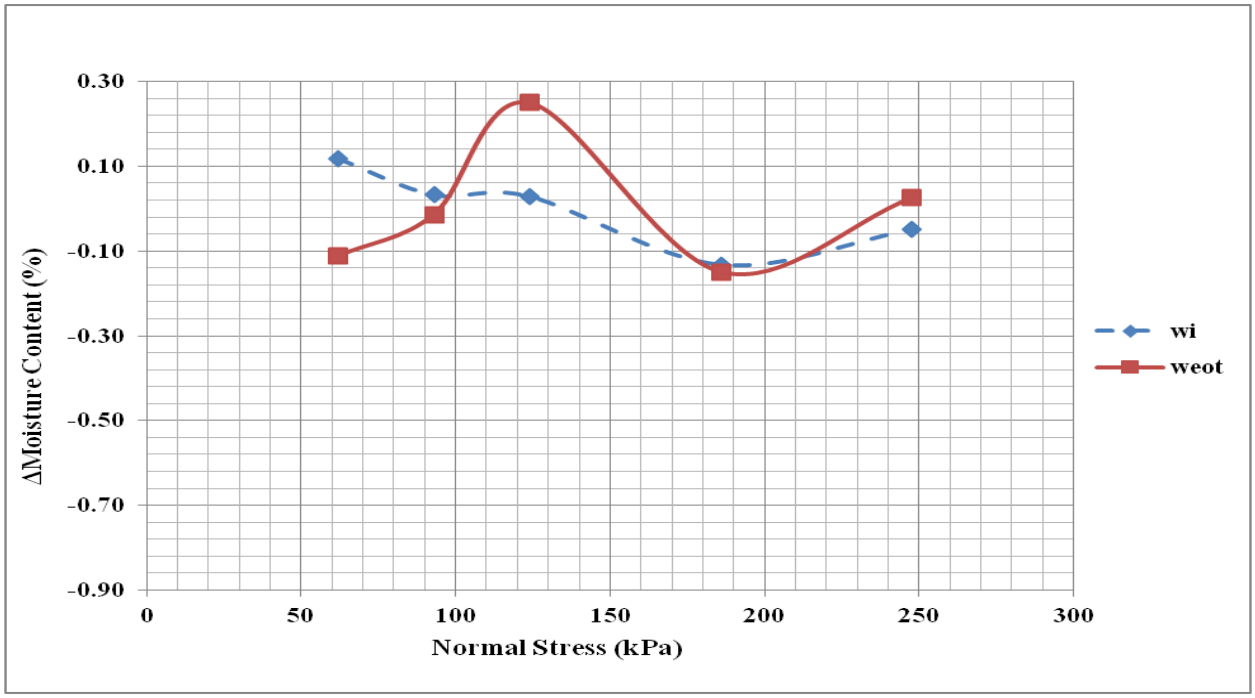

Figure A-14: Change in moisture content vs. normal stress. (6A)

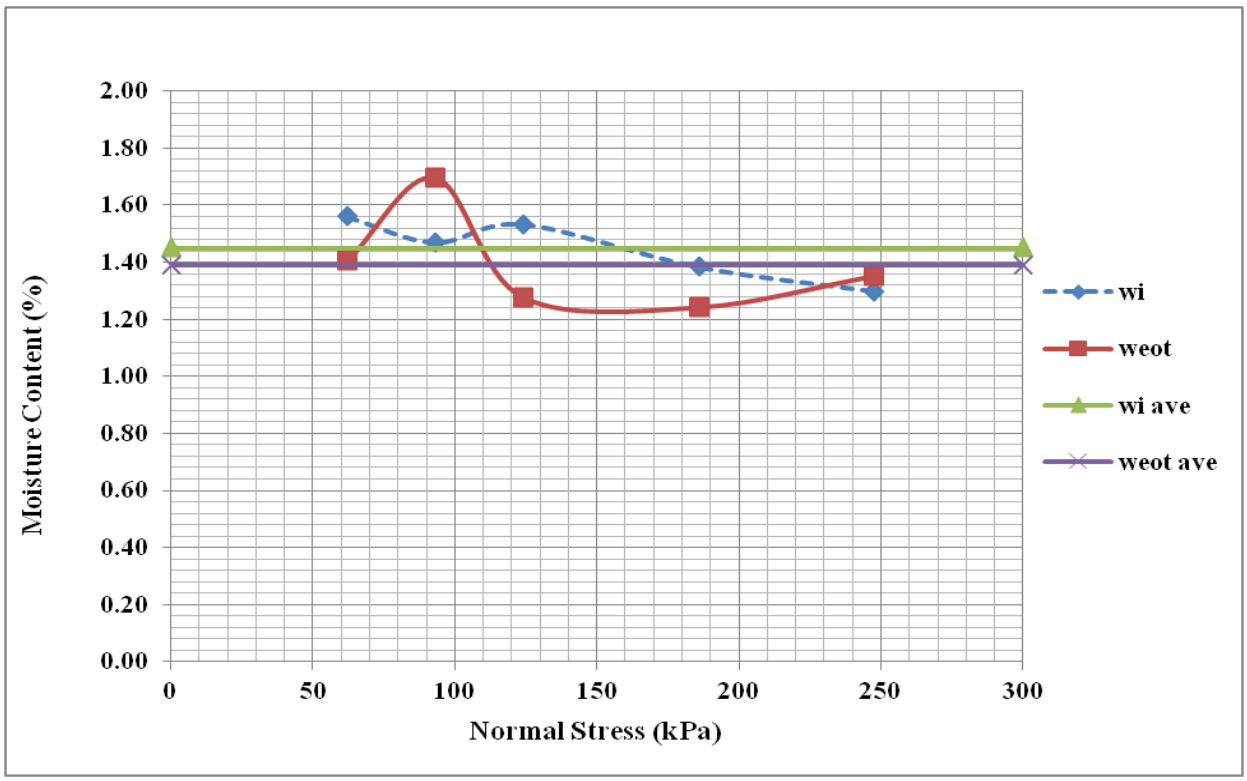

Figure A-15: Moisture content vs. normal stress. (6E)

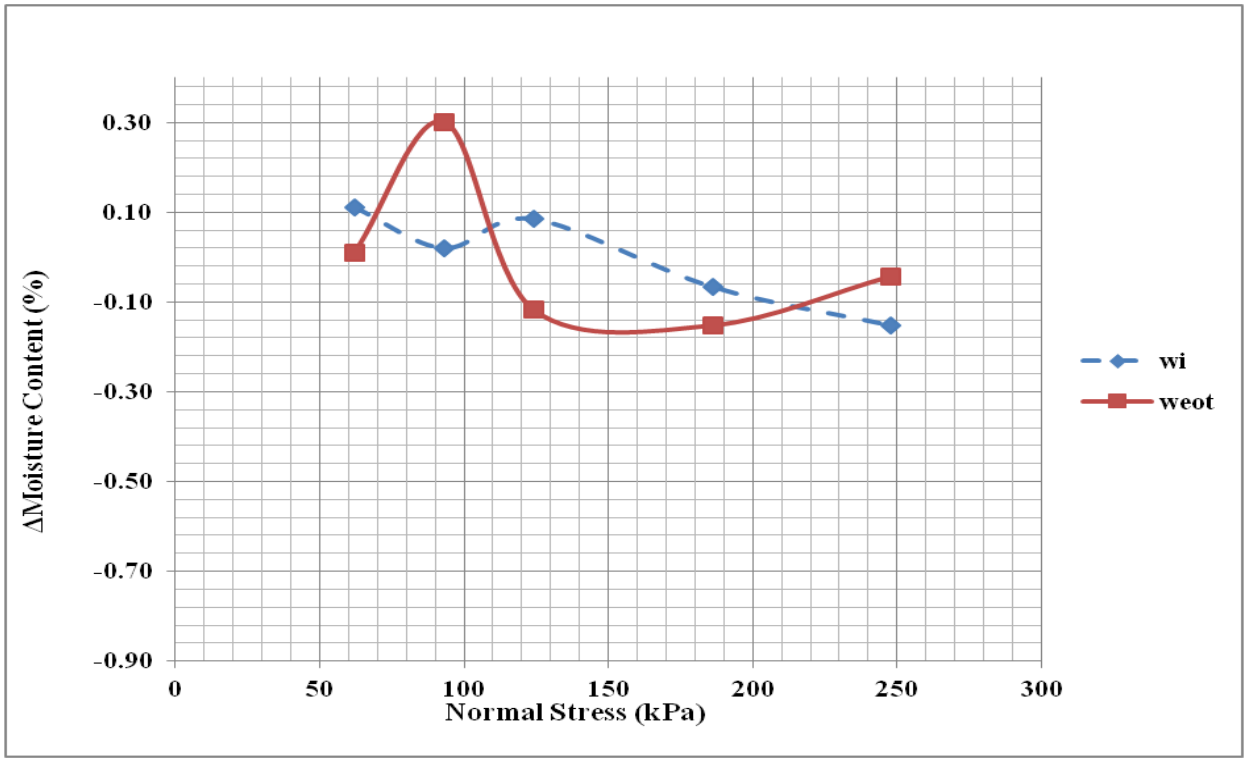

Figure A-16: Change in moisture content vs. normal stress. (6E)

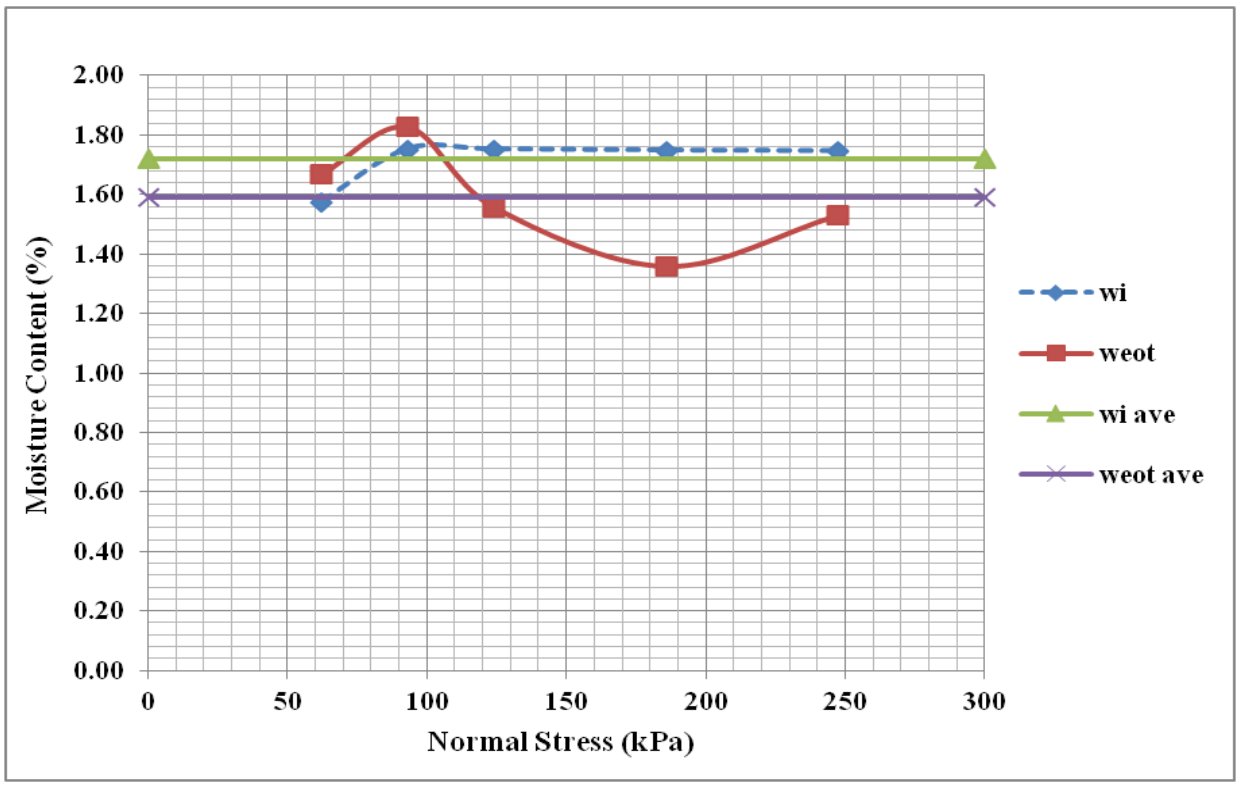

Figure A-17: Moisture content vs. normal stress. (6C)

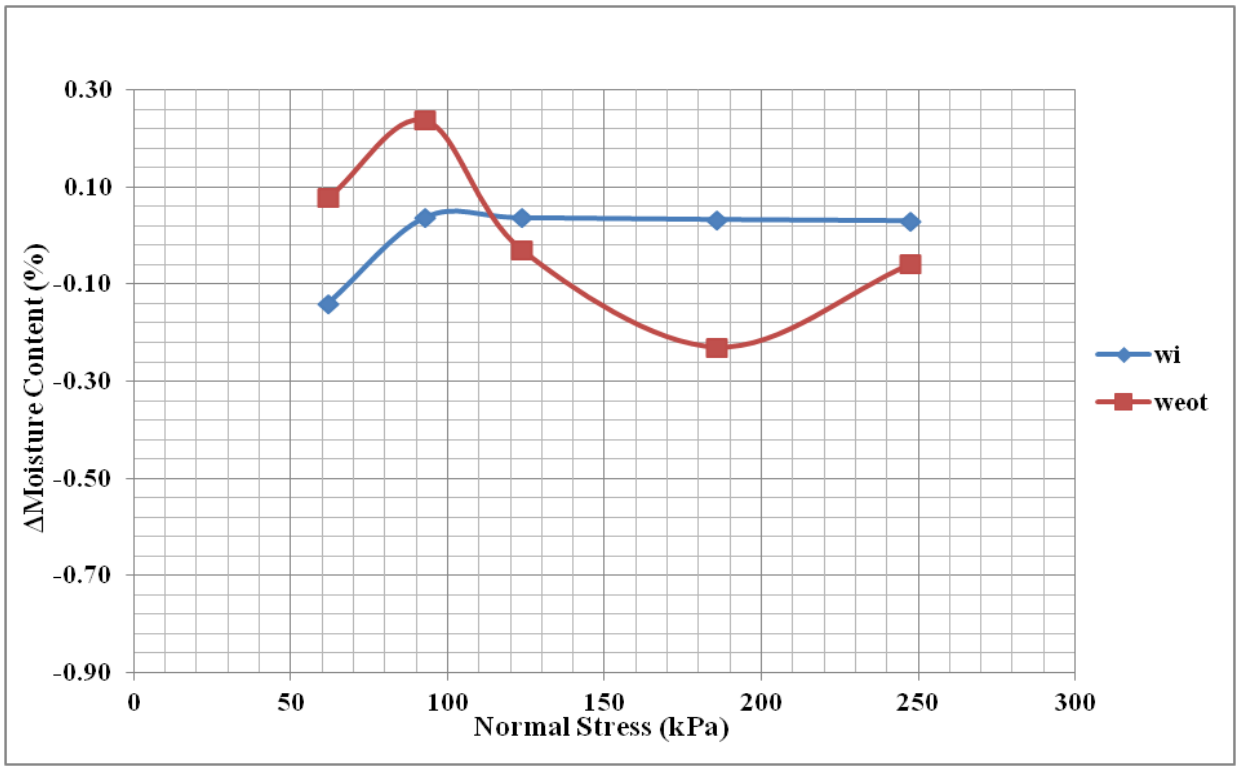

Figure A-18: Change in moisture content vs. normal stress. (6C)

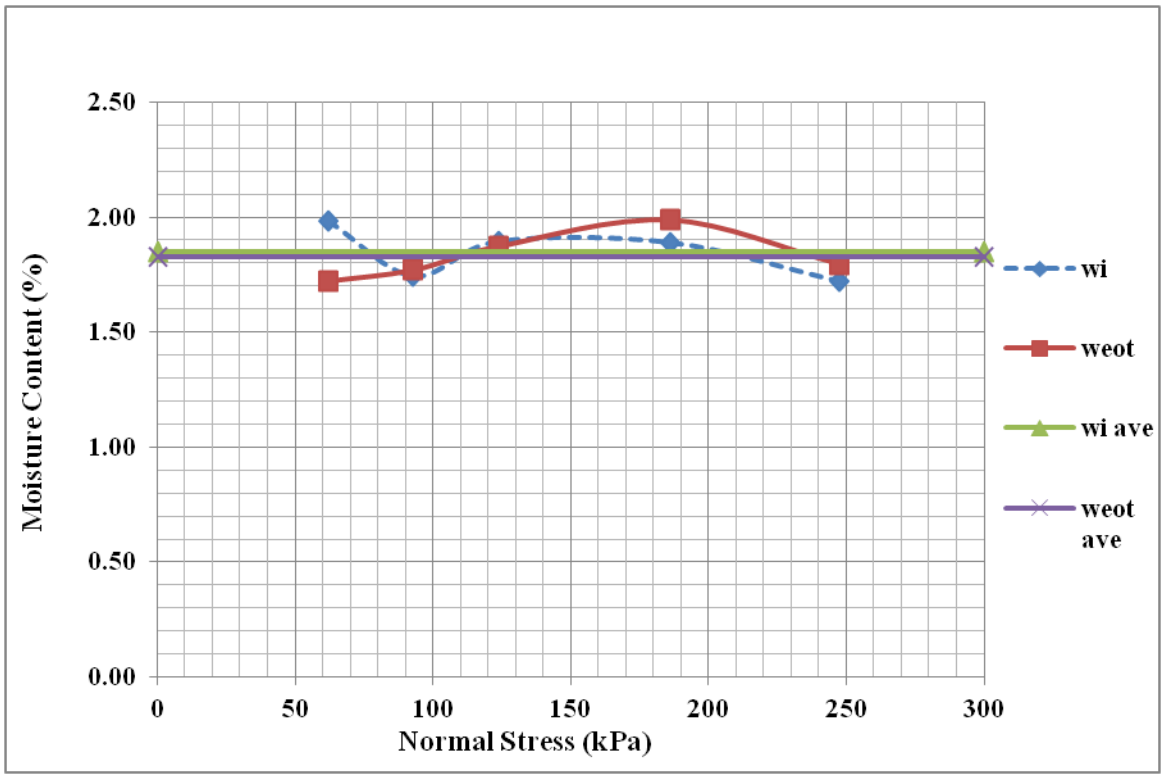

Figure A-19: Moisture content vs. normal stress. (6B)

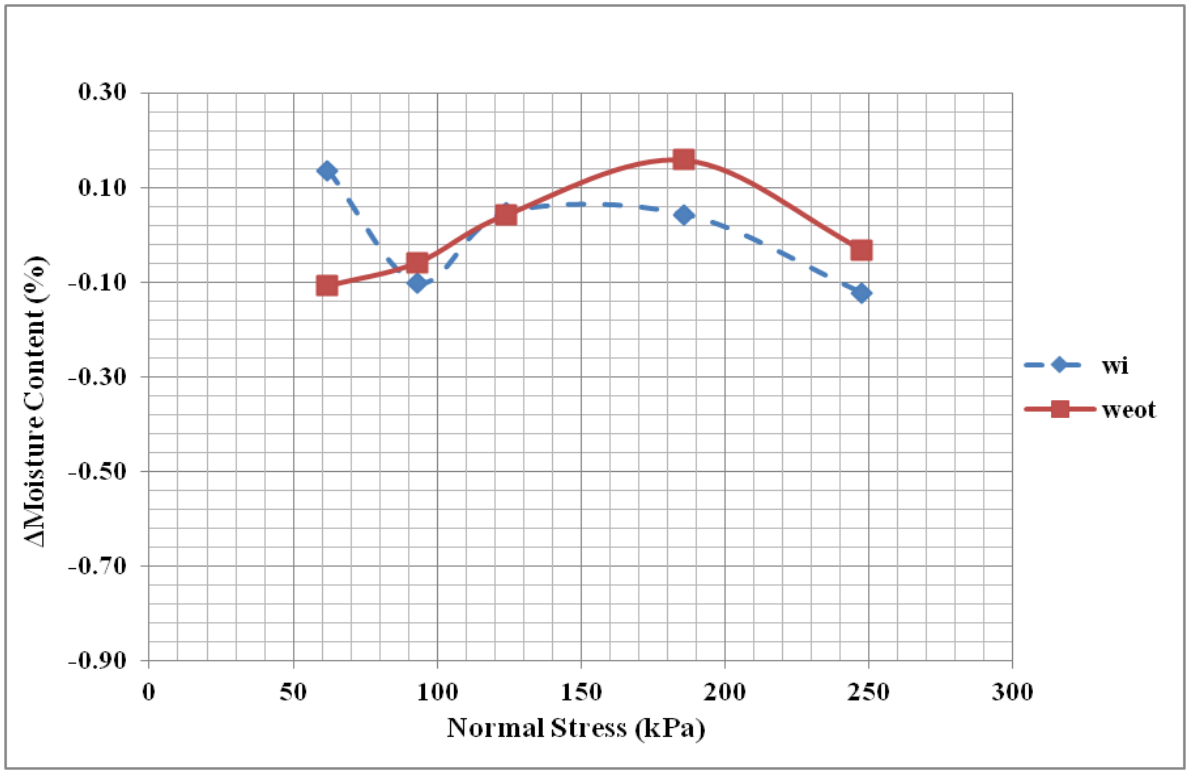

Figure A-20: Change in moisture content vs. normal stress. (6B)